

DEVELOPMENT OF P AND N TYPE CONJUGATED POLYMERS FOR
ELECTROCHROMIC AND ORGANIC SOLAR CELL APPLICATIONS

A THESIS SUBMITTED TO
THE GRADUATE SCHOOL OF NATURAL AND APPLIED SCIENCES
OF
MIDDLE EAST TECHNICAL UNIVERSITY

BY

NAİME AKBAŞOĞLU ÜNLÜ

IN PARTIAL FULFILLMENT OF THE REQUIREMENTS
FOR
THE DEGREE OF DOCTOR OF PHILOSOPHY
IN
CHEMISTRY

SEPTEMBER 2015

Approval of the thesis:

**DEVELOPMENT OF P AND N TYPE CONJUGATED POLYMERS FOR
ELECTROCHROMIC AND ORGANIC SOLAR CELL APPLICATIONS**

submitted by **NAİME AKBAŞOĞLU ÜNLÜ** in partial fulfillment of the requirements
for the degree of **Doctor of Philosophy in Chemistry Department, Middle East
Technical University** by,

Prof. Dr. Gülbin Dural Ünver
Dean, Graduate School of **Natural and Applied Sciences**

Prof. Dr. Cihangir Tanyeli
Head of Department, **Chemistry**

Assoc. Prof. Dr. Ali Çırpan
Supervisor, **Chemistry Dept., METU**

Examining Committee Members:

Prof. Dr. Cihangir Tanyeli
Chemistry Dept., METU

Assoc. Prof. Dr. Ali Çırpan
Chemistry Dept., METU

Prof. Dr. Levent Toppare
Chemistry Dept., METU

Assoc. Prof. Dr. Yasemin Arslan Udum
Advanced Technologies Gazi Universitesi

Assoc. Prof. Dr. Ertuğrul Şahmetlioğlu
Chemistry Department, Nigde University

Date: 11/09/2015

I hereby declare that all information in this document has been obtained and presented in accordance with academic rules and ethical conduct. I also declare that, as required by these rules and conduct, I have fully cited and referenced all material and results that are not original to this work.

Name, Last name: Naime Akbařođlu Ünlü

Signature :

ABSTRACT

DEVELOPMENT OF P AND N TYPE DONOR ACCEPTOR CONJUGATED POLYMERS FOR ELECTROCHROMIC AND ORGANIC SOLAR CELL APPLICATIONS

Akbařođlu Ünlü, Naime

PhD, Chemistry Department

Supervisor: Assoc. Prof. Dr. Ali Çırpan

September 2015, 190 pages

Donor-acceptor (D-A) approach is highly efficient to obtain p-type and n-type materials with desired intrinsic optical and electrochemical properties. Therefore, in this study a series of p-type and n- type DA type conjugated polymers was synthesized with combination of electron donating and electron-withdrawing heterocyclics to understand the effects of structural modifications on electrochemical, optoelectronic and photovoltaic properties. Synthesized polymers were utilized for electrochromic and organic solar cell applications. Conjugated polymers were synthesized either electrochemical or chemical methods. Syntheses of p-type DA polymers were performed

from the coupling reaction of benzotriazole with different donor units, i.e, furan, thieno[3,2-b]thiophene, dithienopyrrole, benzodithiophene. Donor units in molecular design are either used directly to couple with BTz or inserted as π -bridging segments to discuss their effect on optical, electrochemical, electrochromic, and optoelectronic properties. N-type conjugated polymers were developed by NDI and ladder type indacenodithiophene (IDT) and indacenodiselenophene (IDSe) units. N-type conjugated polymers were utilized for all polymer solar cell applications to replace fullerene in bulk heterojunction organic solar cell fabrication. Morphological and light intensity dependent photovoltaic studies were conducted that elucidate the possible loss mechanism in the related solar cells.

Keywords: Electrochromism, organic solar cell, polymer-polymer solar cell, benzotriazole, naphthalene diimide

ÖZ

ORGANİK GÜNEŞ PİLİ VE ELEKTROKROMİK UYGULAMALAR İÇİN P VE N TİPİ DONÖR- AKSEPTÖR KONJÜGE POLİMERLERİN GELİŞTİRİLMESİ

Akbaşođlu Ünlü, Naime

Doktora, Kimya Bölümü

Tez Yöneticisi: Doç. Dr. Ali Çırpan

Eylül 2015, 190 sayfa

Donör-akseptör yaklaşımı istenilen optik elektronik özelliklere sahip p ve n tipi materyallerin sentezi için etkili bir yöntemdir. Bundan dolayı, bu çalışmada yapısal farklılıkların elektrokimyasal, optik, elektrokromik ve fotovoltaiik özelliklerine etkilerinin araştırılması için deđişik elektron alıcı ve verici üniteler birleştirildiđi DA tipi n ve p tipi konjüge polimerler sentezlenmiştir. Sentezlenen polimerler elektrokromik ve organik güneş pili uygulamalarında kullanılmıştır. Polimerler elektrokimyasal ve kimyasal metotlar kullanılarak sentezlenmiştir. P-tipi polimerlerin sentezi benzotriazolün furan, tiyeno[3,2-b]tiyofen, ditiyenopirol ve benzoditiyofen gibi farklı donör üniteleri ile kenetlenme reaksiyona sokulması ile sağlanmıştır. Donör üniteler

optik, elektronik, elektrokromik ve optoelektronik etkilerinin tartiřılması iin ya direkt olarak ya da π -koprüsü olarak kullanılmıřtır. n-tipi konjüge polimerler ise NDI'in indasenoditiyofen (IDT) ve indasenodiselenofen (IDSe) üniteleri ile geliřtirilmiřtir. Bu polimerler polimer-polimer organik güneř pili uygulamalarında fullerenin yerine kullanılmak üzere sentezlenmiřtir. Morfoloji ve ışık řiddetine baėlı fotovoltaik alıřmalar organik güneř pillerindeki kayıp mekanizmalarını aydınlatmak iin gerekleřtirilmiřtir.

Anahtar kelimeler: Elektrokromizm organik güneř pilleri, polimer-polimer güneř pilleri, benzotriazol, naftalin diimid

To my lovely husband and baby

ACKNOWLEDGEMENTS

I wish to express my sincere appreciation to my advisor, Assoc. Prof. Dr. Ali Çırpan for giving opportunity to join in his research group and undertake my graduate research in his research group. It was a long way for me to understand organic electronics since at the beginning of the PhD I have no idea about it. Assoc. Prof. Dr. Ali Çırpan was very supportive and made all the points clear to me. Although, I faced with some problems in my study from time to time, we found a way to handle these obstacles.

I would like to thank to Prof. Dr. Levent Toppare for giving opportunity to work with his research group. Although, I don't know anything about electrochromism and conjugated polymers at the first year of my PhD, I learn lots of valuable knowledge from him and his research group meetings.

I would like to thank to Professor Alex Jen for allowing undertake the research in the area of organic photovoltaic in his research group. I conduct the study entitle as "Indacenodithiophene/selenophene and Naphthalene Diimide n-Type Copolymers for Efficient All-Polymer Solar Cells" in his research group. I also owe a great debt to his research group member: Chang-Zhi Li for brilliant ideas about synthesis of conjugated polymers, Yun-Xiang Xu for his help in organic synthesis, Yue Zhang for organic photovoltaic fabrication and characterization.

During my PhD years, I have an opportunity to work lots of people. At the beginning, I was alone in our research group and we become a big family during years. I also owe a great debt to past and present members of Çırpan research group. All of them provide an amazing working environment to me. Whenever I faced with a problem, they were always there and with me. We had a great experience together about research and life.

To start the working day with them and finish it together was very valuable for me. I want to special thank to Hande Ünay, Şevki Can Cevher, Ozan Erlik, Cansel Temiz and Emre Atoğlu. I will remember Hande Ünay with her support, respect, hardworking, and coffee breaks, Şevki Can Cevher with unbelievable personality (remember the summer we alone in the laboratory), Ozan Erlik with his respect, hardworking and the travels we did together, Cansel Temiz with her smile, positivity and unending excuses, Emre Atoğlu with stubborn personality.

I would like to thank to past and present members of Toppare Research group. Derya Baran and Merve Şendur for electrochemical characterization, Abidin Balan for helping me to understand the concept of structure/ property of DA conjugated polymers and electrochromism, Gönül Hızalan for organic solar cell fabrication and characterization.

I would like to thank to Cihangir Tanyeli and Yasemin Arslan Udum for their valuable idea about my thesis and I would like to thank Esra Yildiz for mobility measurements.

I want to special thank to Şerife Özdemir Hacıoğlu not only for her help about the electrochemical characterization of my polymers but also being a good friend during my MSc and PhD years. Our friendship started at the Organic Chemistry floor and continued at the Toppare research group. I will always remember her and our pregnancy. Doing all the valuable things like being research assistant and pregnant at the same time is very valuable for me. I am sorry but I have to finish my PhD before you.

I would like to thank the friends I have, Sema Demirci, Ece Aktaş, Gözde Öktem, Buket Zaifoğlu and Şebnem Bayseç. I always remember Sema Demirci with her friendship and endless conversation in Seattle, Gözde Öktem with her strong personality and Şebnem Bayseç with her beauty and vulnerability, Buket Zaifoğlu with her enthusiasm. I want to special thank to Ece Aktaş for being with me whenever I fell alone and also being a good friend.

I would like to thank TUBITAK 2214/A fellowship for financial support, METU Central lab for characterization of conjugated polymers and Betül Eymür for NMR analysis.

Finally, I would like to thank my husband, my family, and my lovely baby. They were always support me during my PhD. Whenever I cried or happy, my husband was always there to support me or share my feelings. After my baby born, I found the reason of my life. This was the most tired and valuable experience of my life. Life does not mean anything without her smile and smell.

TABLE OF CONTENT

ABSTRACT	v
ÖZ.....	vii
ACKNOWLEDGEMENTS	x
TABLE OF CONTENT	xiii
LIST OF TABLES	xix
LIST OF FIGURES.....	xx
LIST OF ABBREVIATIONS.....	xxvi
CHACTERS	
INTRODUCTION.....	1
1.1. History of conducting polymers.....	1
1.2. Band gap.....	2
1.3. Charge transport in conjugated polymers	3
1.4. Doping process in conjugated polymers	6
1.5. Synthesis of conjugated polymers.....	7
1.5.1. Chemical synthesis of conjugated polymers	7
1.5.1.1. Suzuki reaction.....	8
1.5.1.2. Stille coupling	9
1.5.2. Electrochemical synthesis of conjugated polymers	9
1.6. Electrochromism	11

1.6.1. Electrochromism in conjugated polymers.....	11
1.7. Organic solar cell	13
1.7.1. Working principle of solar cell.....	13
1.7.2. Solar cell architectures	17
1.7.2.1. Bilayer Heterojunction Device.....	17
1.7.2.2. The bulk-heterojunction organic solar cell.....	18
1.7.3. Fabrication of bulk heterojunction organic solar cell.....	19
1.7.4. Characterization of organic solar cells	20
1.7.4.1. Open circuit voltage	21
1.7.4.2. Short-circuit current	22
1.7.4.3. Fill Factor	22
1.7.5. Donor materials in OSCs fabrication	23
1.7.6. Band gap engineering.....	23
1.7.7. Donor-acceptor theory.....	25
1.7.7.1. Donor units.....	27
1.7.7.1.1. Dibenzene bridged donor units	28
1.7.7.1.2. Dithiophene bridged donor units	29
1.7.7.1.3. Thiophene–benzene fused donor units.....	29
1.7.7.2. Acceptor Units.....	30
1.7.8. Benzotriazole based donor molecules for organic solar cell applications	31
1.7.9. Acceptor materials in organic solar cell.....	33
1.7.10. NDI based acceptor molecules for all polymer solar cell applications	33
1.8. Organic field effect transistor.....	36

1.9. Aim of the study	38
EXPERIMENTAL	41
2.1. A synopsis of materials and methods.....	41
2.2. Gel permeation chromatography	42
2.3. Cyclic Voltammetry	42
2.4. Spectroelectrochemistry	44
2.5. Kinetic studies.....	45
2.6. Device fabrication of OSC	46
2.7. Device Characterization of OSC.....	47
2.8. SCLC mobility measurements	48
2.9. Device Fabrication of OFET	48
2.10. Synopsis of synthetic procedures	49
2.10.1. Synthesis of 2-dodecylbenzotriazole.....	49
2.10.2. Synthesis of 4,7-dibromo-2-dodecylbenzotriazole	50
2.10.3. Synthesis of 2-(bromomethyl)nonadecane.....	51
2.10.4. Synthesis of 4,7-dibromo- 2 -(2-octyldodecyl)-2H-benzo[d][1,2,3] triazole 52	
2.10.5. Synthesis of 2-dodecyl-4,7-di(thieno[3,2-b]thiophen-2-yl)-2H- benzo[d][1,2,3]triazole	53
2.10.6. Synthesis of 2-dodecyl-4,7-di(furan-2-yl)- 2Hbenzo[d][1,2,3]triazole	54
2.10.7. Synthesis of 4-hexyl-4H-dithieno[3,2-b:2' ,3' -d]pyrrole	55
2.10.8. Synthesis of 4-hexyl-2,6-bis(tributylstannyl)-4H- dithieno[3,2-b:2' ,3' - d]pyrrole56	

2.10.9. Synthesis of poly[2-(2-dodecyl-2H-benzo[d][1,2,3]triazol-4-yl)-4-hexyl-4H-dithieno[3,2-b:2',3'-d]pyrrole] (PBTzDTP)	57
2.10.10. Synthesis of poly[2-(5-(2-dodecyl-7-(thiophen-2-yl)-2H-benzo[d][1,2,3]triazol-4-yl)thiophen-2-yl)-4-hexyl-4H-dithieno[3,2-b:2',3'-d]pyrrole] (PTBTzDTP).....	58
2.10.11. Synthesis of poly[2-(5-(2-dodecyl-7-(4-hexylthiophen-2-yl)-2H-benzo[d][1,2,3]triazol-4-yl)-3-hexylthiophen-2-yl)-4-hexyl-4H-dithieno[3,2-b:2',3'-d]pyrrole] (PHTBTzDTP).....	59
2.10.12. Synthesis of 2-(2-octyldodecyl)-4,7-bis(thieno[3,2-b]thiophen-2-yl)-2H-benzo[d][1,2,3]triazole	60
2.10.13. Synthesis of 4,7-di(furan-2-yl)-2-(2-octyldodecyl)-2H-benzo[d][1,2,3]triazole	61
2.10.14. Synthesis of 4,7-bis(5-bromothieno[3,2-b]thiophen-2-yl)-2-(2-octyldodecyl)-2H benzo[d][1,2,3]triazole.....	62
2.10.15. Synthesis of 4,7-bis(5-bromofuran-2-yl)-2-(2-octyldodecyl)-2H-benzo[d][1,2,3]triazole	63
2.10.16. Synthesis of PTTBTBDT	64
2.10.17. Synthesis of PFBTBDT	65
2.10.18. Synthesis of PIDTNDI and PIDSeNDI	66
RESULTS AND DISCUSSION	69
3.1. Furan and thieno[3,2-b]thiophene end capped benzotriazole derivatives.....	71
3.1.1. Synthesis of TTBT and FBT	72
3.1.2. Electropolymerization of TTBT and FBT	73
3.1.3. Spectroelectrochemistry	78
3.1.4. Kinetic Studies	81

3.1.5.	Comparison with other benzotriazole based conjugated polymers.....	84
3.2.	Dithienopyrrole and benzotriazole based conjugated polymers	87
3.2.1.	Synthetic Pathway	88
3.2.2.	Electronic Properties	90
3.2.3.	Optical Studies	91
3.2.4.	Spectroelectrochemical Studies	94
3.2.5.	Kinetic Studies	96
3.3.	Benzodithiophene and benzotriazole based conjugated polymers.....	100
3.3.1.	Synthetic Pathway	101
3.3.2.	Electronic Properties	104
3.3.3.	Optical Properties.....	106
3.3.4.	Spectroelectrochemistry.....	109
3.3.5.	Kinetic Studies	110
3.3.6.	Photovoltaic Properties	113
3.3.7.	Morphology.....	119
3.3.8.	SCLC Mobilities	120
3.4.	Indacenodithiophene/selenophene and Naphthalene Diimide n-Type Copolymers for Efficient All-Polymer Solar Cells.....	124
3.4.1.	Synthesis of PIDTNDI and PIDSeNDI.....	124
3.4.2.	Electronic properties of PIDTNDI and PIDSeNDI.....	125
3.4.3.	Optical Properties of PIDTNDI and PIDSeNDI	127
3.4.4.	OFET mobilities of PIDTNDI and PIDSeNDI	129
3.4.5.	Fabrication of BHJ OSCs.....	131

3.4.6. Morphology	135
3.4.7. SCLC Mobilities	136
3.4.8. Light intensity dependence of J_{sc} and V_{oc}	139
CONCLUSION	143
REFERENCES	147
APPENDICES	155
CURRICULUM VITAE	185

LIST OF TABLES

TABLES

Table 1 Summary of optical and electrochemical properties of benzotriazole based polymers.....	85
Table 2 Summary of colors and kinetic properties of benzotriazole based polymers ...	86
Table 3 Summary of optical and electrochemical properties of PDTPBTz, PDTPTBT and PDTPHTBT.....	93
Table 4 Optical contrast and switching times of the polymers.....	99
Table 5 Summary of optical and electrochemical properties of PFBTBDT and PTTBTBDT.....	108
Table 6 Summary of optical contrast and switching times of PFBTBDT and PTTBTBDT.....	113
Table 7 Photovoltaic performance of PFBTBDT with PC ₇₁ BM in different weight composition.....	115
Table 8 Summary of the performance of OSCs optimization studies.....	117
Table 9 Summary of SCLC mobilities of PFBTBDT:PC ₇₁ BM blends.....	123
Table 10 Molecular weight, optical and electrochemical properties.....	128
Table 11 Organic Field-Effect Transistor (OFET) mobilities of PIDTNDI and PIDSeNDI.....	130
Table 12 Photovoltaic characteristics of all polymer solar cells based on PIDTNDI and PIDSeNDI.....	134
Table 13 SCLC mobilities of PTB7:PIDSeNDI and PBDTTT-E-T:PIDSeNDI BHJ films.....	139

LIST OF FIGURES

FIGURES

Figure 1 A schematic representation of energy gaps in metal (a), insulator (b), and semiconductor (c).....	3
Figure 2 (a) Ground state energy as a function of coordinate for degenerate state (b) solitons in trans-polyacetylene	4
Figure 3 (a) Ground state energy as a function of coordinate for non-degenerate state (aromatic and quinoid form of benzene) (b) doping process of PPy	6
Figure 4 An overview of transition metal catalyzed polycondensation reaction	8
Figure 5 Electropolymerization mechanism of thiophene	10
Figure 6 Allowed transitions of neutral (a) polaron (b) and bipolaron (c) states with the chemical structures of thiophene trimer	12
Figure 7 Working principle of organic solar cell	15
Figure 8 Bilayer device configuration.....	18
Figure 9 Conventional and inverted device configuration	19
Figure 10 Current-voltage curve under illumination and in dark.....	20
Figure 11 Synopsis of factor affecting band gap.....	24
Figure 12 Orbital interaction of donor and acceptor moiety in DA approach	26
Figure 13 Chemical structures of basic donor units	28
Figure 14 Chemical structures of acceptor units.....	30
Figure 15 Overview of the structures and photovoltaic performance of benzotriazole based conjugated polymers	32
Figure 16 Overview of the structures and photovoltaic performance of NDI based conjugated polymers	35

Figure 17 Device configuration of OFETs A) bottom-gate/bottom-contact, B) bottom gate/top-contact, C) top gate /bottom contact, D) top gate/top contact	37
Figure 18 Typical OFET curves.....	38
Figure 19 Cyclic voltamagrom of ferrocene	43
Figure 20 Representative spectroelectrochemistry of an electrochromic conducting polymer	45
Figure 21 Representative kinetic studies of a conjugated polymer.....	46
Figure 22 Chemical structures of donor-acceptor type conjugated polymers developed in this study	70
Figure 23 Chemical structures and (i) donor groups, (ii) abbreviations of BTz bearing DAD type polymers	72
Figure 24 Synthetic routes of TTBT and FBT	73
Figure 25 Electropolymerization of FBT (A) and TTBT (B) in 0.1 M TBAPF ₆ /dichloromethane/acetonitrile solutions at a scan rate of 100 mV/s.....	74
Figure 26 Single scan cyclic voltammograms of PFBT (A) and PTTBT (B) in monomer free, 0.1 M TBAPF ₆ /acetonitrile solvent-electrolyte couple versus Ag wire pseudo reference electrode	76
Figure 27 Cyclic voltammograms of A) PFBT B) PTTBT in 0.1 M TBABF ₆ /ACN at scan rates of 50, 100, 150, 200, and 250 mV/s	77
Figure 28 UV-vis-NIR spectra of PFBT (A) between 0.5 and 1.3 V and PTTBT (B) between 0.5 and 1.4 V	80
Figure 29 Chemical structures and colors of PTTBT and PFBT	81
Figure 30 Percent transmittance changes of PFBT (A) and PTTBT (B)film in monomer free, 0.1 M TBAPF ₆ /acetonitrile solution at its maximum absorption wavelengths	83
Figure 31 Synthetic pathway for benzotriazole and dithienopyrrole based polymers ...	89
Figure 32 Cyclic voltammograms of the polymer films on ITO electrode in 0.1 M TBAPF ₆ , CH ₃ CN solution with a scan rate of 100 mV/s.....	91
Figure 33 Absorption spectra of PDTPTBTz, PDTPTBT, and PDTPTBT in dichloromethane and thin film	93

Figure 34 UV–Vis–NIR spectra of (A) PDTPBTz at potentials between 0.0 and 0.9 V (B) PDTPTBT at potentials between 0 and 0.9 V (C) PDTPHTBT at potentials between 0.0 and 1.6 V	95
Figure 35 Colors of PDTPBTz, PDTPTBT, and PDTPHTBT	96
Figure 36 Percent transmittance changes of PDTPBTz (A), PDTPTBT (B) and PDTPHTBT (C) film in monomer free, 0.1 M TBAPF ₆ /acetonitrile solution at its maximum absorption wavelengths.....	98
Figure 37 Synthetic pathways of PTTBTBDT and PFBTBDT	103
Figure 38 Cyclic voltammograms of the PTTBTBDT and PFBTBDT on ITO electrode in 0.1 M TBAPF ₆ , CH ₃ CN solution with a scan rate of 100 mV/s ((Fc/Fc ⁺ redox couple was used as internal standard).....	105
Figure 39 Cyclic voltammograms of A) PFBTBDT B) PTTBTBDT in 0.1 M TBAPF ₆ /ACN at scan rates of 50, 100, 150, 200, 250, and 300 mV/s.....	106
Figure 40 Absorption spectra of PFBTBDT and PTTBTBDT in chlorobenzene solution and in thin film	108
Figure 41 UV–Vis–NIR spectra of (A) PFBTBDT (B) PTTBTBDT.....	110
Figure 42 Percent transmittance changes of PFBTBDT (A), PTTBTBDT (B) film in monomer free, 0.1 M TBAPF ₆ /acetonitrile solution at its maximum absorption wavelengths.....	112
Figure 43 J-V characteristic of conventional device based on different ratio of PFBTBDT: PC ₇₁ BM	115
Figure 44 J-V characteristic of conventional device based on different ratio of PFBTBDT: PC ₇₁ BM	116
Figure 45 Absorption (A) and (B) incident to photon conversion efficiency (IPCE) spectra of PFBTBDT: PC ₇₁ BM (1:3).....	118
Figure 46 AFM and TEM images of PFBTBDT: PC ₇₁ BM (1:3) with (B) and without methanol treatment (A)	120
Figure 47 SCLC mobilities of PFBTBDT: PC ₇₁ BM.....	122

Figure 48 Synthetic pathways for PIDTNDI and PIDSeNDI	125
Figure 49 Cyclic voltammogram of PIDTNDI and PIDSeNDI on ITO electrode in a 0.1 M Bu ₄ NPF ₆ /ACN solution with a scan rate of 100 mV s ⁻¹	126
Figure 50 Absorption spectra of PIDSeNDI and PIDTNDI in chlorobenzene and thin film	128
Figure 51 Typical transfer curves of PIDTNDI and PIDSeNDI based electron only devices	130
Figure 52 Chemical structures of p-type materials and representative energy levels of p-type and n-type materials	131
Figure 53 Current density-voltage (J-V) characteristics of all-polymer BHJ solar cells with two different donors	133
Figure 54 External quantum efficiency (EQE) spectra of all-polymer BHJ OSCs of PIDSeNDI: PTB7, PIDSeNDI: PBDTT-E-T	135
Figure 55 AFM face and height images of PTB7: PIDSeNDI (A,C) and PBDTTT-E-T: PIDSeNDI (B,D)	136
Figure 56 J-V characteristics under dark for hole-only and electron-only devices consisting of PTB7: PIDSeNDI and PBDTTT-E-T: PIDSeNDI BHJ films. The bias (V) is corrected for built-in voltage, V _{Bi} , arising from different in the work function of the contacts, and the voltage drop due to substrate series resistance (V _{RS}), such that V=V _{APPL} -V _{RS} -V _{Bi} . (V _{APPL} is the applied voltage). The solid lines represent the fitting curves.	138
Figure 57 Light intensity dependence of J _{SC} in BHJ (1: 1) with inverted configuration	140
Figure 58 Light intensity dependence of V _{OC} in BHJ (1:1) with inverted configuration	142
Figure 59 ¹ H NMR of 2-(dodecyl)-4,7-bis(thieno[3,2-b]thiophen-2-yl)-2H-benzo[d][1,2,3]triazole	155
Figure 60 ¹³ C NMR of 2-(dodecyl)-4,7-bis(thieno[3,2-b]thiophen-2-yl)-2H-benzo[d][1,2,3]triazole	156

Figure 61 ¹ H NMR of 2-Dodecyl-4,7-di(furan-2-yl)- 2Hbenzo[d][1,2,3]triazole	157
Figure 62 ¹³ C NMR of 2-Dodecyl-4,7-di(furan-2-yl)- 2Hbenzo[d][1,2,3]triazole	158
Figure 63 HRMS of 2-(dodecyl)-4,7-bis(thieno[3,2-b]thiophen-2-yl)-2H- benzo[d][1,2,3]triazole	159
Figure 64 HRMS of 2-(dodecyl)-4,7-bis(thieno[3,2-b]thiophen-2-yl)-2H- benzo[d][1,2,3]triazole	160
Figure 65 ¹ H NMR of 4-hexyl-4H-dithieno[3,2-b:2' ,3' -d]pyrrole	161
Figure 66 ¹³ C NMR of 4-hexyl-4H-dithieno[3,2-b:2' ,3' -d]pyrrole	162
Figure 67 ¹ H NMR of 4-hexyl-2,6-bis(tributylstannyl)-4H- dithieno[3,2-b:2' ,3' - d]pyrrole	163
Figure 68 ¹³ C NMR of 4-hexyl-2,6-bis(tributylstannyl)-4H- dithieno[3,2-b:2' ,3' - d]pyrrole	164
Figure 69 ¹ H NMR of PDTPBTz	165
Figure 70 ¹ H NMR of PDTPTBT	166
Figure 71 ¹ H NMR of PDTPHTBT	167
Figure 72 ¹ H NMR of 2-(Bromomethyl)nonadecane	168
Figure 73 ¹³ C NMR of 2-(Bromomethyl)nonadecane	169
Figure 74 ¹ H NMR of 4,7-Dibromo-2-(2-octyldodecyl)-2H-benzo[d][1,2,3] triazole	170
Figure 75 ¹³ C NMR of 4,7-Dibromo-2-(2-octyldodecyl)-2H-benzo[d][1,2,3] triazole	171
Figure 76 ¹ H NMR of 4,7-di(furan-2-yl)-2-(2-octyldodecyl)-2H-benzo[d][1,2,3]triazole	172
Figure 77 ¹³ C NMR of 4,7-di(furan-2-yl)-2-(2-octyldodecyl)-2H-benzo[d][1,2,3]triazole	173
Figure 78 ¹ H NMR of 4,7-bis(5-bromofuran-2-yl)-2-(2-octyldodecyl)-2H- benzo[d][1,2,3]triazole	174
Figure 79 ¹ H NMR of 2-(2-octyldodecyl)-4,7-bis(thieno[3,2-b]thiophen-2-yl)-2H- benzo[d][1,2,3]triazole	175

Figure 80 ^{13}C NMR of 2-(2-octyldodecyl)-4,7-bis(thieno[3,2-b]thiophen-2-yl)-2H-benzo[d][1,2,3]triazole	176
Figure 81 ^1H NMR of 4,7-bis(5-bromothieno[3,2-b]thiophen-2-yl)-2-(2-octyldodecyl)-2H benzo[d][1,2,3]triazole	177
Figure 82 ^{13}C NMR of 4,7-bis(5-bromothieno[3,2-b]thiophen-2-yl)-2-(2-octyldodecyl)-2H benzo[d][1,2,3]triazole	178
Figure 83 ^1H NMR of PFBTBDT	179
Figure 84 TGA of PTTBTBDT	180
Figure 85 TGA of PFBTBDT	181
Figure 86 ^1H NMR of PIDTNDI	183
Figure 87 ^1H NMR of PIDSeNDI	183

LIST OF ABBREVIATIONS

CP	Conducting polymers
PA	Polyacetylene
PPy	Polypyrrole
HOMO	Highest occupied molecular orbital
LUMO	Lowest unoccupied molecular orbital
D	Donor
A	Acceptor
OSC	Organic solar cell
OFET	Organic field effect transistor
BHJ	Bulk heterojunction
SCLC	Space charge limiting current
ITO	Indium tin oxide
PEDOT	Poly (3,4-ethylenedioxythiophene)
PSS	Polystyrene sulfonate
SRH	stockley-read hall

V_{oc}	Open circuit voltage
J_{sc}	Short circuit current
FF	Fill factor
PCE	Power conversion efficiency
AM	Air mass
IPCE	Incident photon to current efficiency
EQE	External quantum efficiency
E_g	Bandgap
BLA	Bond length alternation
PITN	poly-isothinaphthene
BTz	Benzotriazole
PC₆₀BM	[6,6]-phenyl C ₆₁ butyric acid methyl ester
PC₇₀BM	[6,6]-phenyl C ₇₁ butyric acid methyl ester
TBAF₆	Tetrabutylammoniumhexafluorophosphate
NDI	Naphthalene diimide
IDT	Indacenodithiophene
IDSe	Indacenodiselenophene
TLC	Thin layer chromatography
TMS	trimethylsilane

NMR	Nuclear magnetic resonance
HRMS	High resolution mass spectroscopy
CV	Cyclic voltammetry
GPC	Gel permeation chromatography
AFM	Atomic force microscopy
TEM	Transmission electron microscopy
TGA	Termogravimetric analysis
DSC	Differential scanning calorimetry
PTFE	Polytetrafluoroethylene
DTP	Dithienopyrrole
BDT	Benzodithiophene

CHAPTER 1

INTRODUCTION

1.1. History of conducting polymers

Development of conducting polymers (CP) was started with the study of Letheby and coworkers in 1862. They synthesized blue-black shiny powder by anodic oxidation of aniline in the presence of dilute sulphuric acid [1]. However, breakthrough of in the area of CP was achieved with the most studied polymer, namely polyacetylene (PA). PA is the simplest conjugated polymer with $-\text{CH}=\text{CH}-$ repeating unit. It was first synthesized by Natta et. al at 1955. However, PA didn't take enough attention up to 1977 due to its irrespective preparation method, air sensitivity, and infusibility [2]. In 1977, the interest on PA increased with the study conducted by Heeger, MacDiarmid, and Shirakawa. Shirakawa and coworker synthesized PA as a bright, glistening silvery film instead of black powder due to addition of a thousand times more catalyst into reaction medium. After this finding, Shirakawa, Heeger, and MacDiarmid studied the properties of this silvery film and they decided to expose polymer to bromine vapor. Conductivity of polymer films was measured by four-probe method and found that it increased by 10 million times in a few minutes. They also discovered the importance of dopant concentration. It was found that PA could be transferred from insulator to a semiconductor or fully metal depending on dopant concentration [3].

Intrinsic optical and electrochemical properties such as redox behavior (p- and n-dupability) and color change during doping process triggered the usage of PA in “plastic

electronics". Heeger, MacDiarmid, and Shirakawa were awarded with the Nobel Prize in Chemistry in 2000 for "*the discovery and development of electrically conducting polymers*" [4].

Although, PA showed fascinating properties, its instability, and insolubility prevented its use in different applications [5]. After this discovery different conjugated polymer such as polyfuran, polypyrrole, polythiophene and polyaniline, and their derivatives, were synthesized to circumvent these problems. These polymers mostly showed similar properties with high stability and processability [6].

1.2. Band gap

The electrical properties of semiconductors depend on their discrete energy states that are generated from bonding and antibonding molecular orbitals. The band gap is determined by the energy difference between valance (the highest occupied band) and conduction band (lowest unoccupied band). They can be wide, narrow or zero depending on the nature of materials. **Figure 1** depicts the representative energy gap of metal, insulator and semiconductor.

Band gap of metals are zero and they can conduct electricity because of partially filled energy bands. Differently, valence band is fully occupied and conduction band is fully empty for insulators and semiconductors. Most of the conventional polymers have been counted as insulator since the difference between valance and conduction band is wide. In contrast, band gap of semiconductors is narrow and conjugated polymers are counted as semiconductors since band structure of them are changed by removal or adding of electron and they become conductive [7].

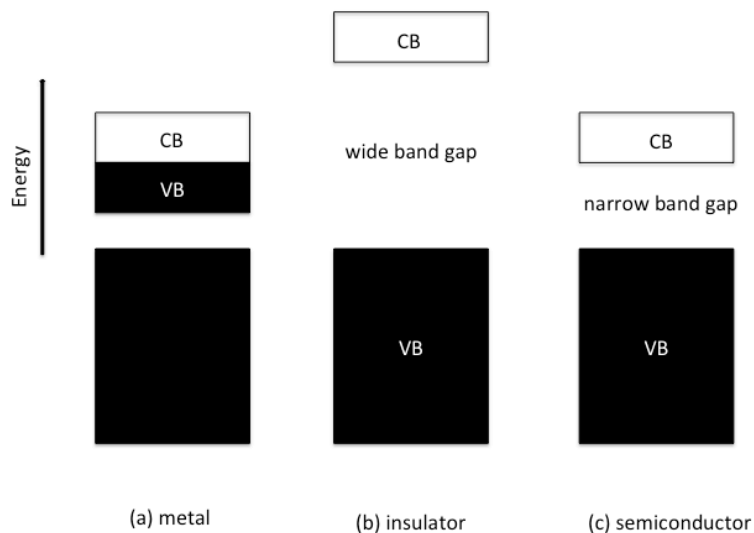


Figure 1 A schematic representation of energy gaps in metal (a), insulator (b), and semiconductor (c)

1.3. Charge transport in conjugated polymers

Conjugated polymers do not possess intrinsic charge carriers in their neutral state hence oxidation and reduction process is needed for the formation of charge carriers. Therefore, they are exposed to reducing and oxidizing agents. This process is known as doping that converts insulating neutral conjugated polymer into an ionic complex consisting of charge carriers. Conducting polymers can easily be oxidized or reduced due to their small ionization potentials or large electron affinities [8]. Therefore, π -electrons can be easily removed or added to form a polymeric ion without disruption of the sigma bonds. Charge carriers like polarons, bipolarons, solitons, free carriers etc. are generated after the doping process. These terms are named according to the degeneracy state of conducting polymers in their ground states [9].

Formation of solitons takes place for the system having degenerate ground state with isoenergetic regions. PA is one of the popular examples for this situation (**Figure 2 (a)**). Solitons can be neutral, positive, and negative as depicted in **Figure 2 (b)**. For a neutral chain, defect occurs at the interface and neutral soliton or uncharged soliton with $\frac{1}{2}$ spin forms [10]. When one electron removed or added to the neutral state, negative or positive soliton with no spin can form. Further removal or addition of electron resulted in the formation of dication that can be freely moved along the polymer chain.

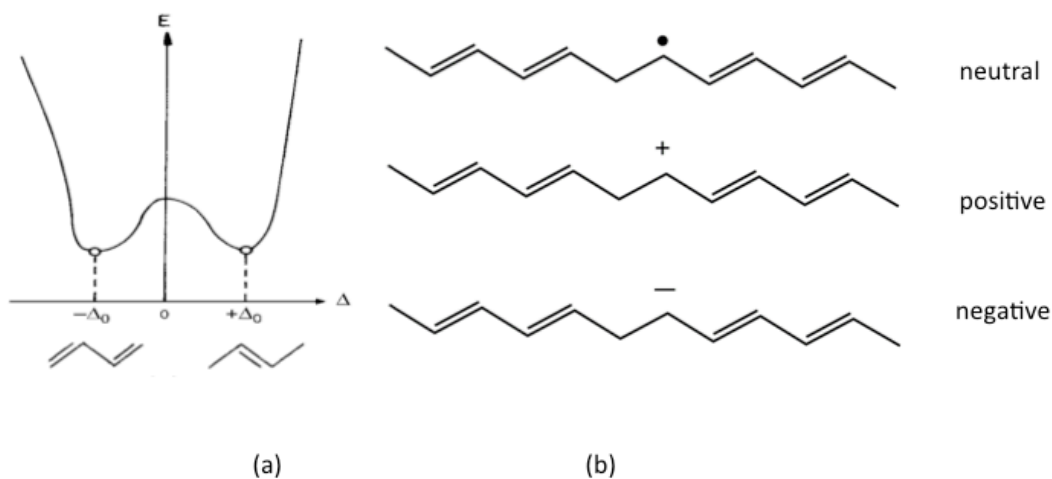


Figure 2 (a) Ground state energy as a function of coordinate for degenerate state (b) solitons in trans-polyacetylene

Different from the PA system, most of the conjugated system has non-degenerate ground states known as aromatic and quinoid forms (**Figure 3(a)**). Therefore, defect or distortion created in the polymer chain resulted in the formation of polaron [11]. When electron is removed from polymer, distortion in the ground state geometry takes place, as shown in **Figure 3(b)** on the structure polypyrrole (PPy). Depending on the addition or removal of electron polaron can be radicalic anion or cation with a spin of $1/2$.

Formation of polaron resulted in the creation of new localized electronic states in the band gap. This causes an upward and downward shift of the highest occupied molecular orbital (HOMO) and a lowest unoccupied molecular orbital (LUMO) respectively. In the case of PPy, this shift is about 0.5 eV from the band edges [12].

Further oxidation of polymer chain causes the removal of electron from either the polaron or the polymer chain. Removal of electron from polaron causes the formation of two positive charge resulted in the formation of bipolaron. Formation of bipolaron is thermodynamically more favorable due to decrease in ionization potential. This finding was supported by theoretical calculation and found that bipolaron energy is 0.4 eV lower than polaron energy [8]. In the case of PPy, bipolaron states are about 0.75 eV away from the band edges. If doping process continue, more bipolaron can be created that can merge to form continuous bipolaron states. Then, metal-like conductivity causes due to combination of CB and VB.

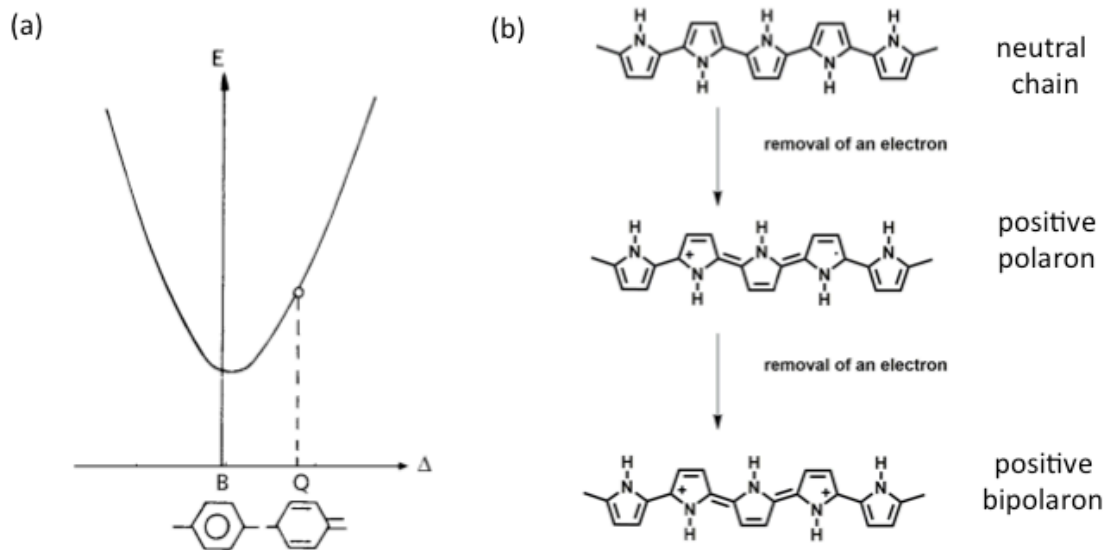
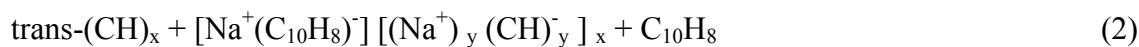


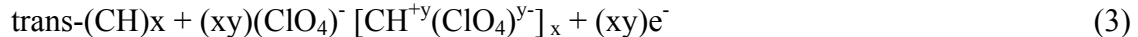
Figure 3 (a) Ground state energy as a function of coordinate for non-degenerate state (aromatic and quinoid form of benzene) (b) doping process of PPy

1.4. Doping process in conjugated polymers

Doping of conjugated polymers can be achieved by chemical and electrochemical process. Chemical doping is achieved by electron acceptors and donor. For example, oxidation of trans-polyacetylene is achieved with iodine (equation 1). Similarly, reduction of it is achieved with electron donor that is $(\text{Na}^+)(\text{C}_{10}\text{H}_8)^-$ in equation 2 [7].



Electrochemical doping can be done by applying potential between a positive electrode that is coated with polymer (i.e, trans-polyacetylene) and a negative electrode. LiClO_4 in polypropylene carbonate is utilized as supporting electrode. Doping of polymers is achieved with following equation (3) [7].



Electrochemical doping has several advantages over chemical doping. Firstly, doping level can be controlled by controlling current passage. Secondly doping-dedoping is highly reversible and there is no need to remove side products. Finally, p and n doping of conjugated polymers can be done with dopant species that cannot be used in chemical doping. However both methods has a disadvantage in terms of dopant ion since they have counter ions to stabilize the charges on conducting polymer that can cause structural deformation affecting conductivity [7].

1.5. Synthesis of conjugated polymers

1.5.1. Chemical synthesis of conjugated polymers

Transition-metal-catalyzed polycondensation reaction is commonly utilized for the synthesis of conjugated polymers. General mechanism of coupling reaction is summarized in **Figure 4**. Suzuki and Stille coupling reactions are preliminary used coupling reaction to develop DA conjugated polymers. Several factors including reactivity of monomers, solvent, end group and the stoichiometry of monomers affect the molecular weight of resulting polymers so they should be optimized [13].

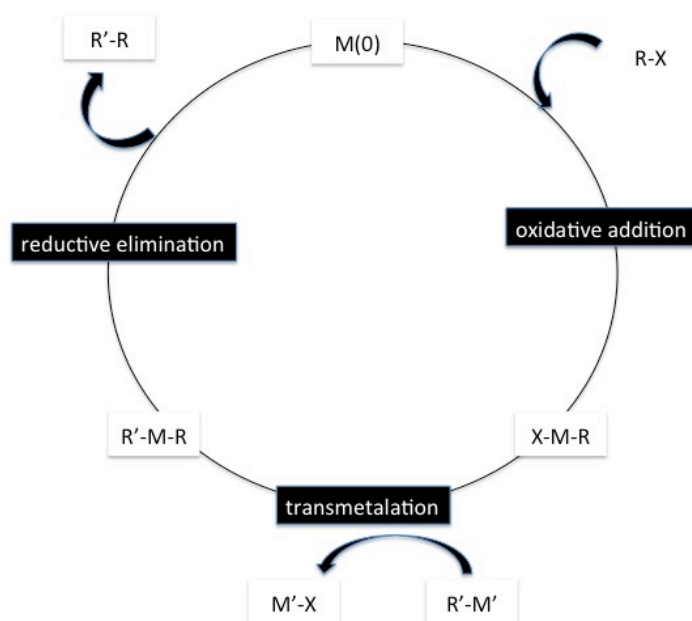


Figure 4 An overview of transition metal catalyzed polycondensation reaction

1.5.1.1. Suzuki reaction

Suzuki and coworkers discovered Suzuki coupling reaction in 1979 [14]. They showed the coupling of boronic acid of one alkenyl and the halogen of the other alkenyl. Mechanism of Suzuki cross coupling reaction starts with the synthesis of aryl halide with $Pd(0)$ catalyst by oxidative addition. Organometallic compound acts as the source of the organic group by transmetalation. $Pd(II)$ intermediate forms and undergoes reductive elimination [15].

Base is one of the necessities of Suzuki coupling and it enhances the reactivity of boronate anion [15]. Suzuki cross coupling reaction shows high tolerance to a wide range of functional groups. Side products and reagents are not toxic compared to Stille

coupling. However, purification of monomers containing boronic acid is difficult that affects the molecular weight of polymers. Generally, Suzuki reaction is preferred for benzene-based compounds such as the preparation of fluorene and carbazole based conjugated polymers [13].

1.5.1.2. Stille coupling

Stille and coworkers [16] and Migita and coworker [17] discovered this coupling reaction almost at the same time in the late 1970s. Aryl and alkenyl stannanes used as an organometallic compound. The basic mechanism of Stille coupling involves oxidative addition of Pd from the aryl halide, transmetallation, and reductive elimination.

Stille coupling is suitable for polymerization of electron-rich compound (i.e, thiophene, furan, selenophene etc.). The Stille reaction requires milder reaction conditions, lower oxygen sensitivity and shows high tolerance over most functional groups. Stannylated monomers and its side products are toxic that is the major drawbacks of this coupling reaction [13].

1.5.2. Electrochemical synthesis of conjugated polymers

Electropolymerization is performed by dissolving a monomer in a solvent/ electrolyte couple. Hence, the choice of solvent and electrolyte is crucial since both of them should be stable at the oxidation potential of the monomer. Besides, they should provide a conductive medium. Acetonitrile or propylene carbonate generally used as the solvents due to their very large potential window and high relative permittivity. Cyclic voltammetry is utilized for electropolymerization and characterization of the polymer films. It is suitable for studying the reversibility of electron transfer because the

oxidation and reduction can be monitored in the form of a current–potential diagram [18].

An electrogenerated cation radicals form as a reactive species at electropolymerization in the first step. Then these cations couple with each other to form dimers. Polymer films forms a sequence of radical coupling and electrochemical reoxidation [19]. These reactions are followed general E(CCE)n mechanism as depicted in **Figure 5**.

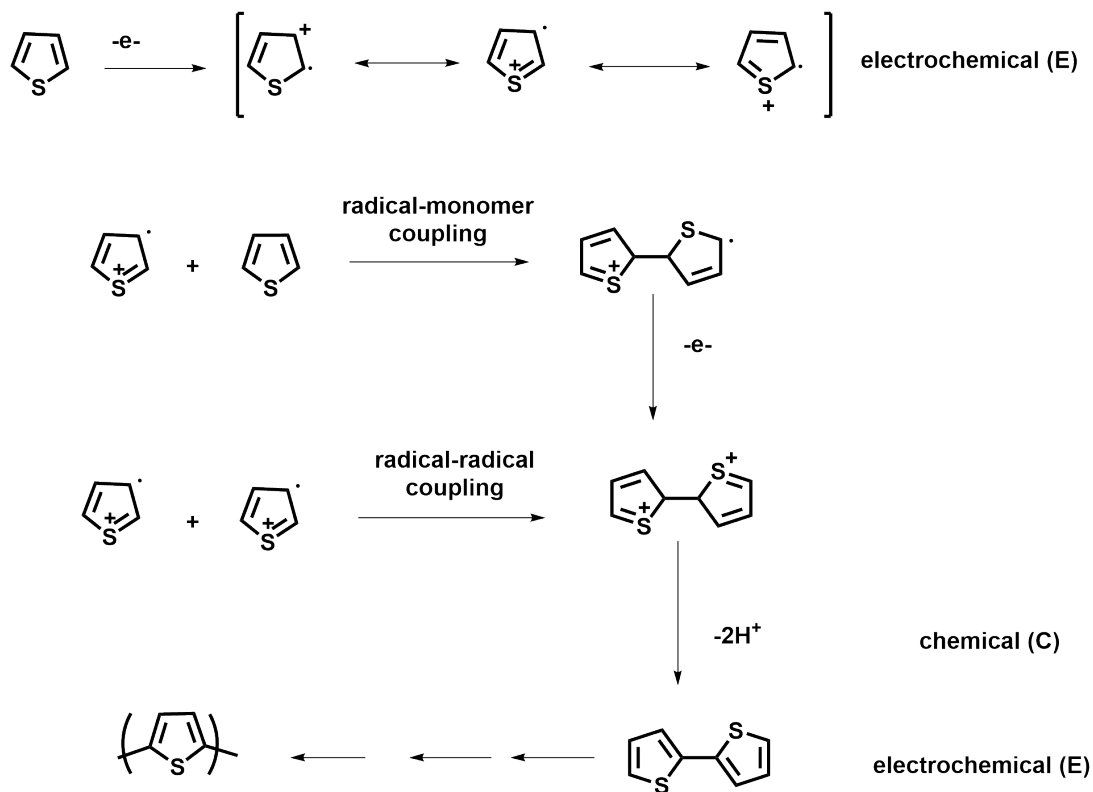


Figure 5 Electropolymerization mechanism of thiophene

1.6. Electrochromism

Chromism is defined as color change as a result of applied physical or chemical stimuli. Chromism is classified according to these stimuli, i.e thermochromism (color change by heat), photochromism (color change by UV light), solvatochromism (color change by solvent), ionochromism (color change by ions) and electrochromism [20]. Change in electromagnetic radiation in terms of absorption, reflection or transmission is observed for electrochromic materials during electrochemical oxidation and reduction reaction. Electrochromism is defined as the reversible color change upon applied potential. Color change is generally observed between a colored and a transmissive state, but sometimes more than one-colored states can be seen for polyelectrochromic (multichromic) materials [11].

The most of the electrochromic materials were inorganic such as transition metal oxides (tungsten oxide, WO_3), viologens and Prussian Blue [20,21]. However, after the discovery of conductivity in polyacetylene upon doping, conjugated polymers have aroused great attention and they were used another class of electrochromic materials due to their fascinating advantages over inorganic counterparts. Fast switching times, high optical contrast, processability, and tunability of optical and electrochemical properties through structural modifications are some advantages of conjugated polymers. Structural modification is the key point for most of the electrochromic properties such as processability and attainability of different color [11].

1.6.1. Electrochromism in conjugated polymers

Optical properties of conjugated polymers are determined by band gap (E_g). Charge injection onto polymer backbone that is responsible from change in optical properties

and electrochromism. Introduction of new intra-band states cause the formation of new optical transitions at lower energies. Electronic transition occurs between HOMO and LUMO when minimum energy applied that is equal or greater than band gap. Upon oxidation (p-doping), electrons are removed from HOMO and single charged species with spin $\frac{1}{2}$ form that is known as polaron (radicalic cation). Thus resulting change from aromatic to quinoid structure and an upward and downward shift of HOMO and LUMO, respectively. Further removal of electron from conjugated polymers causes the formation of bipolaron that is spinless. Two energy levels are formed in the band gap that is occupied by electrons or holes and transition from HOMO is only possible due to unoccupied bipolaron levels. Thus cause the further shift in absorption to low energy [11]. Allowed transition of neutral, polaron and bipolaron states were depicted in **Figure 6**.

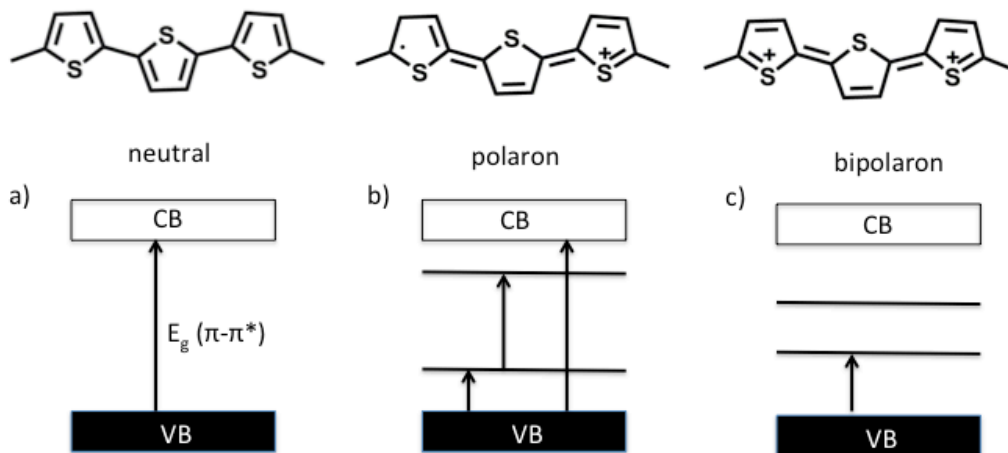


Figure 6 Allowed transitions of neutral (a) polaron (b) and bipolaron (c) states with the chemical structures of thiophene trimer

1.7. Organic solar cell

Photovoltaics convert light into electrical energy. They are aimed to utilize in power supply for off-grid professional devices, supply system and electricity generation. They are classified as an important class of sustainable energy sources as an alternative to fossil fuels since there is no harmful emission, transformation of matter, production of noise, and other by-products. Currently, silicon solar cells cover most part of the market of photovoltaics. However, silicon cell technology is not cheap. Therefore, organic solar cells are developed as an alternative to inorganic solar cells. Solution-processable organic solar cells (OSCs) have aroused great attention due to their diverse advantages such as low cost, light weight, ease of fabrication by large-scale, and roll- to-roll printing techniques, feasibility of flexible devices and tunability of physiochemical properties. However, organic solar cells suffer from long-term stability and low performance. Inorganic and organic solar cell have some distinctions in terms of mobility, absorption profile, creation of free charges or excitons [22,23].

1.7.1. Working principle of solar cell

In the first step, photon is absorbed by photoactive material and an electron is excited from the HOMO to the LUMO energy level of conjugated polymers. After absorption of light, strong Coulombic attraction exists between electron and hole pair as a result of low dielectric constant and localized electron and hole wavefunctions. This bound electron-hole pair is known as exciton. The exciton binding energy is in the range of 0.1-1.4 eV that is much higher than room temperature energy kT .

Exciton can travel to a certain distance before recombination process and the average distance is known as *exciton diffusion length*. This distance is generally in the range of

5-70 nm. When exciton diffuses to the donor-acceptor interface that is heterojunction created with two different organic materials with correctly aligned band levels (donor and acceptor), *photoinduced charge transfer* takes place from LUMO level of the donor to LUMO level of the acceptor. This process can take place when the difference between the HOMO energy level of donor material and the LUMO energy level of acceptor material is equal to exciton binding energy. This charge transfer is competitive with luminescence process (time scale 1ns) but it is more favorable and fast since the time scale of charge transfer is in the range of 45 fs in polymer-fullerene system. As a result of photoinduced charge transfer, geminate pairs; electrons on acceptor and holes on donor are generated. Then, they are transported for charge separation.

Drift and diffusion currents are the main driving forces for charge transportation. Drift current is generated as a result of potential gradient within the solar cell. Potential gradient is necessary to overcome columbic attraction of geminate pairs for fully charge dissociation and to circumvent monomolecular recombination. Potential is generated as a result of the built-in potential due to the work function difference between the electrodes. High work function anode and low work function cathode creates this field. Drift current changes as a result of applied external bias and it is dominated when internal field is large. Another charge transport mechanism is diffusion current that is the result of concentration gradient within the solar cell. The concentration of holes and electrons are high near the heterojunction. Then, they diffuse from heterojunction and cause diffusion current. The diffusion current is dominated when internal field is near to zero.

Charge carrier mobilities of the active layer are limiting factors for charge transport since electron and hole mobilities of active layer are relatively low compared to that of inorganic semiconductors. The large imbalance between electron and hole mobilities resulted in space charge limiting currents (SCLC). Therefore, balance between hole and electron mobilities is highly desired for the efficient solar cells.

After creation of free charges, they are transported to the appropriate electrodes for charge extraction. Holes are transported through the polymer to the anode and electrons are transported through the fullerene to the cathode. Alignment of work function of cathode and anode is crucial for efficient charge transport. HOMO energy level of conjugated polymers should match with work function of anode while LUMO energy level of it should match with work function of cathode to create ohmic contact. Therefore, different kinds of anode and cathode are utilized for efficient charge extraction that is dependent on the fabrication of solar cell [24-30].

In summary, working principle of solar cell involves following 3 critical steps (**Figure 7**);

- Photon absorption by active layer and exciton formation
- Photoinduced charge transfer (exciton dissociation) and mobile carriers generation at donor-acceptor interface
- Charge carrier diffusion to respective electrodes and collection of charges

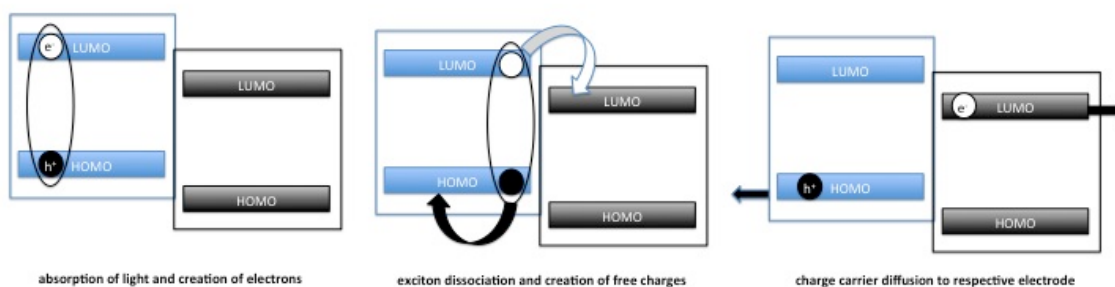


Figure 7 Working principle of organic solar cell

As described above, light-induced charge generation in OSC is observed in a multistep process. However, depending on the dominated recombination process, generated

charges can be lost [31]. Therefore, recombination is the main limiting factor that affects efficiency of OSCs. Monomolecular and bimolecular recombinations are the main types of recombination observed in OSCs that occur at the interface where they dissociate. Monomolecular recombination takes place before creation of free charges and bimolecular recombination takes place afterwards [32].

Monomolecular recombination is defined as any first order recombination, which occurs by recombination of electron and hole that generated from the same exciton. It is known as either Shockley-Read-Hall recombination (SRH) or geminate recombination. Electron and hole recombination take place through a trap site or recombination center is known as SRH recombination. Any impurities in polymer and fullerene and inappropriate phase separation act as a trap site and contribute to a trap-assisted recombination. In addition to SRH recombination, charge-carrier-concentration gradients can cause first-order recombination due to a large imbalance between holes and electrons. This imbalance will result in recombination of excess electrons with holes via first-order process [33]

Bimolecular recombination is referred as second-order recombination. It occurs by the recombination free electrons and holes that do not generate from the same exciton. This kind of recombination is known either Langevin or non-geminate recombination and is observed at the interface rather than the bulk of the material. It is the dominant loss mechanism in OSCs since the charge-carrier mobilities of conjugated polymers are low. Therefore, after creation of free charges (electrons on fullerene and holes on conjugated polymers), they encountered each other and recombine before reaching their respective electrodes [34].

1.7.2. Solar cell architectures

1.7.2.1. Bilayer Heterojunction Device

The first generation of organic photovoltaic solar cells was developed by bilayer heterojunction device architecture (**Figure 8**). Fabrication of bilayer heterojunction device is performed with the configuration of anode/hole transport layer/active layer/electron transport layer/cathode. The hole and electron transport layer are used to modify the work function of the electrodes to create an ohmic contact. First example of bilayer device configuration was implemented by Tang et al. and they constructed photovoltaic cell with a phthalocyanine derivative (p-type) and a perylene derivative (n-type). Power conversion efficiency was about 1% [35].

The main drawback of this configuration is the short exciton diffusion length. Thus, it limits thickness of active layer (100 nm). However, this thickness is more than exciton diffusion length (10-20 nm). Excitons are only generated in the small area between the donor and acceptor interface. Therefore, recombination of excitons is observed after the generation of exciton. Only the excitons generated within the exciton diffusion length can reach the interface and contribute to efficiency of solar cell [29].

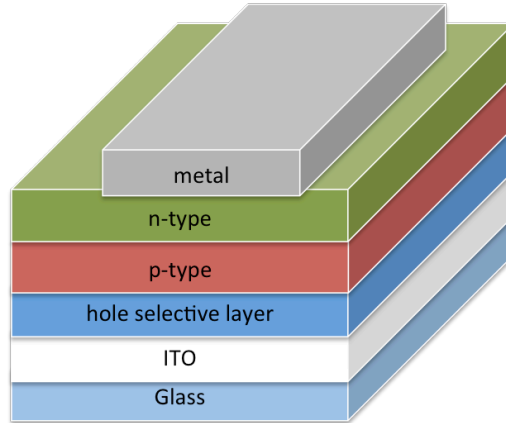


Figure 8 Bilayer device configuration

1.7.2.2. The bulk-heterojunction organic solar cell

Yu et al. first introduced bulk heterojunction (BHJ) concept by blending donor and acceptor material together to achieve an interpenetrating network with a large D-A interfacial area. They also take into account of exciton diffusion length and required thickness for light absorption to overcome the problems faced within bilayer device configuration [36]. In this way, interpenetrated network was formed to separate exciton into free charges via ultrafast charge transfer that cause enhanced quantum efficiency. These interpenetrated networks create suitable channels for transportation of holes and electrons. However, the major breakthrough and rapid development of BHJ solar cells arose from the discovery of efficient photoinduced electron transfer in conjugated polymer-fullerene composites [37]. After this discovery, buckminsterfullerene (C₆₀) derivative became solution processable by structural modification and utilized for n-type material for device fabrication.

1.7.3. Fabrication of bulk heterojunction organic solar cell

Fabrication of BHJ OSCs can be achieved with two types of device configuration. **Figure 9** shows conventional and inverted device configuration. In the conventional BHJ OSC approach, ITO/hole transport layer/ active layer/ metal configuration is utilized. PEDOT:PSS is often used as a hole transport layer to planarize ITO electrode surface and increase its work function for effective hole collection and active layer is sandwiched between anode (ITO) and low work function metal (Ca/Al and LiF/Al). However, stability was the main problem in this design since low work function metals (Ca and Al) are vulnerable to oxidation. This decreases device life times under ambient conditions. Therefore, inverted BHJ OSC configuration was developed to overcome this problem. In this configuration, the polarity of the electrode is reversed compared to that of the conventional structure. ITO/ electron transport layer/ active layer/ hole transport layer/ metal configuration is developed. ZnO or TiO_x used as an electron transport layer between ITO and active layer to collect electrons selectively whereas MoO_x are inserted as electron and hole transporting layer between active layer and metal to collect holes selectively. Metals with high work function such as Ag were utilized [38].

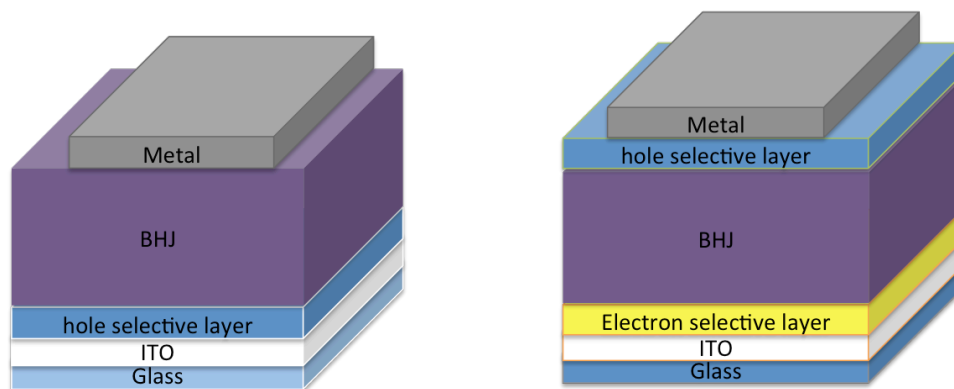


Figure 9 Conventional and inverted device configuration

1.7.4. Characterization of organic solar cells

OSCs are typically characterized under the illumination of AM 1.5 G solar spectrum. The power conversion efficiency (PCE) of organic solar cell is dictated by three parameters namely open circuit voltage (V_{OC}), short circuit current (J_{SC}) and fill factor (FF) and these are shown in **Figure 10**. PCE can be calculated by equation 4

$$\eta = \frac{J_{sc} V_{oc} FF}{P_{in}} \quad (4)$$

where P_{in} is light power incident on the device, V_{OC} is open circuit voltage, J_{SC} is short circuit current and FF is fill factor.

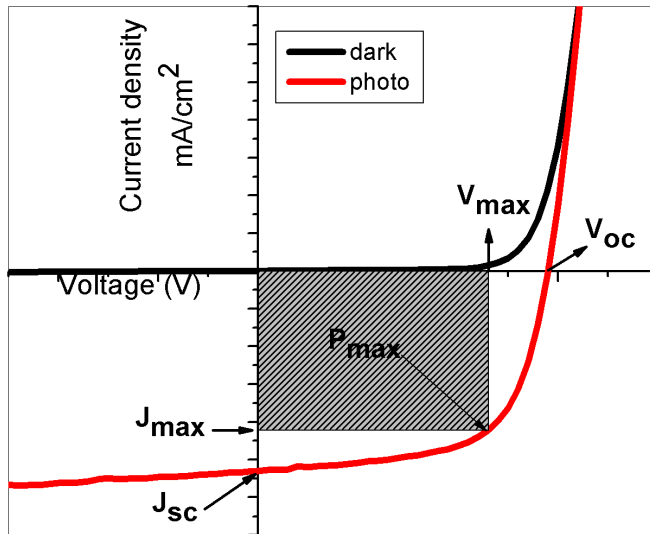


Figure 10 Current-voltage curve under illumination and in dark

1.7.4.1. Open circuit voltage

The open circuit voltage (V_{OC}) is defined as the maximum voltage delivered by the solar cell when the current is zero [35]. Several studies were conducted to understand the factor affecting V_{OC} . One of the famous studies was conducted by Brabec et al. [36,37]. They studied the effect of different metals with work function that varied from 2.87 eV (Ca) and 4.28 eV (Au). They fabricated solar cells using poly(2-methoxy-5-(3', 7'-dimethyloctyloxy)-1,4-phenylenevinylene) (MDMO-PPV) as the donor and fullerene derivatives as the acceptor. They found that V_{OC} is determined by the LUMO energy level of the acceptor rather than work function of cathode. Similarly, Scharber et al. studied the effect of different donor units with different HOMO energy level and found that V_{OC} is also affected by HOMO energy level of the donor unit and they have proposed the equation 5 to define V_{OC} [39,40].

$$V_{OC} = \frac{1}{q} \cdot (|E_{HOMO,D}| - |E_{LUMO,A}|) - 0.3V \quad (5)$$

q: elementary charge,

$E_{HOMO,D}$: HOMO level energy of the donor

$E_{LUMO,A}$: LUMO level energy of the acceptor

1.7.4.2. Short-circuit current

The short circuit current (J_{SC}) is defined as the current that flows when $V_{OC}=0$. J_{SC} is strongly affected by the number of absorbed photons, efficiency of charge separation, and mobility of charge carriers [32].

1.7.4.3. Fill Factor

It is defined as the ratio of maximum power to the incident power in the device and formulated as equation 6 and showed in **Figure 10**.

$$FF = \frac{J_{max}V_{max}}{J_{sc}V_{oc}} \quad (6)$$

Fill factor is determined by series (R_s) and shunt resistance (R_{sh}). R_s affects the applied voltage. If it is large, less voltage drop on the diode and resulted in slower increase of J with V . R_{sh} cause the division on current and if it is amount is less, less current is observed since current flows on R_{sh} . Therefore, linear increase with increasing voltage is observed. Both situations affect the squareness of curve. In addition to these resistances, fill factor is affected by carrier recombination and carrier lifetime. These two parameters affects extractable current from the device since enhancement in charge mobility can increase the charge transport near short-circuit conditions. Besides, carrier lifetimes affect charge extraction near V_{OC} condition due to creation of free charges [32,41,42].

1.7.5. Donor materials in OSCs fabrication

Polymers, small molecules, and oligomeric units with suitable physicochemical properties can be utilized as donor materials for fabrication of BHJ OSCs. Highly efficient donor molecules should have following properties:

1. Broad and strong absorption band in visible and near- infrared region to harvest sun light efficiently to increase J_{SC}
2. Suitable alignment of HOMO and LUMO for efficient charge separation and higher V_{OC}
3. High charge carrier mobility to overcome recombination process and facilitate the charge transport efficiency for high FF and J_{SC}
4. High processability for solution processing in fabrication OSCs
5. Suitable morphology, and nanoscale phase separation for effective charge separation and extraction

All these requirements are interconnected with each other; therefore careful molecular design is necessity of development of efficient donor molecules. Almost all properties of conjugated polymers are related to band gap and several strategies were developed to control it [27].

1.7.6. Band gap engineering

Band gap (E_g) is defined as the energy difference between HOMO and LUMO energy level. Optical and electrochemical properties of the conjugated polymers strongly affected from this value. Therefore, most of the studies have been dedicated to develop strategies to modulate band gap and these studies showed that band gap of the conjugated polymer is determined by five parameters, i.e, bond length alternation (E^{dr}),

interannular rotations ($E^{\delta r}$), aromatic resonance energy (E^{res}), substitution effect (E^{sub}), and intermolecular interaction (E^{int}) and these parameters have been summarized on **Figure 11** [11,43].

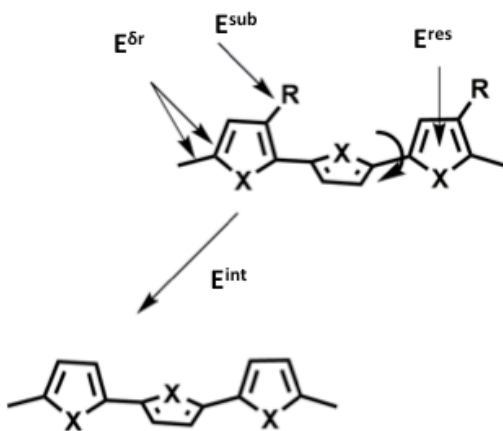


Figure 11 Synopsis of factor affecting band gap

Polyaromatic systems contain alternating double and single bonds. Delocalization of π -electrons cause the conversion of double bond into single bond and single bond into double bond. Therefore, polyaromatic-conjugated system contains two nondegenerate energy states known as aromatic and quinoid forms [44]. Aromatic form is energetically more stable whereas quinoid form is less stable. Although, quinoid form is less energetic owing to destruction of aromatic stabilization energy to adopt this form, it has smaller band gap compared to aromatic form [45]. Therefore, if quinoid form of the polymaromatic system is more dominated in ground state, it is expected that this system will have smaller band gap. This situation is explained by bond length alternation (BLA), whose definition is the difference between single and double bond lengths. BLA is the major factor affecting band gap ($E^{\delta r}$). Besides, BLA also depends on aromatic

resonance energy of aromatic unit that defined as the energy needed to limit π -electron delocalization (E^{res}). Less aromatic compounds have a tendency to adopt quinoid form and lower band gap. For example, aromatic resonance stabilization energy of benzene (1.56 eV) is higher than thiophene (1.26 eV) and thiophene more easily adapt to quinoid form so polythiophene has lower band gap. Further modification by combining benzene and thiophene on the structure of poly- isothianaphthene (PITN) cause low band gap as small as 1 eV due to further stabilization of quinoid form compared to thiophene and benzene aromatic units. [46].

Besides, it is possible to control steric and electronic effects on polymer chain by structural modification, which has an impact on interannular rotation [11]. Interannular rotation is single bond between adjacent aromatic unit and it prevents π -orbital interaction. Several strategies have been developed to control this interaction. For example, chemical rigidification results in planarization to enhance π -orbital interaction to increase conjugation and delocalization. Thus lowering band gap and BLA [11,46].

Additionally, electron withdrawing or donating groups can be introduced on polyaromatic system to modulate HOMO and LUMO energy level and to change band gap [11,46]. In general, electron-donating group cause high-lying HOMO energy level whereas electron withdrawing one resulted in low-lying LUMO energy level.

1.7.7. Donor-acceptor theory

Among all band gap-engineering strategies, donor-acceptor (D-A) approach is the most efficient strategy to tune band gap of polyaromatic systems. In this approach, electron rich (donor) and electron deficient (acceptors) units are alternated along the polymer backbone. Polymers with low band gaps as small as 0.5 eV, was reported with the study of ten Hoeve and coworkers in 1993. In this study, squaric and croconic acid was

utilized as strong acceptor units and combined with different donor segments and polymers with low band gaps compared to their counterparts, have been synthesized [46,47]. This situation was explained by the rules of perturbation theory. The formation of new high-lying HOMO and low-lying LUMO energy levels from the hybridization of the molecular orbital between the donor and acceptor segment was found as the explanation for this statement (**Figure 12**) [47].

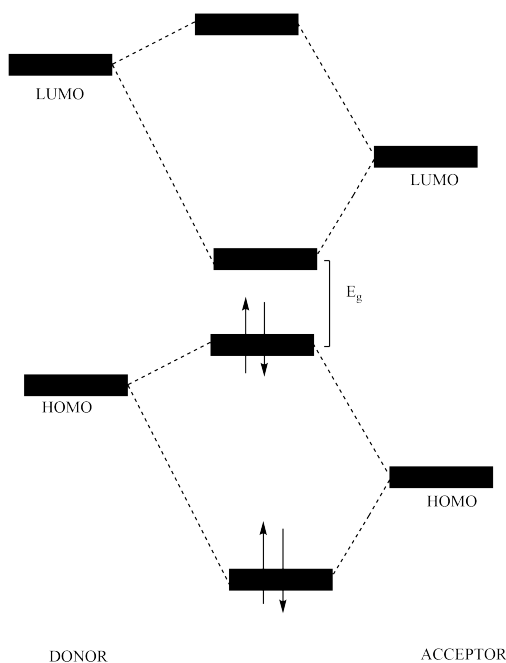


Figure 12 Orbital interaction of donor and acceptor moiety in DA approach

Although, origin of donor-acceptor approach depends on the synthesis of low band gap polymers, it is note taking to state that this motivation provides control over both band gap and energy levels of the conjugated polymers. The alignment of energy levels and magnitude of band gap strongly affected by donor and acceptor strength and their combinations because HOMO and LUMO energy levels of polymer are mainly located

on acceptor and donor units, respectively. Low, medium, and large band gap polymers can be synthesized from strong donor-strong acceptor, strong donor-weak acceptor (or vice versa), weak donor- weak acceptor combination, respectively [48].

1.7.7.1. Donor units

Donor units are electron-donating compounds and classified as weak, medium and strong according to their strength. There are three main types of donor units i.e, dibenzene bridged, dithiophene bridged and thiophene-benzene fused units that were constructed from dibenzene and dithiophene units and their chemical structures are depicted in **Figure 13** [48].

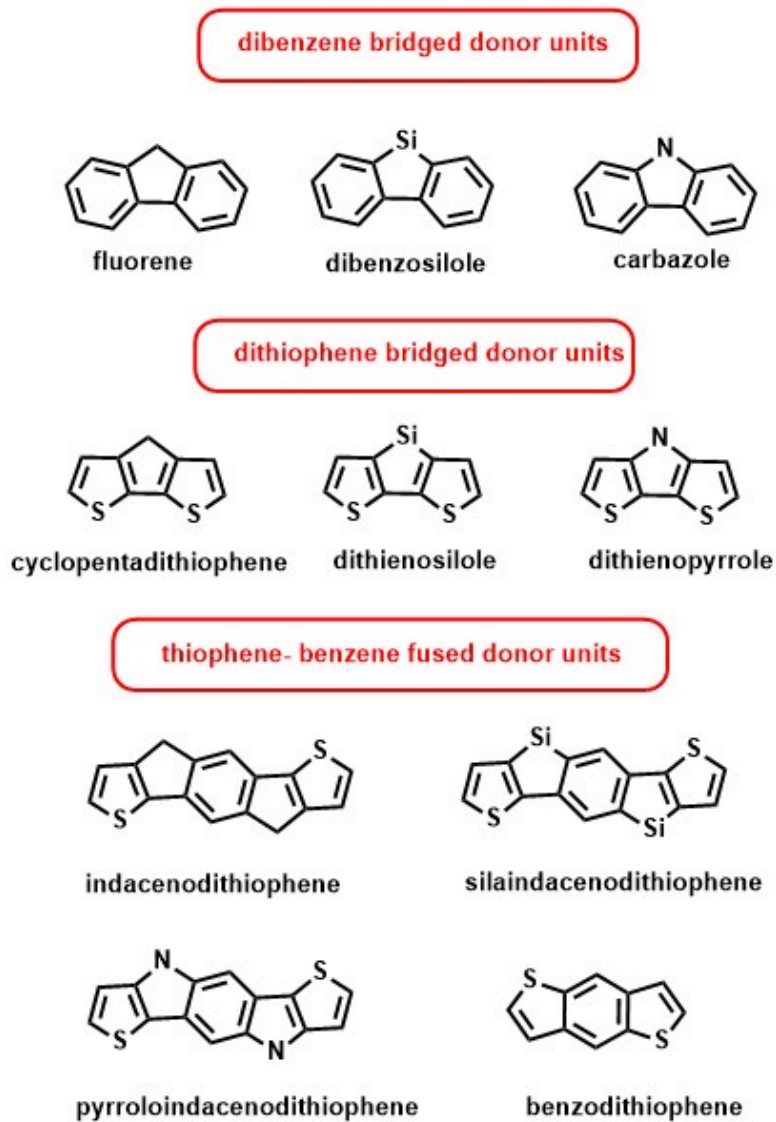


Figure 13 Chemical structures of basic donor units

1.7.7.1.1. Dibenzene bridged donor units

These types of donor units were counted as weak donors due to electron-deficient nature of the benzene. Although, optical and electronic properties of donor unit change by

molecular modification with the insertion of different atom (carbon, nitrogen and silicon), DA polymers, which contain one of these units, generally exhibit relatively large bandgap and narrow light absorption [48].

1.7.7.1.2. Dithiophene bridged donor units

Dithiophene bridged donor units are the strongest donor units among dibenzene bridged and thiophene-benzene fused donor units since orbital mixing of these donor units with acceptor units is strong due to robust electron delocalization. Besides, planarity of D-A copolymer is really high. Different atoms (carbon, nitrogen and silicon) can also be inserted as bridging atoms, which dramatically affect electronic and optical properties of resulting polymers [48].

1.7.7.1.3. Thiophene–benzene fused donor units

These types of donor units are ideal ones, which are developed from the combination of thiophene and benzene unit. Coplanar geometry of these units increases the effective conjugation length and π -electron delocalization. At the meantime, HOMO energy level of this unit stabilizes due to electron-deficient nature of benzene unit that is very crucial parameter for OSC applications [48].

1.7.7.2. Acceptor Units

Acceptor units are electron deficient units. They contain imine bond (C=N) or carbonyl (C=O) group on their backbones. Electron accepting ability of acceptor units are determined from the alignment of LUMO energy level and strong electron accepting units has low-lying LUMO energy level. Acceptor units are divided into three categories according to their strength, where their chemical structures and names are summarized in **Figure 14** [48].

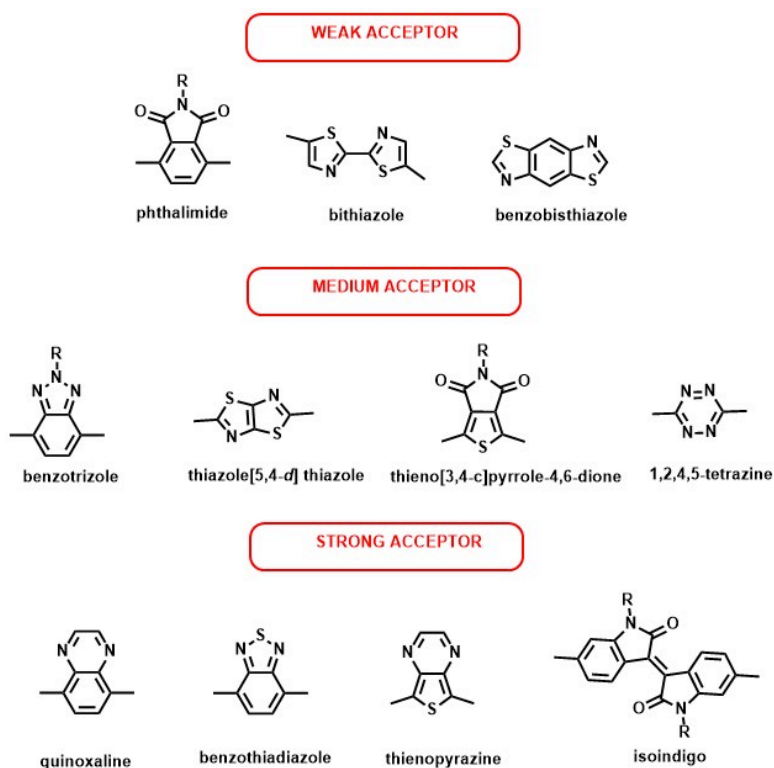


Figure 14 Chemical structures of acceptor units

1.7.8. Benzotriazole based donor molecules for organic solar cell applications

Benzotriazole (BTz) is one of the benzazole derivatives that contains nitrogen atom in its structure. This nitrogen atom makes this unit more basic and electron rich compared to its counterparts. Therefore, alkyl chains can be anchored onto benzotriazole rather than other donor units in molecular design. Therefore, polymer backbone adopts more planar structure by preventing steric hindrance. Thus enhances hole mobility of polymer due to close packing of polymer chain. Benzotriazole is counted in the class of medium strength acceptor units due to its electron rich nature that result large band gap due to high-lying LUMO energy level. Although, it is thought that this is one of the disadvantages of BTz based conjugated polymer due to less solar spectrum harvesting, thus enhances V_{OC} . Besides, this property makes this polymer suitable for tandem solar cell applications [49-51].

Benzotriazole was copolymerized with carbazole, fluorene, silafluorene benzodithiophene and dithienosilole for OSC applications [50-56]. Besides, electron-withdrawing fluorine groups were anchored onto BTz structure to decrease HOMO and LUMO energy level simultaneously [50]. **Figure 15** shows an overview of the structures and photovoltaic performance of benzotriazole based conjugated polymers.

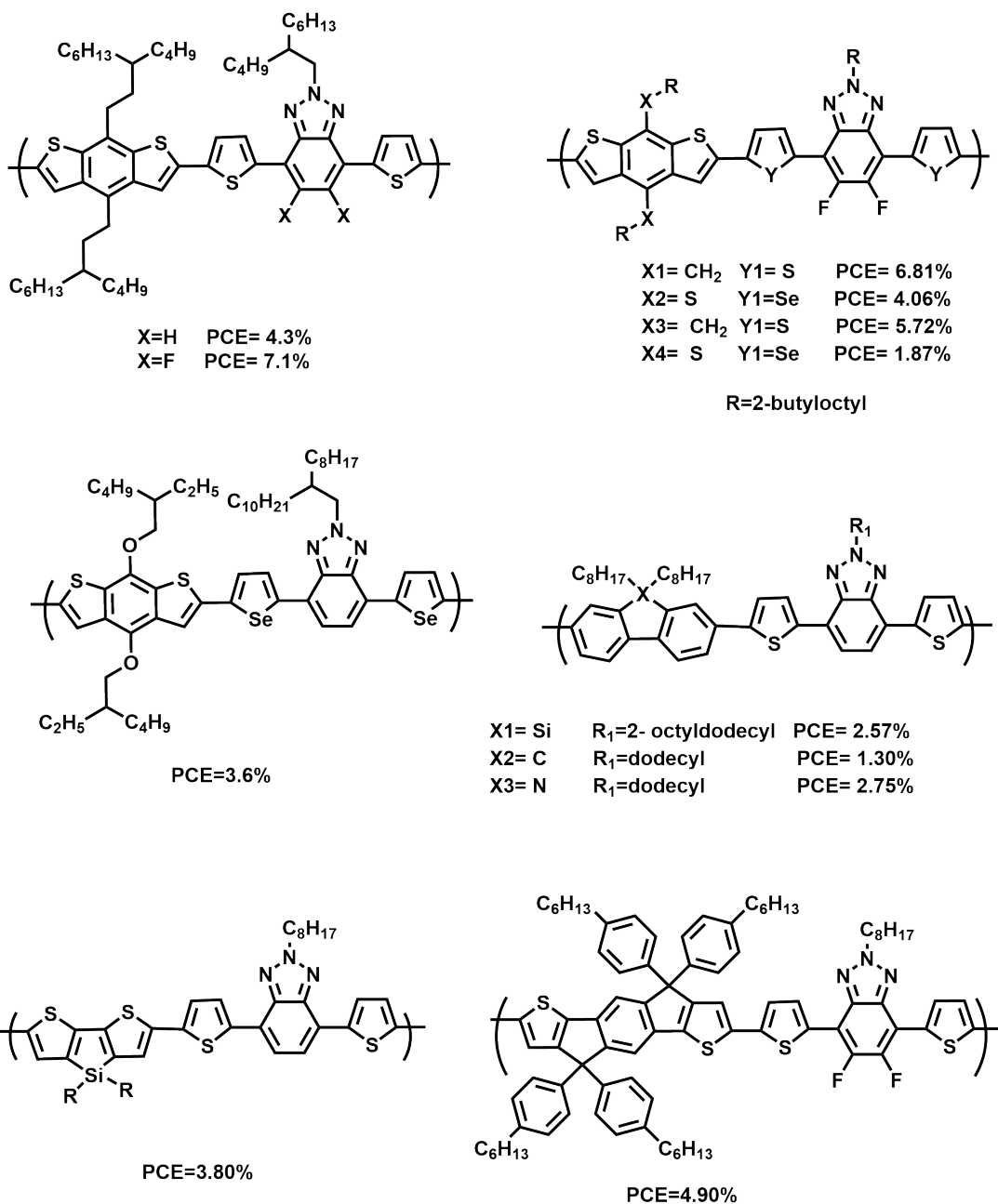


Figure 15 Overview of the structures and photovoltaic performance of benzotriazole based conjugated polymers

1.7.9. Acceptor materials in organic solar cell

[6,6]-Phenyl-C61-butyric acid methyl ester (PC₆₀BM) and its C₇₀ derivative (PC₇₀BM) have been dominantly used as the acceptors in OSCs. PC₇₀BM has a stronger absorption in visible region than C₆₀BM. However its expensive purification procedures limits the usage of this material in OSCs applications. Suitable LUMO energy level and low time scale for photoinduced charge transfer, their ability to accept up to six electrons are the some advantages of fullerenes [30, 57]. Therefore, fullerene and its derivatives are the most successful electron acceptor materials in OSCs. However, there are some drawbacks of fullerene derivatives, (i) they have low absorption profile (absorption in the visible-near IR region is weak), (ii) their photochemical and chemical stability is poor, (iii) controlling phase-separation kinetics is difficult due to their much higher rates of molecular diffusion and crystallization compared to donor molecules, (iv) manipulation of HOMO and LUMO energy level is difficult and (v) synthesis and purification of them are expensive [58,59]. Therefore, recently different n-type small molecules or conjugated polymers have been developed to replace fullerene derivatives. These molecules are also utilized to exceed the open circuit voltage (V_{OC}) limit impinged by fullerene derivatives [60].

1.7.10. NDI based acceptor molecules for all polymer solar cell applications

Among all acceptor units, naphthalene diimide (NDI) based copolymers are suitable building blocks for the development of n-type semiconductors. NDI based conjugated polymers not only exhibit high electron mobility and low-lying LUMO energy level but also show suitable physical properties such as, solubility, crystallization and self-assembly capacity that can be controlled by substitution of different alkyl chains from

N-position of the imide ring [61,62] Although, their unique properties of all polymer solar cell, PCEs based on polymer-polymer solar cell was relatively low and few researches have been reported PCE over 2% in the past [63-66].

The main problem of all polymer solar cells is the morphology control since low entropy of mixing of the polymers prevents proper phase separation. Thus enhances bimolecular and geminate recombination of charges [67]. Therefore, optimization studies like thermal annealing, usage of solvent and solvent mixtures, and solvent additives were used to circumvent these problems [63-66, 68]. In addition to these optimizations, suitable choice of p-type polymers with appropriate absorption profile, energy level and suitable miscibility become crucial to get high performance solar cell. Nowadays PCEs around 7% were reported. Structures of NDI based n-type polymers are utilized for solar cell applications are depicted in **Figure 16** [60, 65, 68, 69].

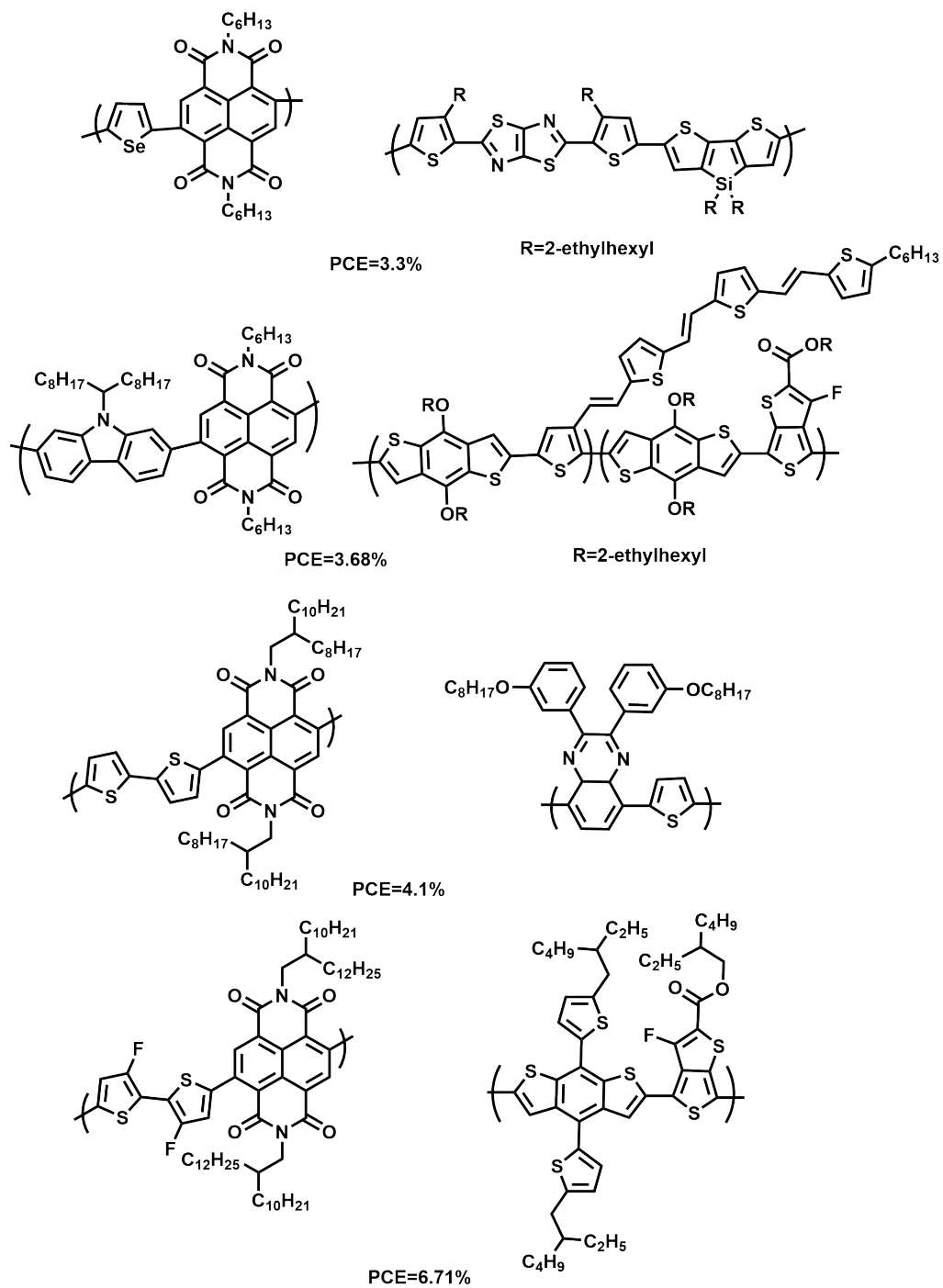


Figure 16 Overview of the structures and photovoltaic performance of NDI based conjugated polymers

1.8. Organic field effect transistor

Organic field effect transistors (OFETs) are one of the application areas of conjugated polymers and they are utilized to determine the charge transport properties of conjugated polymers. OFETs consist of three parts, i.e., an insulator, semiconducting material, and three electrodes (source, drain and gate). In the fabrication of OFETs, highly doped silicon generally used as a gate electrode, SiO_2 , Al_2O_3 and Si_3N_4 are utilized as inorganic insulator and high work function metals (i.e, gold) is preferred as source and drain electrodes. Voltage is applied to gate and drain electrode. Negative and positive charges can be induced to the source channel depending on applied potential. If the applied potential to the gate is positive, negative charges are induced at the source or if the applied potential is negative, positive charges are induced at the source.

Bottom gate/bottom contact (BG/BC), bottom gate/top-contact (BG/TC), top gate /bottom contact (TG/BC), and top gate/top contact (TG/TC) are types of the OFETS that are categorized according to their fabrication type and operation mode [70]. Device configuration of OFET is depicted on **Figure 17**.

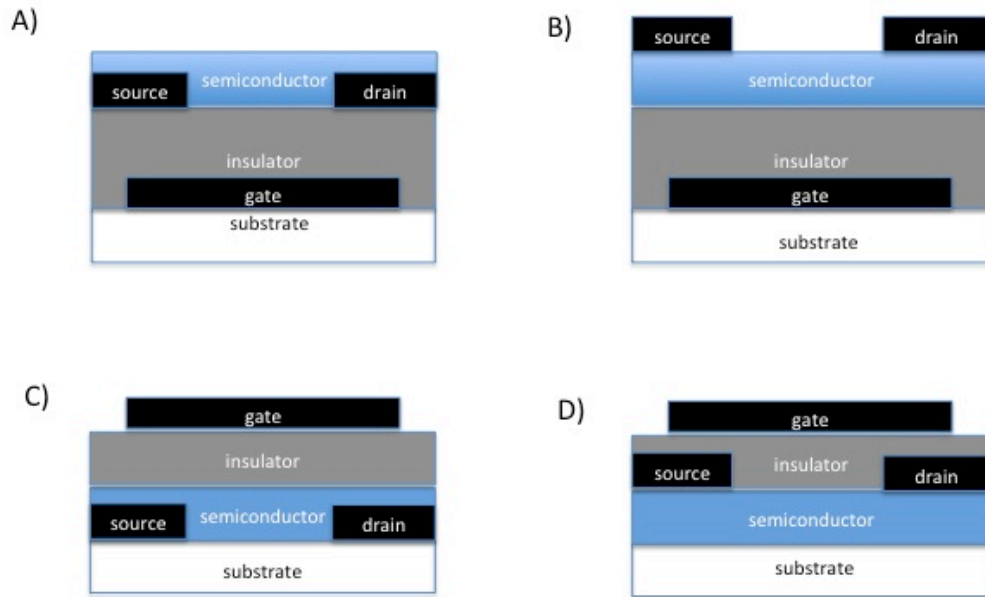


Figure 17 Device configuration of OFETs A) bottom-gate/bottom-contact, B) bottom gate/top-contact, C) top gate /bottom contact, D) top gate/top contact

Figure 18 depicts the typical OFET curves. Charge mobilities are calculated from saturated region with equation 7 and linear region with equation 8:

$$I_{ds,sat} = \frac{W}{2L} \cdot C_i \cdot \mu \cdot (V_g - V_{Th})^2 \quad (7)$$

$$I_{ds,lin} = \frac{W}{L} \cdot C_i \cdot \mu \cdot (V_g - V_{Th})^2 \quad (8)$$

where $I_{ds,sat}$ is drain current, W is channel width, L is channel length, C_i is capacitance, V_g is gate voltage, and V_{Th} is threshold voltage.

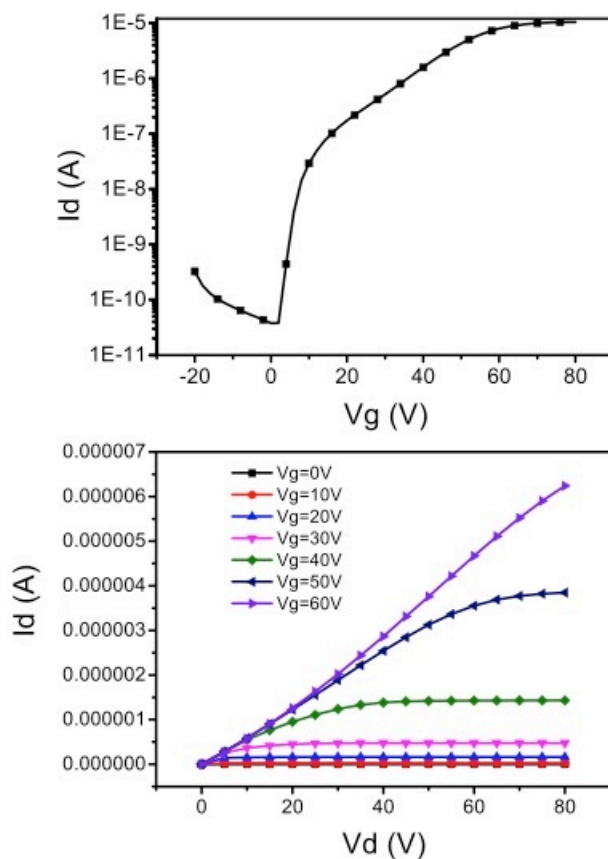


Figure 18 Typical OFET curves

1.9. Aim of the study

As mentioned before, donor-acceptor (D-A) approach is highly effective to obtain p-type and n-type materials with desired intrinsic optical and electrochemical properties. Therefore, in this work series of π -conjugated polymers was synthesized with combination of electron donating and electron-withdrawing heterocyclics to understand the effects of structural modifications on electrochemical and optoelectronic properties and we developed p and n type DA type conjugated polymers for electrochromic and organic solar cell applications. Conjugated polymers were synthesized via either

electrochemical or chemical methods. In the first part of the study benzotriazole was selected as a acceptor segment for development of p-type conjugated polymers and it coupled with different donor units, i.e, furan, thieno[3,2-b]thiophene, dithienopyrrole, benzodithiophene. Donor units in molecular design were selected according to their strength and their expectable effect on optical and electronic properties of resulting polymers. Besides, they are inserted either as donor or π -bridging units (furan, thieno[3,2-b]thiophene, thiophene, 3-hexylthiophene). The effects of these donor units on optical, electrochemical, electrochromic, and photovoltaic properties of conjugated polymers were investigated. In the second part of the study, NDI was selected as an acceptor unit and coupled with ladder type indacenodithiophene (IDT) and indacenodiselenophene (IDSe) units to synthesize novel n-type conjugated polymers for all polymer solar cell applications to replace fullerene in bulk heterojunction organic solar cell fabrication. Morphological and light intensity dependent photovoltaic studies were conducted that elucidate the possible loss mechanism in the related solar cells.

CHAPTER 2

EXPERIMENTAL

2.1. A synopsis of materials and methods

All chemicals and reagents were obtained from commercial sources and used without further purification. Tetrahydrofuran (THF) and toluene were dried over metallic sodium and benzophenone. Purification of monomers was done by column chromatography. TLC was utilized to monitor the reaction. Structures of monomers and polymers were proven by nuclear magnetic resonance (NMR) spectra recorded on a Bruker Spectrospin Avance DPX-400 Spectrometer with trimethylsilane (TMS) as the internal reference in deuterated chloroform solution. High-resolution mass spectrometer (HRMS) studies were done with a Waters SYNAPT MS system to verify molecular weight of monomers. Electrochemical and chemical polymerization (Stille Coupling) were performed to synthesize polymers. Purification of chemically synthesized polymers was done by Soxhlett extraction to get rid of any palladium catalyst residue and oligomeric units. Electrochemical properties and redox behavior of monomers and polymers were performed using a Voltalab 50 potentiostat in three-electrode cell consisting of an ITO-coated glass slide as the working electrode, Pt wire as the counter electrode, and Ag wire as the pseudo reference electrode (calibrated against Fc/Fc^+). Cyclic Voltametry (CV) was performed 0.1 M tetrabutylammonium hexafluorophosphate solution (TBAF_6) in acetonitrile. Both HOMO and LUMO energy levels were calculated by taking normal hydrogen electrode value as -4.8 eV or 4.75 eV and electrochemical band gap were calculated from HOMO and LUMO energy levels. Spectroelectrochemical and optical

studies of the polymers and monomers were investigated by Varian Carry 500 UV-Vis spectrophotometer. Molecular weight of the polymers was determined by gel permeation chromatography (GPC) (Polymer Laboratories PL-GPC 220) using o-dichlorobenzene (DCB), tetrahydrofuran (THF) and chloroform (CHCl_3) as mobile phase and polystyrene as standard. Thermal properties of the polymer were analyzed by thermal gravimetric analysis (TGA) (PerkinElmer Pyris 1 TGA) under nitrogen atmosphere at a heating rate of $10\text{ }^\circ\text{C}/\text{min}$. Differential Scanning Calorimetry (DSC) (Perkin Elmer Differential Scanning Calorimetry) was utilized to determine phase transitions of polymers.

2.2. Gel permeation chromatography

All synthetic polymers show a distribution of molecular weights, which may be averaged in several ways. Any physical or performance property of a polymer may be related to one or more average molecular weights, the type of average is determined by the physical averaging process, inherent in the method used to measure the property. Many polymers have distributions of other molecular parameters, such as chemical composition, stereoregularity, and chain branching.

In the GPC experiment, size, or their hydrodynamic volume because of their ability to penetrate part of the pores volume of the gel particles, i.e., the stationary phase separates polymer molecules. As the sample moves along the column with the mobile phase, the largest molecules are almost entirely excluded from the pores of the stationary phase, whereas the smallest find almost all the stationary phase accessible. The smaller the molecule, the more of the stationary phase volume is accessible to it and the longer it stays in that phase. Consequently, small molecules are eluted from the column later [71].

2.3. Cyclic Voltammetry

Cyclic voltammetry (CV) is a versatile tool to examine redox behavior of electroactive species as well as HOMO and LUMO energy levels. Current change as a function of applied potential is measured in CV studies. Three-electrode system is utilized for CV

studies, namely, reference (Ag), working (ITO) and counter electrode (Pt). Working electrode is the electrode where electrochemical reactions take place. Its potential difference is known when potential difference between working electrode and reference electrode is taken into account [72].

In CV experiments, electroactive species diffuses from solution to the surface of electrode where electrochemical reaction takes place. After electrochemical reaction, if product is soluble, it diffuses back to the solution. Typical shape of voltammogram for is depicted in **Figure 19**.

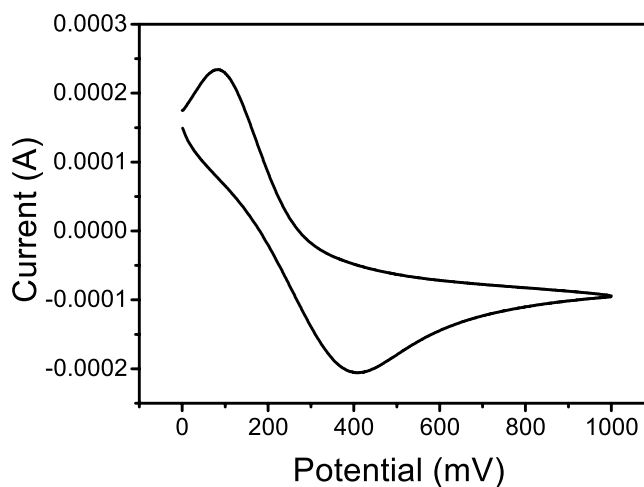


Figure 19 Cyclic voltammogram of ferrocene

The intensity of peak current is evaluated with the following equation known as Randles-Sevcik equation [72]

$$i_p = (2.69 \times 10^5) n^{1.5} A D^{0.5} C^b v^{0.5}$$

where A is the area of the electrode, C^b is the bulk concentration of the electroactive species, D is its diffusion coefficient and, v is the scan rate. This equation is applicable to 'reversible' all-solution systems.

Electrochemical behaviour of an electrochemically or chemically synthesized polymer is analyzed in a supporting electrolyte. The polymer is immobilized at the electrode surface and diffusion cannot take place. Therefore, peak current dependence on scan rate is analyzed according to immobilized redox centers with the following equation [73]:

$$i_p = n^2 F^2 \Gamma \frac{v}{4RT}$$

Here, Γ is the total amount of electroactive species. This equation gives the relation between current and scan rate. If scan rate is linearly dependent on scan rate, then process is called as diffusion controlled.

2.4. Spectroelectrochemistry

Spectroelectrochemical techniques have been utilized to gain a deeper insight into electrochromic processes of conjugated polymers. The evolution of the radical carriers (polaron and bipolaron) during p-doping process can be probed by recording in situ visible and NIR spectra as a function of applied electrode potential. Figure 20 depicts spectroelectrochemistry spectra of conjugated polymers. Neutral state polymers have characteristic of a $\pi-\pi^*$ interband transition. Upon doping process, this band decreases, new bands are intensified due to formation of polaron, which appears at lower energy. Further oxidation causes the formation of bipolaron.

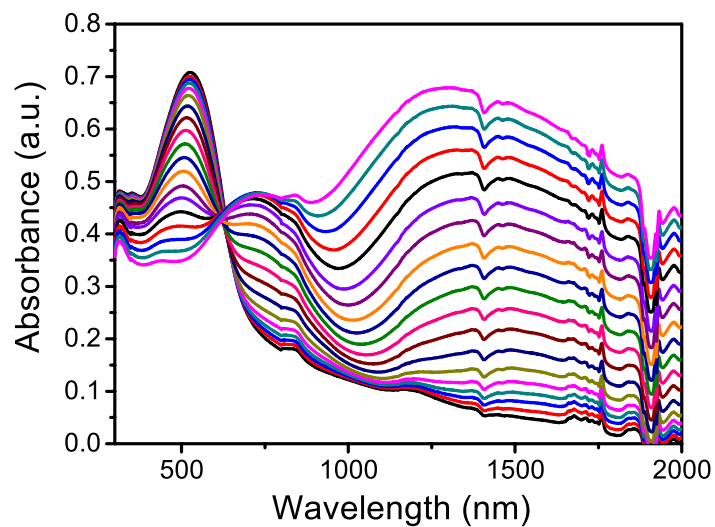


Figure 20 Representative spectroelectrochemistry of an electrochromic conducting polymer

2.5. Kinetic studies

Kinetic studies were performed to monitor transmittance change as a function of time by sweeping the potentials between neutral and fully oxidized states at maximum absorption wavelengths of polymer films (**Figure 21**). During the experiment, optical contrasts of the polymer films at corresponding wavelengths were recorded using a UV-vis-NIR spectrophotometer. Chronoamperometry was utilized to monitor switching times and contrast.

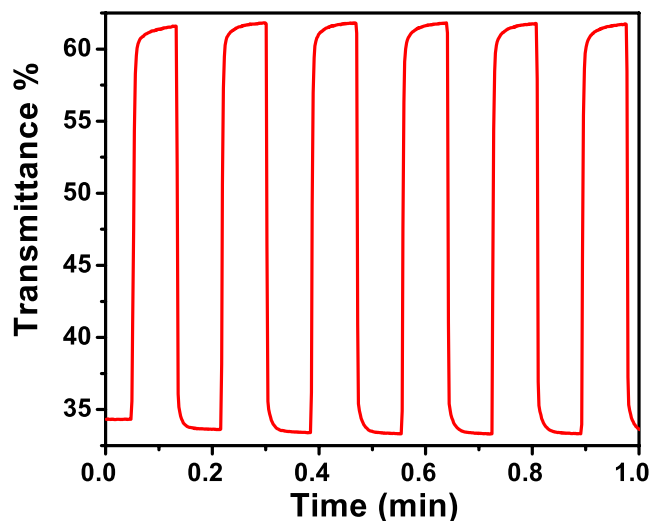


Figure 21 Representative kinetic studies of a conjugated polymer

2.6. Device fabrication of OSC

ITO coated glass substrates ($15 \Omega \text{ sq}^{-1}$) were cleaned with toluene, detergent, water, acetone, and isopropyl alcohol in 15 minutes with ultrasonic bath. Subsequently, oxygen plasma treatment was performed in Harrick Plasma Cleaner to get rid of any remaining organic component. For conventional device fabrication, PEDOT: PSS was spin coated onto pre-cleaned ITO-coated glass substrate at 5000 rpm and annealed at 150°C for 10 min to remove residual water. Active layer was prepared by dissolving polymers and PC_{71}BM with different weight ratio in different solvents and filtered through polytetrafluoroethylene (PTFE) filter ($0.2 \mu\text{m}$) to have a homogenous solution. Then active layer was spin coated on PEDOT: PSS layer. After that, calcium (20 nm) and aluminum (80 nm) were deposited with thermal deposition technique. Shadow masks were used to define the OSC active area (0.06 cm^2) of the devices.

For inverted device fabrication, the ZnO precursor solution was prepared by dissolving zinc acetate dehydrate $\text{C}_4\text{H}_6\text{O}_4\text{Zn} \cdot 2(\text{H}_2\text{O})$ (99.5 %, Merck 1g) and monoethanolamine

(HOCH₂CH₂NH₂, 98 % Acros, 0.28 g) in 2-methoxyethanol (CH₃OCH₂CH₂OH, Aldrich, 98 %, 10 mL) under stirring for 8 h for hydrolysis reaction and aging. Thin layer of sol-gel ZnO (~30 nm) was spin-coated onto pre-cleaned ITO-coated glass substrates at 4000 rpm and then annealed at 200 °C for 1 h in air since crystallinity of the ZnO sol-gel was increased by thermal annealing that enhanced conductivity and mobility. The substrates were then transferred into a nitrogen-filled glovebox. Subsequently, the active layer (~90 nm) was spin-coated on the ZnO layer from a homogeneous solution. The solution was prepared by dissolving the PTB7 (or PBDTTT-E-T) and **PIDTNDI** or **PIDSeNDI** with weight ratio of 1:1 in o-dichlorobenzene overnight and filtered through a PTFE (polytetrafluoroethylene) filter (0.2 μm). After that, an 8 nm-thick MoO₃ film and 100 nm Ag were deposited to complete the inverted devices structure. Shadow masks were used to define the OSC active area (10.08×10⁻² cm²) of the devices.

2.7. Device Characterization of OSC

The current density-voltage (J-V) characteristics of unencapsulated photovoltaic devices were measured under N₂ using a Keithley 2400 source meter. A 300 W xenon arc solar simulator (Oriel) with an AM 1.5 global filter operated at 100 mW/cm² was used to simulate the AM 1.5G solar irradiation. The light intensity was measured with a Newport Optical Powermeter 1916-C radiant power meter. The illumination intensity was corrected by using a silicon photodiode with a protective KG5 filter calibrated by the National Renewable Energy Laboratory (NREL). The EQE system uses a lock-in amplifier (Stanford Research Systems SR830) to record the short circuit current under chopped monochromatic light. The absorption spectra were measured using a Perkin-Elmer Lambda-9 UV-visible spectrophotometer. Tapping-mode AFM images were taken on a Veeco multimode AFM with a Nanoscope III controller.

2.8. SCLC mobility measurements

Space charge limited currents have been tested in electron-only devices with a configuration of ITO/Al/BHJ/Ca/Al and hole-only devices with a configuration of ITO/PEDOT: PSS/BHJ/MoO₃/Ag. The devices were prepared following the same procedure described in the experimental section for photovoltaic devices, except that of the metal electrode. The mobilities were determined by fitting the dark current to the model of a single carrier SCLC current with field dependent mobility, which is described as

$$J = \frac{9\epsilon_r\epsilon_0\mu_0V^2}{8L^3} \exp\left(\beta \frac{V}{L}\right)$$

Where J is the current, μ_0 is the zero-field mobility, ϵ_0 is the permittivity of free space, ϵ_r is the relative permittivity of the material, V is the effective voltage, and L is the thickness of the active layer.

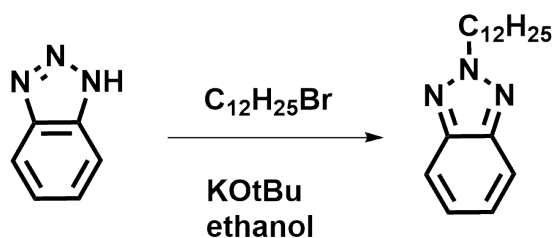
2.9. Device Fabrication of OFET

Transistors were fabricated through the top-contact and bottom-gate geometry. The silicon substrate (with a 300 nm thermal oxide layer) were cleaned by sequential ultrasonication in acetone and isopropyl alcohol for 15 min followed by air plasma treatment and the oxide layer was passivated with a thin divinyltetramethyldisiloxane-bis(benzocyclobutene) (BCB) buffer layer. The 1 wt% BCB precursor solution in toluene was spun onto the silicon oxide at 4000 rpm and subsequently annealed at 250 °C overnight. **PIDTNDI** and **PIDSeNDI** thin films were spin-coated at 1000 rpm from 5mg/mL polymer solution in o-dichlorobenzene. Interdigitated source and drain electrodes ($W = 1000$ nm, $L = 20/30/50$ nm) were defined by evaporating Ag (100 nm)

through a shadow mask from the resistively heated Mo boat at 10^{-7} Torr. OFET characterization was carried out in a N_2 -filled glovebox using an Agilent Model 4155B semiconductor parameter S6 analyzer.

2.10. Synopsis of synthetic procedures

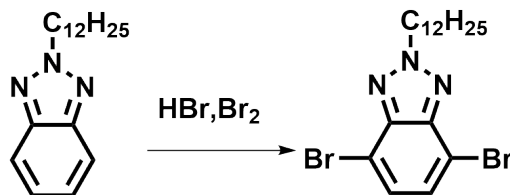
2.10.1. Synthesis of 2-dodecylbenzotriazole



It was synthesized using the modified procedure as reported elsewhere [74]. A mixture of 1,2,3-benzotriazole (5.0 g, 42 mmol), potassium tert-butoxide (5.0 g, 44 mmol) and bromododecane (12.2 g, 49 mmol) in 50 mL methanol was refluxed for 12 h. After cooling to room temperature, the solvent was evaporated. The residue was dissolved in $CHCl_3$ and extracted with brine. The organic extract was dried over $MgSO_4$ and the solvent was evaporated under reduced pressure. The resulting crude compound was purified by silica gel column using a mixture of hexane/DCM (1:2) as the eluent to give colorless oil (3.7 g, 31%)

1H NMR (400 MHz, $CDCl_3$, δ): 7.76 (m, 2H), 7.26 (m, 2H), 4.62 (t, $J=7.1$ Hz 2H), 2.12 (m, 2H), 1.25-1.15 (m, 18H), 0.78 (t, $J=6.0$ Hz, 3H) ^{13}C NMR (100 MHz, $CDCl_3$, δ): 144.3, 126.1, 117.9, 56.6, 31.8, 30.0, 29.5, 29.4, 29.4, 29.3, 29.3, 29.0, 26.5, 22.6, 14.0

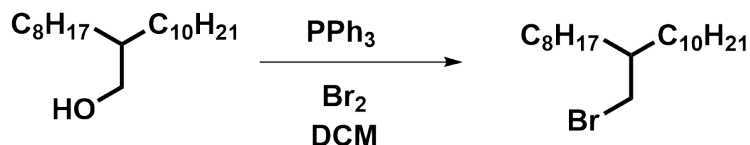
2.10.2. Synthesis of 4,7-dibromo-2-dodecylbenzotriazole



It was synthesized using the modified procedure as reported elsewhere [74]. A mixture of 2-dodecylbenzotriazole (3.7 g, 13.1mmol) and an aqueous HBr solution (5.8 M, 15 ml) was stirred for 1 h at 100°C. Bromine (5.9 g, 36 mmol) was added, and the mixture was stirred for 12 h at 135°C. After cooling to room temperature, residue was extracted with CHCl₃ and NaHCO₃. The organic layer was dried over MgSO₄ and the solvent was evaporated under reduced pressure. The product was purified by column chromatography using CHCl₃: hexane (1:1). The pure product was obtained as light yellow oil (4.3 g, 75%).

¹H NMR (400MHz, CDCl₃, δ): 7.36 (s, 2H), 4.60 (t, J=7.0 Hz, 2H), 2.10 (m, 2H), 1.38-1.12 (m, 18H), 0.80 (t, J=6.9 Hz, 3H). ¹³C NMR (100 MHz, CDCl₃, δ): 143.7, 129.4, 109.9, 57.4, 31.8, 30.1, 29.5, 29.5, 29.4, 29.4, 29.3, 28.9, 26.4, 22.6, 14.0

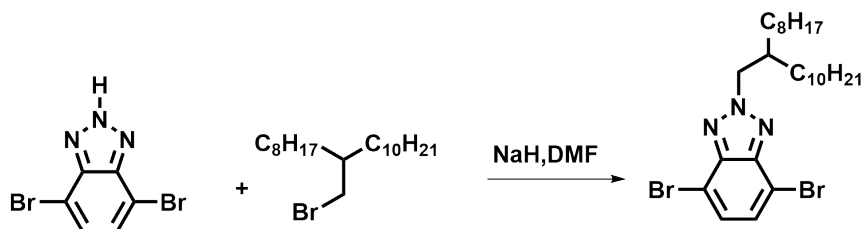
2.10.3. Synthesis of 2-(bromomethyl)nonadecane



2-Octyldodecanol (1.94 g, 6.5 mmol) was dissolved in 50 mL CH₂Cl₂ and PPh₃ (1.79 g (6.825 mmol) was added to the solution at 0°C. Br₂ (15.4 mmol) was added to this mixture. The mixture was kept at 0°C for 30 min and then warmed up to RT for another 1 hour. After completion of reaction, it was poured into 50 mL saturated NaHSO₃ and extracted with NaHSO₃, brine and water. After drying over MgSO₄, the solvent was removed and the crude product was purified by column chromatography using hexane. The pure product was obtained as colorless oil (2.23 g, 95%).

¹H NMR (400 MHz, CDCl₃, δ): 3.37(d, J =4.7 Hz, 2H), 1.52 (m, 1.46–1.57, 1H), 1.20 (m, 1.15–1.32, 32 H), 0.81 (t, J =6.58 Hz, 6H).¹³C NMR (100 MHz, CDCl₃, δ): 39.6, 39.5, 32.59, 31.9, 29.8, 29.7, 29.6, 29.5, 29.4, 29.3, 26.6, 22.7, 14.1

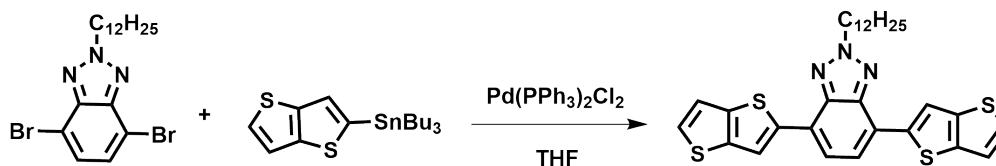
2.10.4. Synthesis of 4,7-dibromo-2-(2-(2-octyldodecyl)-2H-benzo[d][1,2,3]triazole



To a solution of 4,7-dibromo-1H-benzo[d][1,2,3]triazole (2 g, 7.22 mmol) in 10 mL of anhydrous dimethylformamide (DMF) at 0°C was added NaH (0.21 g, 8.75 mmol). Then 2-(bromomethyl)nonadecane (8.46 mmol, 3.04 g) was added into the reaction medium and the resulting mixture was stirred overnight at room temperature. It was then poured into brine and extracted with ethylacetate. After drying over MgSO₄, the solvent was removed. The crude product was purified by column chromatography using dichloromethane: hexane (1:1). The pure product was obtained as pale yellow oil (1.4 g, 34%).

¹H NMR (400 MHz, CDCl₃, δ): 7.32 (s, 2H), 4.59 (d, J=7.3 Hz, 2H), 2.25 (m, 2.19–2.30, 1H), 1.13(m, 1.08–1.30, 32H), 0.78 (m, 0.75–0.80, 6H). ¹³C NMR (100 MHz, CDCl₃, δ): 141.4, 127.2, 107.8, 58.9, 36.8, 29.7, 29.6, 29.4, 29.0, 27.6, 27.4, 27.3, 27.2, 27.1, 27.0, 23.8, 20.5, 20.4, 11.9

2.10.5. Synthesis of 2-dodecyl-4,7-di(thieno[3,2-b]thiophen-2-yl)-2H-benzo[d][1,2,3]triazole

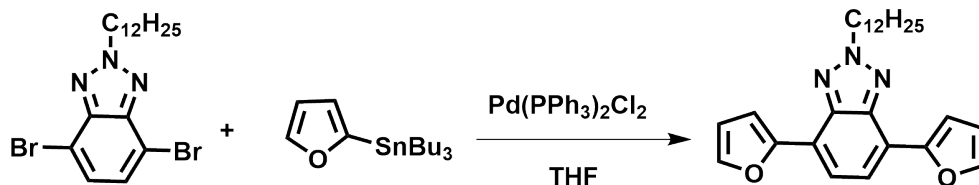


Tributyl(thieno[3,2-b]thiophen-2-yl)stannane [75] (2.03 g, 4.73 mmol) and 4,7-dibromo-2-dodecyl-2H-benzo[d][1,2,3]triazole (524 mg, 1.18 mmol) were charged in a 50 mL three-neck flask. After adding THF (10 mL), the mixture was bubbled with argon to remove O₂. Then dichlorobis(triphenylphosphine)palladium(II) (150 mg, 0.21 mmol) were added and the mixture was bubbled once more. Then the mixture was heated at 100 °C for 24 hours. The volatiles were removed under reduced pressure and the residue was purified by silica gel chromatography using chloroform-hexane as an eluent. The product was obtained as a yellow solid with a yield of 45%.

¹H NMR (400 MHz, CDCl₃, δ): 8.34 (s, 2H), 7.55 (s, 2H), 7.34 (d, J=5.2 Hz, 2H), 7.22 (d, J=5.1 Hz, 2H), 4.78 (t, J=7.03 Hz, 2H), 2.21–2.11 (m, 2H), 1.4–1.11 (m, 18H), 0.79 (t, J= 7.0, 3H). ¹³C NMR (100 MHz, CDCl₃, δ): 141.0, 140.8, 139.5, 137.8, 126.7, 123.3, 121.6, 118.9, 118.6, 55.9, 30.9, 29.1, 28.6, 28.4, 28.3, 28.0, 25.6, 21.6, 13.1.

HRMS-ESI⁺ (m/z): [M⁺] Calculated for C₃₀H₃₃N₃S₄ 563.1557, found 563.1563.

2.10.6. Synthesis of 2-dodecyl-4,7-di(furan-2-yl)-2Hbenzo[d][1,2,3]triazole



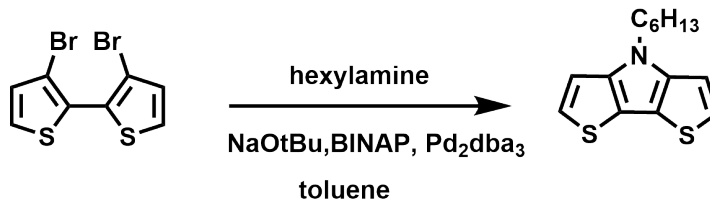
Tributyl(furan-2-yl)stannane (1.43 g, 4 mmol) and 4,7-dibromo-2-dodecyl-2Hbenzo[d][1,2,3]triazole (443 mg, 1 mmol) were charged in a 50 mL three-neck flask. After adding THF (10 mL), the mixture was degassed with argon to remove O₂. Dichlorobis(triphenylphosphine)palladium(II) (80 mg, 0.11 mmol) was added and the mixture was degassed once more. Then the mixture was heated at 100 °C for 24 hours. The volatiles were removed under reduced pressure and the residue was purified by silica gel chromatography using chloroform-hexane as an eluent. The pure product was obtained as a pale yellow solid with a yield of 43%.

¹H NMR (400 MHz, CDCl₃, δ): 7.73 (s, 2H), 7.48 (d, J=2.08 Hz, 2H), 7.37 (d, J = 2.92 Hz, 2H), 6.52 (q, J=1.56 Hz, 2H), 4.73 (t, J =7.25 Hz, 2H), 2.06–2.16 (m, 2H), 2.1–2.16 (m, 2H), 1.11–1.40 (m, 16H), 0.8 (t, J=6.67 Hz, 3H)

¹³C NMR (100 MHz, CDCl₃, δ): 149.3, 141.1, 139.5, 119.2, 118.2, 110.9, 109.3, 55.5, 30.6, 28.8, 28.3, 28.2, 28.1, 28.0, 27.8, 25.3, 21.4, 12.8

HRMS-ESI⁺ (m/z): [M⁺] Calculated for C₂₆H₃₃N₃O₂ 419.2573, found 419.2569.

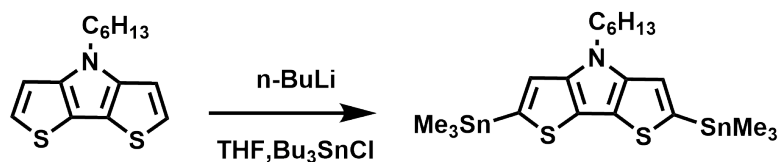
2.10.7. Synthesis of 4-hexyl-4H-dithieno[3,2-b:2',3'-d]pyrrole



3,3'-Dibromo-2,2'-bithiophene (1.95 g, 6.00 mmol), NaOtBu (1.09 g, 11.4 mmol), Pd₂dba₃ (0.18 mmol), and 2,2'-bis(diphenylphosphino)-1,1'-binaphthyl (BINAP, 0.45 g, 0.72 mmol) were dissolved in dry toluene (20 mL) and solution was purged with argon for 20 min. Then, hexyl amine (0.491 g, 4.87 mmol) was added and the mixture was stirred at 110°C under inert atmosphere for 12 h. The reaction mixture was poured into water and extracted with ethyl acetate. The combined organic layers were dried over MgSO₄ and the solvent was removed under reduced pressure. The crude product was purified through column chromatography (silica gel, dichloromethane:hexane, 1:1) to afford a yellow liquid with a yield of 50% (0.789 g, 3 mmol).

¹H NMR (400 MHz, CDCl₃, δ): 7.04 (d, J = 5.30 Hz, 2H), 6.93 (d, J = 5.30 Hz, 2H), 4.11 (t, J = 7.90 Hz, 2H), 1.75–1.83 (m, 2H), 1.15–1.30 (m, 6H). ¹³C NMR (100 MHz, CDCl₃, δ): 144.2, 122.0, 110.2, 46.7, 30.7, 29.6, 25.9, 21.8, 13.3.

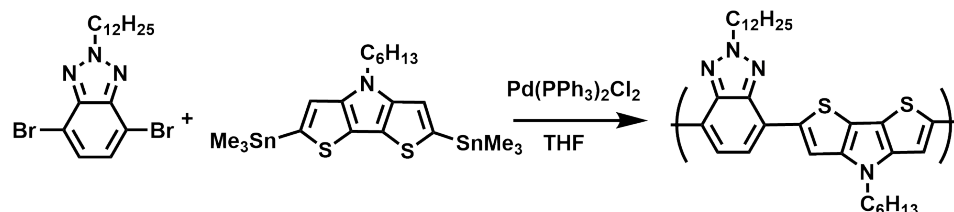
2.10.8. Synthesis of 4-hexyl-2,6-bis(tributylstannyl)-4H-dithieno[3,2-b:2',3'-d]pyrrole



n-BuLi (2.2 mmol 2.5 M in hexane, 2.2 eq.) was added via syringe to the solution of 4-hexyl-4H-dithieno[3,2-b:2',3'-d]pyrrole (0.263 g, 1 mmol, 1 eq.) in dry THF at $-78\text{ }^{\circ}\text{C}$ under inert atmosphere. After addition of n-BuLi, reaction mixture was stirred at room temperature for 1 h. Then reaction was cooled to $-78\text{ }^{\circ}\text{C}$ and a solution of Bu₃SnCl (2.2 mmol, 2.2 eq.) in dry THF (10 mL) was drop wise added. After stirring overnight at room temperature, water was added and extraction was done with chloroform. The combined organic layers were dried over MgSO₄ and the solvents were removed under reduced pressure. The crude product was obtained as a yellow liquid made use of in polymerization reaction without further purification with a yield of 60% (0.505 g, 0.6 mmol).

¹H NMR (400 MHz, CDCl₃, δ): 7.18 (s, 2H), 4.12 (t, J = 6.90 Hz, 2H), 1.75-1.85 (m, 2H), 1.48-1.57 (m, 12H), 1.20-1.33 (m, 24H), 1.08-1.3 (m, 6H), 0.83 (t, J = 7.3 Hz, 21H). ¹³C NMR (100 MHz, CDCl₃, δ): 146.9, 117.0, 110.7, 95.3, 46.3, 30.4, 27.9, 26.8, 26.2, 26.1, 21.5, 16.5, 12.7, 9.9

2.10.9. Synthesis of poly[2-(2-dodecyl-2H-benzo[d][1,2,3]triazol-4-yl)-4-hexyl-4H-dithieno[3,2-b:2',3'-d]pyrrole] (PBTzDTP)

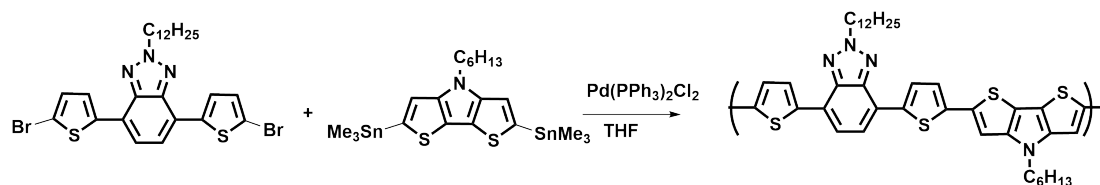


4-Hexyl-2,6-bis(tributylstannyl)-4H-dithieno[3,2-b:2',3'-d]pyrrole (1 mmol) and 4,7-dibromo-2-dodecyl-2H-benzo[d][1,2,3] triazole (1 mmol) were dissolved in dry THF. The mixture was purged with nitrogen for 30 min and heated under reflux. Then dichlorobis(triphenylphosphine)-palladium(II) (10% by mol) and CuO (10 mg) were added to the reaction mixture. The mixture was heated for 3 days. 2-Bromobenzene and 2-tributyl(thiophen-2-yl)stannane were added to the reaction mixture as the end-capper. Polymer was then precipitated into methanol and then washed sequentially with methanol and acetone in a Soxhlet extractor. The polymer was then extracted with chloroform and concentrated under vacuum. Then, it was precipitated into methanol to afford purple solids (0.153 mg, 28%)

GPC: Number-average molecular weight (M_n) = 72.1 kDa, polydispersity index (PDI) = 7.9

¹H NMR (400 MHz, CDCl₃, δ): 7.98 (BTz), 7.01 (DTP), 4.74 (N-CH₂), 4.10 (N-CH₂, BTz), 1.82 (CH₂), 1.18 (CH₂), 0.81 (CH₃)

2.10.10. Synthesis of poly[2-(5-(2-dodecyl-7-(thiophen-2-yl)-2H-benzo[d][1,2,3]triazol-4-yl)thiophen-2-yl)-4-hexyl-4H-dithieno[3,2-b:2',3'-d]pyrrole] (PTBTDTP)

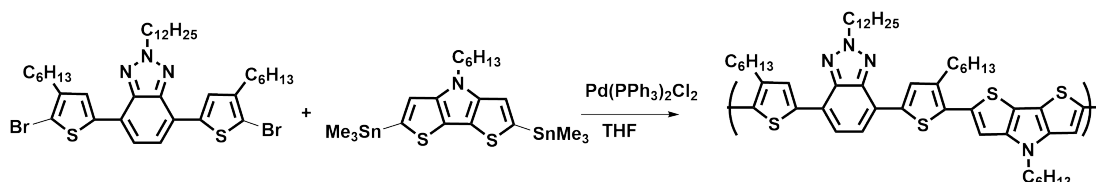


The same procedure was applied for the polymerization using 4-hexyl-2,6-bis(tributylstannyl)-4H-dithieno[3,2-b:2',3'-d]pyrrole (1mmol) and 4,7-bis(5-bromothiophen-2-yl)-2-dodecyl-2H-benzo[d][1,2,3]triazole [76] (1mmol). **PTBTDTP** was obtained as a red solid with a yield of 37% (0.263 g).

GPC: $M_n = 3.2$ kDa, PDI = 6.7

^1H NMR (400 MHz, CDCl_3 , δ): 7.92 (BTz), 7.42 (thiophene), 7.07 (thiophene), 6.90 (DTP), 4.72 (N- CH_2 , DTP), 4.08 (N- CH_2 , BTz), 2.16 (CH_2), 1.79 (CH_2), 1.18 (CH_2), 0.79 (CH_3)

2.10.11. Synthesis of poly[2-(5-(2-dodecyl-7-(4-hexylthiophen-2-yl)-2H-benzo[d][1,2,3]triazol-4-yl)-3-hexylthiophen-2-yl)-4-hexyl-4H-dithieno[3,2-b:2',3'-d]pyrrole] (PHTBTDTP)

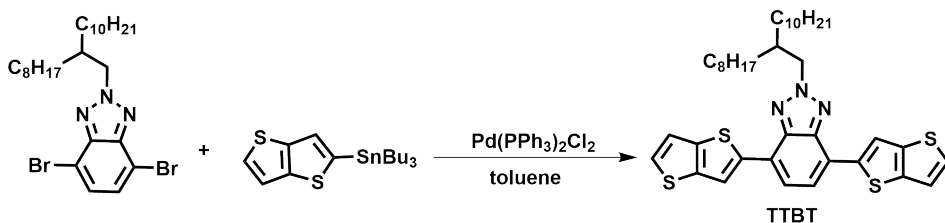


The same procedure was applied for the polymerization reaction using 4-hexyl-2,6-bis(tributylstannyl)-4H-dithieno[3,2-b:2',3'-d]pyrrole (1mmol) and 4,7-bis(5-bromo-4-hexylthiophen-2-yl)-2-dodecyl-2H-benzo[d][1,2,3]triazole [76] (1mmol). **PHTBTDTP** was obtained as a red solid with a yield of 29% (0.255 g).

GPC: Mn = 6.3 kDa, PDI = 5.1

¹H NMR (400 MHz, CDCl₃, δ): 7.89 (BTz), 7.52 (3-hexylthiophene), 7.06 (DTP), 4.79 (N-CH₂, DTP), 4.15 (N-CH₂, BTz), 2.86 (CH₂), 2.16 (CH₂), 1.83 (CH₂), 1.73 (CH₂), 1.18 (CH₂), 0.81 (CH₃)

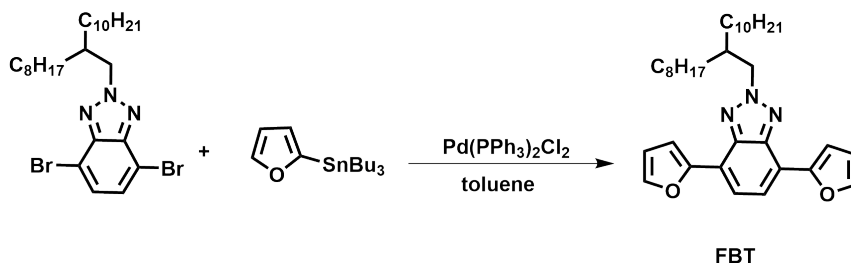
2.10.12. Synthesis of 2-(2-octyldodecyl)-4,7-bis(thieno[3,2-b]thiophen-2-yl)-2H-benzo[d][1,2,3]triazole



4,7-Dibromo-2-(2-octyldodecyl)-2H-benzo[d][1,2,3]triazole (557.45 mg, 1 mmol) and tributyl(thieno[3,2-b]thiophen-2-yl)stannane (1.7 g, 4 mmol) were dissolved in 5 mL toluene. After the mixture was degassed with argon to remove O₂, dichlorobis(triphenylphosphine)palladium(II) (70.1 mg, 0.1 mmol) and tri-*o*-tolylphosphine (121 mg, 0.4 mmol) were added and the mixture was degassed once more. Then the mixture was heated at 120 °C for 24 hours. The volatiles were removed under reduced pressure and the residue was purified by silica gel chromatography using petroleum ether: dichloromethane (5:1). The pure product was obtained as a pale yellow solid with a yield of 76% (520 mg).

¹H NMR (400 MHz, CDCl₃, δ): 8.34 (s, 2H), 7.54 (s, 2H), 7.34 (d, J = 5.18 Hz, 2H), 7.22 (d, J = 5.15 Hz, 2H), 4.70 (d, J = 6.71 Hz, 2H), 2.25- 2.35 (m, 1H), 1.12-1.40 (m, 36H), 0.75-0.88 (m, 6H). ¹³C NMR (100 MHz, CDCl₃, δ): 186.5, 172.6, 141.8, 140.4, 138.8, 127.7, 124.2, 122.4, 121.4, 119.9, 119.5, 31.9, 31.8, 29.9, 29.6, 29.6, 29.3, 26.2, 22.6, 14.1

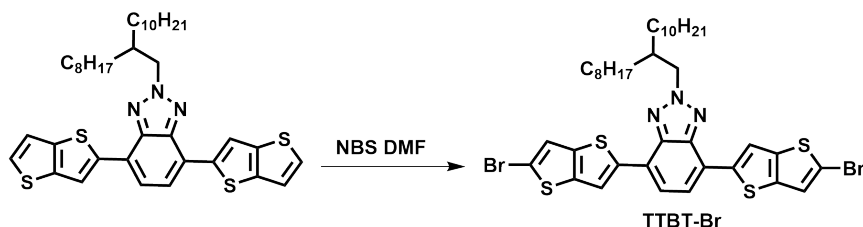
2.10.13. Synthesis of 4,7-di(furan-2-yl)-2-(2-octyldodecyl)-2H-benzo[d][1,2,3]triazole



4,7-Dibromo-2-(2-octyldodecyl)-2H-benzo[d][1,2,3]triazole (650 mg, 1.46 mmol) and tributyl(furan-2-yl)stannane (1.616 g, 3.1 mmol) were dissolved in 5 mL toluene. After the mixture was degassed with argon to remove O₂, dichlorobis(triphenylphosphine)palladium(II) (102 mg, 0.146 mmol) and tri-tolylphosphine (177 mg, 0.584 mmol) were added and the mixture was degassed once more. Then the mixture was heated at 120 °C for 24 hours. The volatiles were removed under reduced pressure and the residue was purified by silica gel chromatography. The pure product was obtained as a pale yellow solid with a yield of 77.7% (275 mg).

¹H NMR (400 MHz, CDCl₃, δ): 7.80 (s, 2H), 7.54 (d, J = 1.65 Hz, 2H), 7.45 (d, J = 3.36 Hz, 2H), 6.59 (d,d J = 1.77 Hz, 2H), 4.72 (d, J = 6.65 Hz, 2H), 2.25-2.35 (m, 1H), 1.20-1.42 (m, 36H), 0.84-0.90 (m, 6H). ¹³C NMR (100 MHz, CDCl₃, δ): 167.1, 150.6, 142.3, 140.6, 120.3, 119.4, 112.1, 110.6, 31.9, 31.8, 31.4, 29.8, 29.6, 29.5, 29.2, 26.2, 22.6

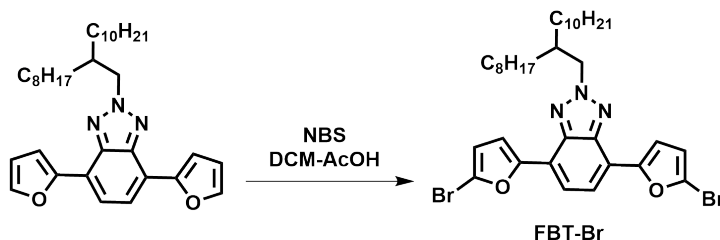
2.10.14. Synthesis of 4,7-bis(5-bromothieno[3,2-b]thiophen-2-yl)-2-(2-octyldodecyl)-2H benzo[d][1,2,3]triazole



4,7-Bis(5-bromothieno[3,2-b]thiophen-2-yl)-2-(2-octyldodecyl)-2H-benzo[d][1,2,3] triazole (390 mg, 0.576 mmol) was dissolved in DMF and NBS (235.79 mg, 1.38 mmol) was added to reaction medium in portion under dark. Reaction mixture was stirred at room temperature for 16 hours after the completion of addition. Product was precipitated out and collected by filtration. The crude product was washed with ethanol and dichloromethane. Pure compound was obtained as a yellow solid with a yield of 62.5% (300 mg).

^1H NMR (400 MHz, CDCl_3 , δ): 8.23 (s, 2H), 7.52 (s, 2H), 7.21 (s, 2H), 4.69 (d, $J = 6.76$ Hz, 2H), 2.25- 2.32 (m, 1H), 1.12-1.40 (m, 36H), 0.75-0.84 (m, 6H) ^{13}C NMR (100 MHz, CDCl_3 , δ): 140.7, 140.1, 139.5, 136.6, 122.9, 121.4, 121.2, 118.3, 113.0, 59.1, 38.1, 30.9, 30.5, 28.9, 28.6, 28.5, 28.3, 25.2, 21.6, 13.0

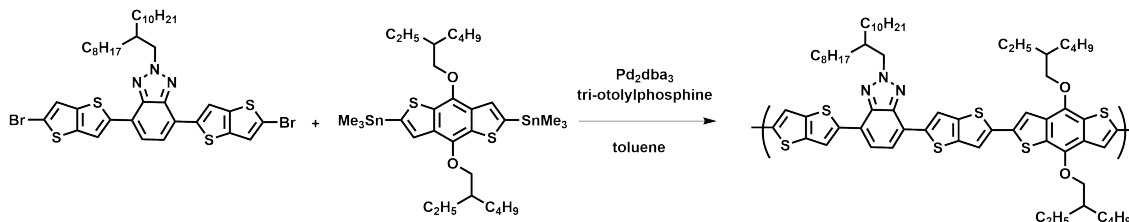
2.10.15. Synthesis of 4,7-bis(5-bromofuran-2-yl)-2-(2-octyldodecyl)-2H-benzo[d][1,2,3]triazole



4,7-Di(furan-2-yl)-2-(2-octyldodecyl)-2H-benzo[d][1,2,3]triazole (275 mg, 0.517 mmol) was dissolved in dichloromethane (10 mL) and glacial acetic acid (10 mL). NBS (211.63 mg, 1.18 mmol) was added to reaction medium temperature in portion under darkness. The reaction mixture was stirred for 16 hours and washed with dichloromethane and water. Organic phase was dried over MgSO_4 . Solvent was evaporated under reduced pressure and crude product was purified through column chromatography (petroleum ether: dichloromethane, 1:7) Pure product was obtained as a pale yellow solid with yield of 42% (150 mg). Stability of the compound was low so used directly for polymerization reaction.

^1H NMR (400 MHz, CDCl_3 , δ): 7.67 (s, 2H), 7.32 (d, $J = 3.40$ Hz, 2H), 6.42 (d, $J = 3.35$ Hz, 2H), 4.62 (d, $J = 6.61$ Hz, 2H), 2.15- 2.23 (m, 1H), 1.10-1.33 (m, 36H), 0.76-0.83 (m, 6H)

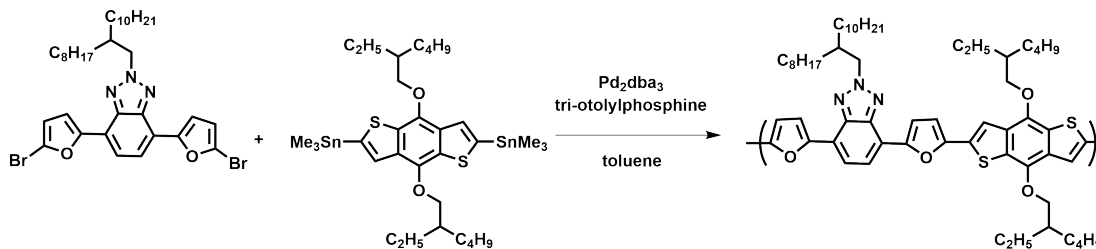
2.10.16. Synthesis of PTTBTBDT



4,7-Bis(5-bromothiopheno[3,2-b]thiophen-2-yl)-2-(2-octyldodecyl)-2H benzo[d][1,2,3] triazole (120 mg, 0.144 mmol) and 2,6-bis(trimethylstannyl)-4,8-bis(2-ethylhexyloxy)benzo[1,2-b:4,5-b']dithiophene (116.7 mg, 0.1512 mmol) were dissolved in 4 mL of dry toluene and solution was deoxygenated by bubbling nitrogen through the solution for 30 min. Pd₂(dba)₃ (5% mmol, 7.22 mg) and tri-o-tolylphosphine (40% mmol, 18.34 mg) was added reaction medium and system was deoxygenated by bubbling nitrogen through the solution for 10 min. Then solution was heated to 120 °C for 24 hours. 2-Bromothiophene and 2-tributylstanylthiophene was added to reaction medium as end-cappers. The polymer was then precipitated into methanol and then washed sequentially with methanol, acetone, and hexane in a Soxhlet extractor. The polymer was then extracted with chloroform, passed through a plug of silica gel and concentrated under vacuum. Then, it was precipitated into methanol to afford purple solids (120 mg, 74.3%).

GPC and NMR of polymer were not be taken due to low solubility of polymer

2.10.17. Synthesis of PFBTBDT



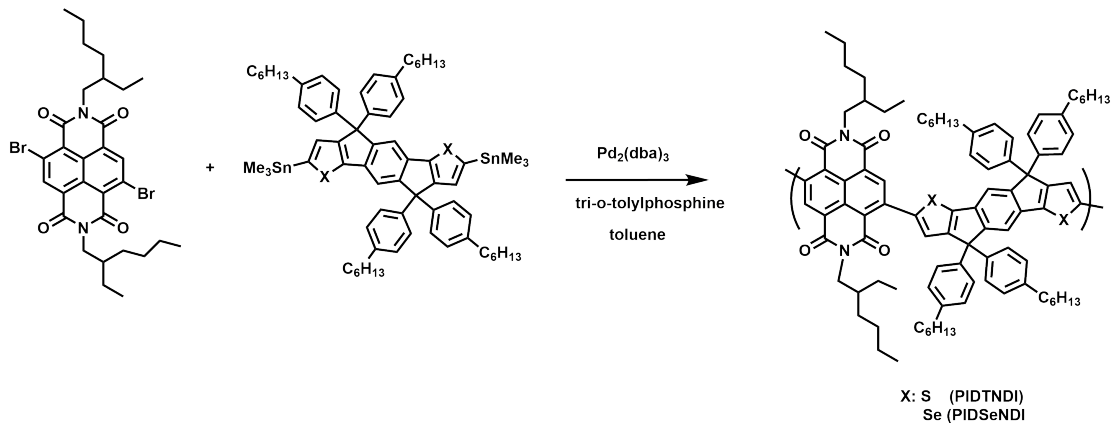
4,7-Bis(5-bromofuran-2-yl)-2-(2-octyldodecyl)-2H-benzo[d][1,2,3] triazole

(100 mg, 0.145 mmol) and 2,6-bis(trimethylstannyl)-4,8-bis(2-ethylhexyloxy)benzo [1,2-b:4,5- b'] dithiophene (117 mg, 0.1525 mmol) were dissolved in 4 mL of dry toluene and solution was deoxygenated by bubbling nitrogen through the solution for 30 min. Pd₂(dba)₃ (5% mmol, 7.66 mg) and tri-*o*-tolylphosphine (40% mmol, 18.5 mg) was added reaction medium and system was deoxygenated by bubbling nitrogen through the solution for 10 min. Then solution was heated to 120 °C for 24 hours. 2-bromothiophene and 2-tributylstanylthiophene was added to reaction medium as end-cappers. The polymer was then precipitated into methanol and then washed sequentially with methanol, acetone, and hexane in a Soxhlet extractor. The polymer was then extracted with chloroform, passed through a plug of silica gel and concentrated under vacuum. Then, it was precipitated into methanol to afford red solids (120 mg, 84.7%).

GPC: M_n =17.5 kDa, PDI 1.83

¹H NMR (500 MHz, CDCl₃) δ: 7.54, 6.79, 6.49, 4.67 (br), 4.16 (br), 1.1- 2.05 (br m), 0.75-0.9 (br m)

2.10.18. Synthesis of PIDTNDI and PIDSeNDI



4,4,9,9-Tetrakis(4-hexylphenyl)-2,7-bis(trimethylstannyl)-indaceno[1,2-b:5,6-b']dithiophene (IDT-ditin) and 4,4,9,9-Tetrakis(4-hexylphenyl)-2,7-bis(trimethylstannyl)-indaceno[1,2-b:5,6-b']diselenophene (IDSe-ditin) were synthesized according to previously published procedure [77]. IDT-ditin (150 mg, 0.121 mmol) and NDI (76.6 mg, 0.118 mmol) (for PIDTNDI) or IDSe-ditin (150 mg, 0.113 mmol) and NDI (69.8 mg, 0.1077 mmol) (for PIDSeNDI) were dissolved in 4 mL of dry toluene and solution was degassed with freeze/pump/throw cycles to get rid of oxygen. $\text{Pd}_2(\text{dba})_3$ (5% mmol) and tri-*o*-tolylphosphine (40% mmol) was added reaction medium and mixture was degassed two more times. Then solution was heated to 120 °C for two days. 2-bromothiophene and 2-tributylstanylthiophene was added to reaction medium as end-cappers. The polymer was then precipitated into methanol and then washed sequentially with methanol, acetone, and hexane in a Soxhlet extractor. The polymer was then extracted with chloroform, passed through a plug of silica gel and concentrated under vacuum. Then, it was precipitated into methanol to afford green solids.

PIDTNDI (yield: 80 mg, 48%)

GPC: $M_n = 57.2$ kDa, PDI 2.02.

^1H NMR (500 MHz, CDCl_3) δ 8.79 (s), 7.56 (s), 7.33 (s), 7.30 (br s), 7.14 (s), 7.13 (s), 4.13 (br), 2.55-2.68 (br m), 1.90- 2.20 (br m), 1.60-1.69 (br m), 1.26-1.45 (br m), 0.85-0.98 (br m)

PIDSeNDI (yield: 120 mg, 75%)

GPC: $M_n = 34.2$ kDa, PDI 1.88

^1H NMR (500 MHz, CDCl_3) δ 8.78 (s), 7.51 (s), 7.45 (s), 7.13 (s), 7.11 (s), 4.10 (br), 2.55-2.65 (br m), 1.8- 1.99 (br m), 1.59-1.67 (br, m) 1.21-1.41 (br m), 0.85-0.95 (br m)

CHAPTER 3

RESULTS AND DISCUSSION

Chemically and electrochemically synthesized conjugated polymers based on donor-acceptor (DA) approach were developed for electrochromic and organic solar cell application. Structure of p-type conjugated polymers based on benzotriazole (BTz) and n-type conjugated polymers based on naphthalenedimide (NDI) that were synthesized in the content of this thesis are outlined in **Figure 22**. BTz based conjugated polymers are developed for electrochromic and organic solar cell applications. NDI based conjugated polymers are developed for nonfullerene all polymer solar cell applications.

BTz were coupled with dithienopyrrole (DTP), benzodithiophene (BDT), furan, and thieno[3,2-*b*]thiophene and their optical, electrochemical, electrochromic, and photovoltaic properties were investigated. Donor units were selected according to their strength to control band gap that specifically changes optical and electronic properties and to improve electrochromic properties in terms of switching time and optical contrast.

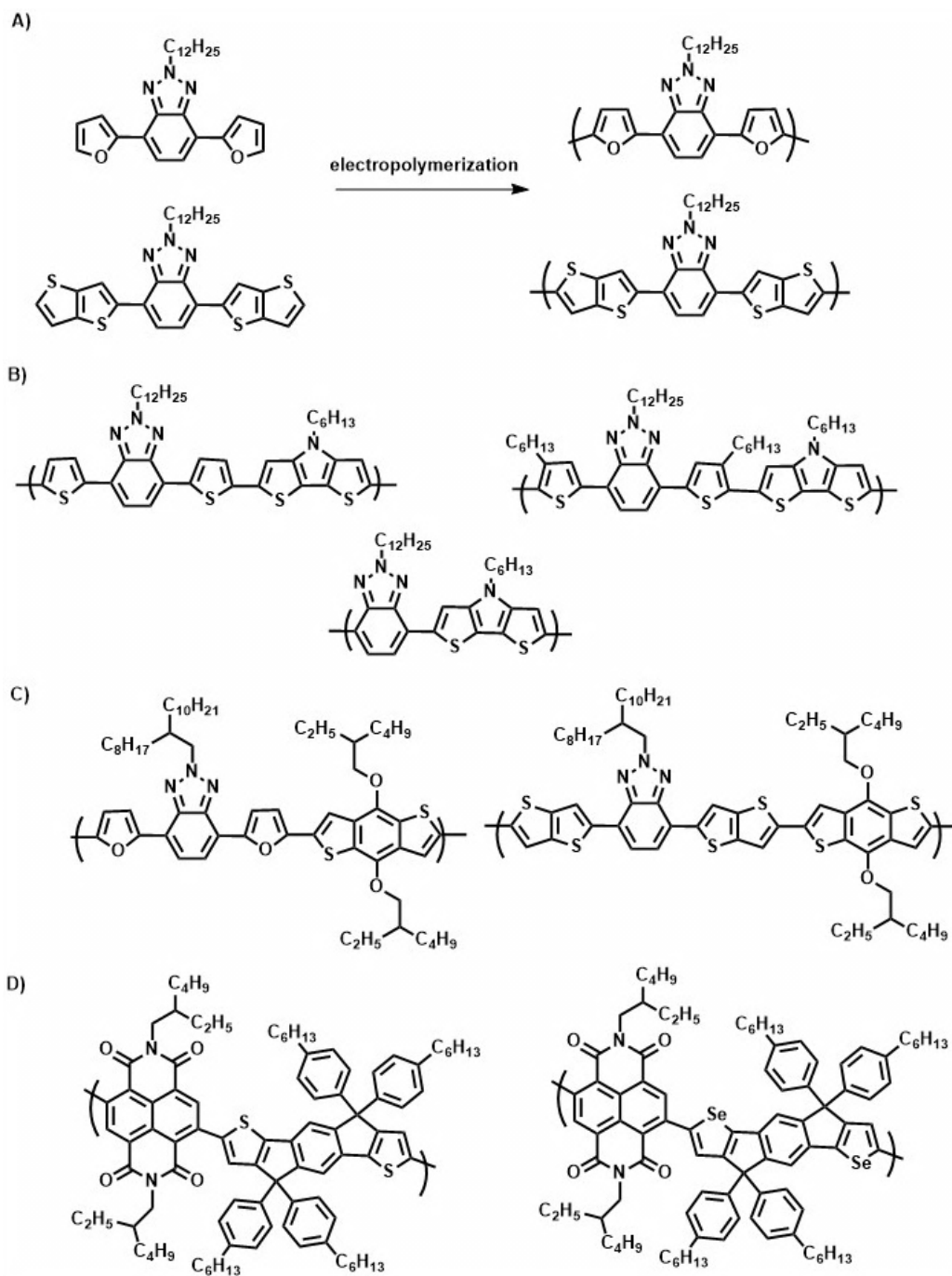


Figure 22 Chemical structures of donor-acceptor type conjugated polymers developed in this study

3.1. Furan and thieno[3,2-*b*]thiophene end capped benzotriazole derivatives

In the first part, BTz were selected as an acceptor units and coupled with furan and thieno[3,2-*b*]thiophene to investigate the effect of different donor units on electrochromic properties. BTz bearing conjugated polymers reveal tremendous electronic and optical properties by altering the D groups [74, 78-81]. These promising results have driven our curiosity to synthesize new DAD type monomers by changing D groups. Structure of BTz based polymers synthesized in this study and previous studies outlined in **Figure 23**.

Furan is a less studied five-membered heterocycle compared to their analogs (i.e, thiophene, selenophene and pyrrole) since furan can undergo ring-opening side reactions during polymerization in the presence of Bronsted acid and resulting polymers show low stability [82]. Besides, polymers are likely to overoxidize by oxidative electrochemical polymerization of furan [83]. DA theory and electropolymerization of terfuran have been developed in order to circumvent these problems [84]. Therefore, in this study DA approach was utilized to synthesize furan containing conjugated polymers. In addition to furan, thieno[3,2-*b*]thiophene is utilized another donor unit to couple with BTz. Thieno[3,2-*b*]thiophene not only has fused structure that facilitates high delocalization of the π -electrons over the polymer backbone by increasing planarity and linearity of polymer backbone but also causes red-shifted absorption and reduced band gap compared to their single counterpart (thiophene) [85-87]. Therefore, coupling BTz with furan and thieno[3,2-*b*]thiophene will not only provide significant information about their effect on optical, electronic, and electrochromic applications but also will provide good comparison of BTz containing polymers in terms of aromaticity and donor strength.

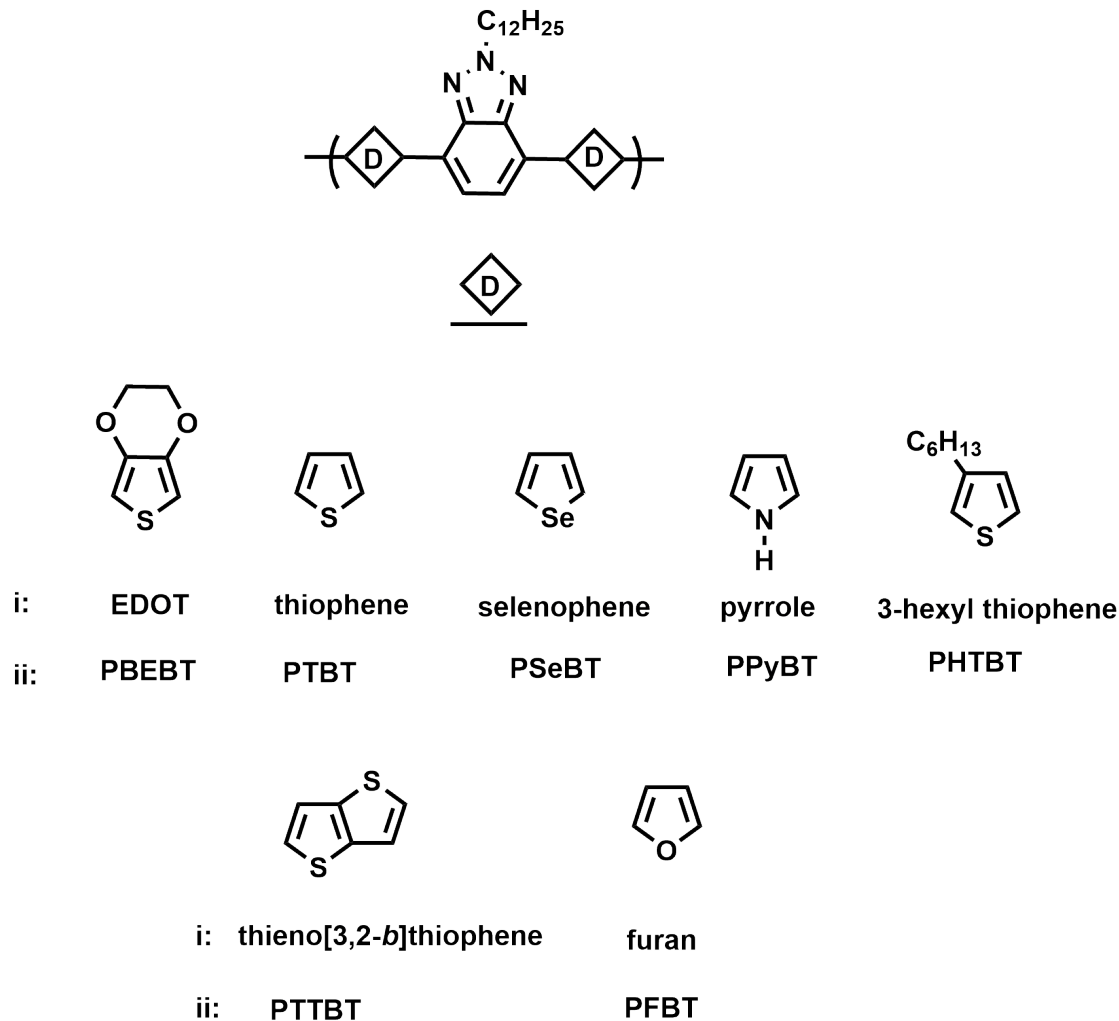


Figure 23 Chemical structures and (i) donor groups, (ii) abbreviations of BTz bearing DAD type polymers

3.1.1. Synthesis of TTBT and FBT

The synthetic route to **TTBT** and **FBT** is depicted in **Figure 24**. 4,7-dibromo-2-dodecyl-2Hbenzo[d][1,2,3]triazole (**2**) [74] and tributyl(thieno[3,2-*b*]thiophen-2-yl)stannane (**4**) [75] were synthesized according to previously published procedures. Stille coupling of **2**

with **3** and tributyl(furan-2-yl)stannane (**4**) afforded **TTBT** and **FBT** as yellow solid and a light yellow solid in 45% and 43% yields, respectively.

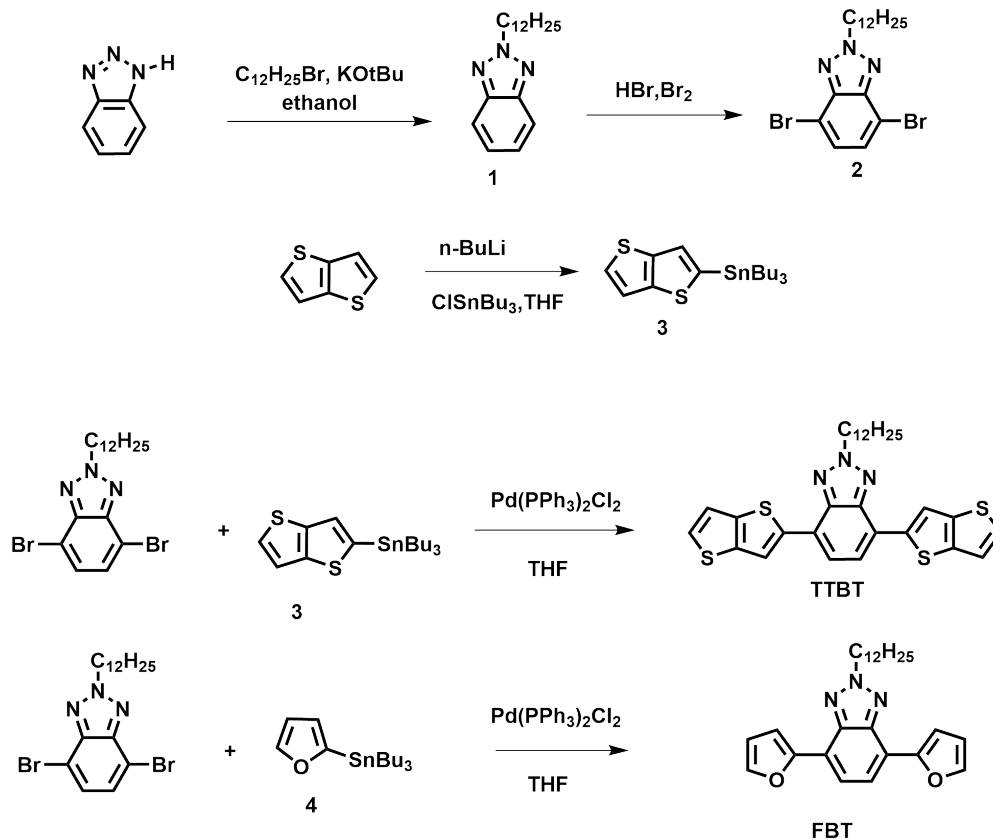


Figure 24 Synthetic routes of **TTBT** and **FBT**

3.1.2. Electropolymerization of **TTBT** and **FBT**

Electropolymerization of **FBT** and **TTBT** was performed with cyclic voltammetry. It was performed in a 0.1 M $TBAPF_6$ and 1×10^{-2} M monomer solution (**FBT** or **TTBT**) between the potentials -0.3 and 1.25 V for **FBT** and -0.15 and 1.4 V for **TTBT** at a scan

rate of 100 mV/s (**Figure 25**) vs Ag wire reference electrode. Electrochemical polymerizations were carried out in 1 mL, 5:95 (v:v) , ACN:DCM mixture for **FBT**. Although, both monomers bear dodecyl pendant chains on BTz unit, **TTBT** was less soluble in ACN due to fused structure of thieno[3,2-*b*]thiophene. Therefore, more DCM was added to solution in order to acquire sufficient solubility and electrochemical polymerization was achieved in 1 mL, 50:50 (v:v) DCM/ACN mixture for **TTBT**.

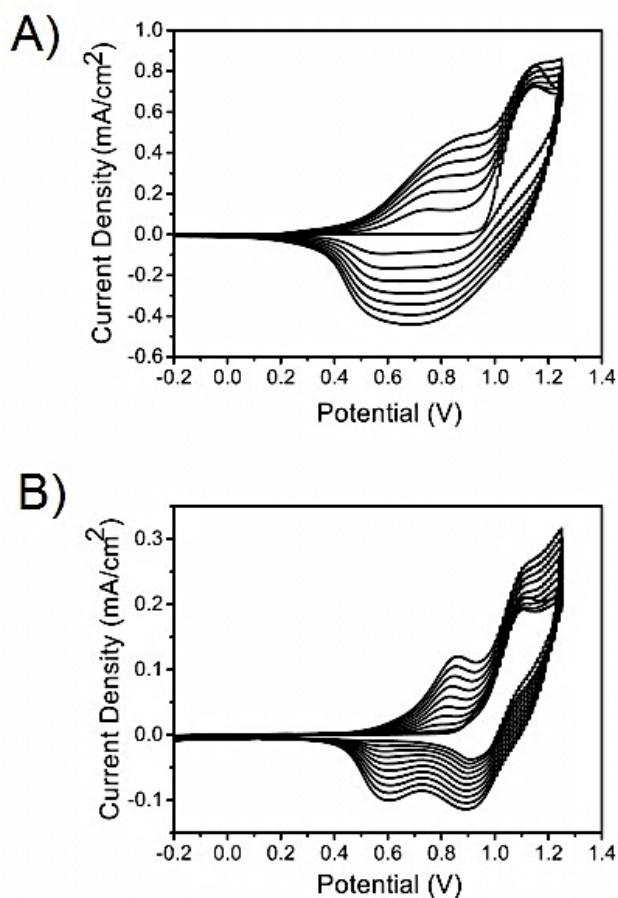


Figure 25 Electropolymerization of FBT (A) and TTBT (B) in 0.1 M TBAPF₆/dichloromethane/acetonitrile solutions at a scan rate of 100 mV/s

As mentioned before, monomer oxidation of **FBT** was very critical since high oxidation potential of furan prevents the formation of proper polyfuran film due to overoxidation of polymer film. Monomer oxidation should be lower than oxidation potential of furan (1.7 V) to circumvent this problem. As shown in **Figure 26**, **FBT** monomer oxidation was observed at 1.15 V. This value is quite lower than oxidation potential of furan (1.7 V) [88, 89] or even than that of terfuran (1.5 V) [84]. Relatively low oxidation potential of **FBT** allowed formation of conducting polymer film on ITO. After the first cycle, oxidation peak at 0.8 V and its reverse cathodic peak at 0.6 V appeared.

Similarly, electrochemical polymerization of **TTBT** was achieved by CV. Monomer oxidation of **TTBT** was 0.1 eV higher than **FBT** and appeared at 1.25 V. After the first cycle, oxidation peak at 0.96 V and its reverse cathodic peak appeared at 0.6 V. Repetitive cycles accompanied with increase in current density for polymers redox couple clearly indicates the increasing conducting surface area of the electrode due to formation of conjugated polymer film on ITO surface.

After electropolymerization of **FBT** and **TTBT**, single scan cyclic voltammograms of **PFBT** and **PTTBT** were recorded in a monomer free solution of 0.1 M TBAPF₆/acetonitrile solvent-electrolyte couple versus Ag wire pseudo reference electrode to confirm polymers electrochromic behavior (i.e its color change upon applied potential). **PFBT** oxidation peak observed at 0.88 V with a reversible couple at 0.55 V whereas **PTTBT** oxidation peak observed at 0.96 V with a reversible couple at 0.6 V.

As a common property for all BTz based polymers, **PFBT** and **PTTBT** also revealed n doping properties confirmed with reversible redox couples at -2.3/-1.50 V and -1.99/-1.58 V, respectively versus the same reference electrodes. HOMO and LUMO energy level of **PFBT** and **PTTBT** were determined from oxidation and reduction onset potentials. Corresponding HOMO-LUMO energy level of **PFBT** and **PTTBT** was calculated as -5.36/ -3.4 and -5.24/-3.22, respectively. **PFBT** and **PTTBT** possess

electrochemical band gap (E_g^{oc}) of 1.96 and 2.02 eV, respectively. **PTTBT** revealed relatively higher HOMO energy level compared to **PFBT**.

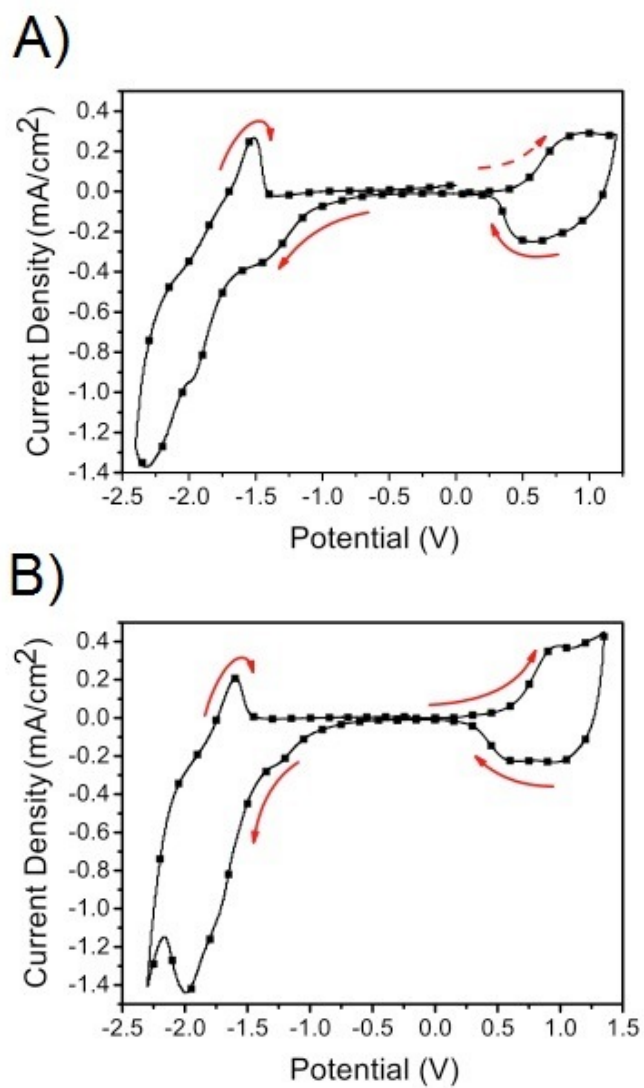


Figure 26 Single scan cyclic voltammograms of PFBT (A) and PTTBT (B) in monomer free, 0.1 M TBAPF₆/acetonitrile solvent-electrolyte couple versus Ag wire pseudo reference electrode

The scan rate dependence of peak currents was examined in a monomer-free electrolyte solution (Figure 27). A linear relationship between the peak current and scan rate illustrates that the films were well adhered and the electrochemical processes were reversible and non-diffusion-controlled.

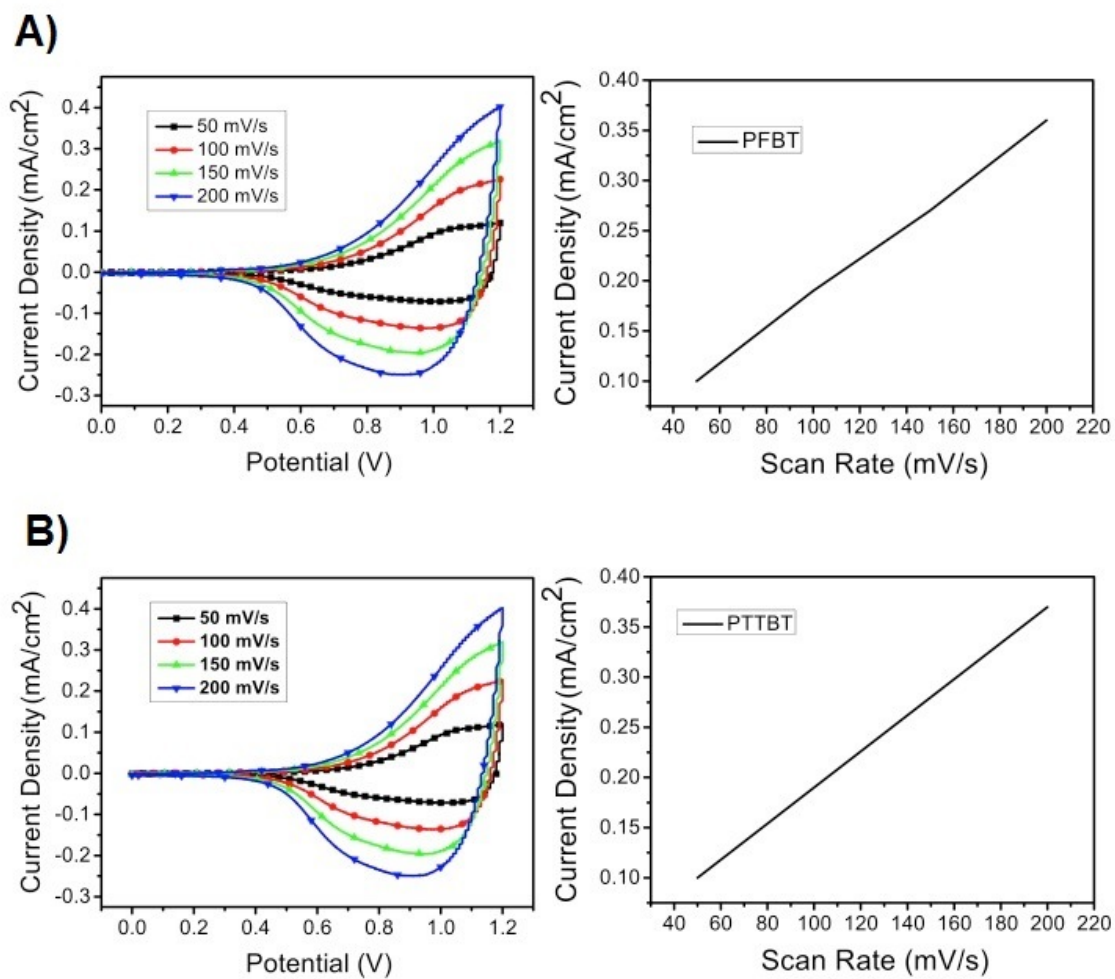


Figure 27 Cyclic voltammograms of A) **PFBT** B) **PTTBT** in 0.1 M TBABF₆/ACN at scan rates of 50, 100, 150, 200, and 250 mV/s

3.1.3. Spectroelectrochemistry

Spectroelectrochemical properties of the **PFBT** and **PTTBT** were investigated between 0.5 and 1.4 V and 0.5 and 1.3 V in 0.1 M TBAPF₆/ ACN electrolyte-solvent couple and UV-vis-NIR spectra were recorded upon external bias. Electrochemically produced polymer films on ITO were reduced to their neutral states at -0.5 V constant potential in order to remove any trapped charge and dopant ion during electrochemical polymerization prior to spectroelectrochemical analysis. The absorbance changes were noted as the potential was gradually increased. As seen in **Figure 28**, **PTTBT** has a dominant wavelength in the visible region centered at 500 nm whereas **PFBT** revealed a relatively red shifted maximum absorption in the visible region at 524 nm. Optical band gaps (E_g^{opt}) for **PTTBT** and **PFBT** calculated from the onsets of π - π^* transitions as 1.87 eV and 1.9 eV, respectively. Calculated electrochemical band gaps were comparatively higher than the ones estimated from π - π^* transition (optical band gap) since after absorption of light, bound electron and hole pairs (exciton) forms in optical studies in contrast to the ions in the electrochemical one. In addition to this, polymer interchain interaction and interface barrier between polymer film and electrode surface can cause this difference [87].

Upon stepwise oxidation of **PTTBT**, the absorption in the visible region started to decrease as the new bands were intensified at 710 nm and 1220 nm. The increased absorbance in the electronic absorption spectra of the polymer films in lower energy regions indicates the formations of charge carriers such as polarons and bipolarons. Since polymer switched between red and blue as its two extreme states, partial oxidation of the polymer film resulted in different transition colors (**Figure 29**). Polaronic absorption at 710 nm emerged with oxidation was tailed into the visible region, which contributed to the color of the polymer. However, well separation of neutral and polaronic absorption bands from each other hindered the observation of black color,

which was detected for **PFBT** where an identical intensity for neutral and polaronic bands was achieved. Instead, different shades of brown and green colors were observed at different doping levels due to different contributions of absorption bands to the resulting color. Neutral and fully oxidized state absorption maxima of the polymer films in the visible were different by ca. 25 nm. Although, thieno[3,2-*b*]thiophene has more electron rich compound compared to furan, λ_{max} of **PFBT** in the neutral film was red shifted to 525 nm. Stepwise oxidation resulted in a different spectral response for **PFBT** compared to its BTz analogues. All other Btz based DAD type polymers revealed formation of simultaneous polaronic and bipolaronic bands at early doping stages, bipolaronic absorption of **PFBT** was not obviously appeared as for the others. Nonetheless, small fractions of bipolaronic transitions were formed between band gap states as a consequence of electronic coupling on the polymer backbone, which was confirmed by a decrease in polaron absorption bands at potentials higher than 1.0 V.

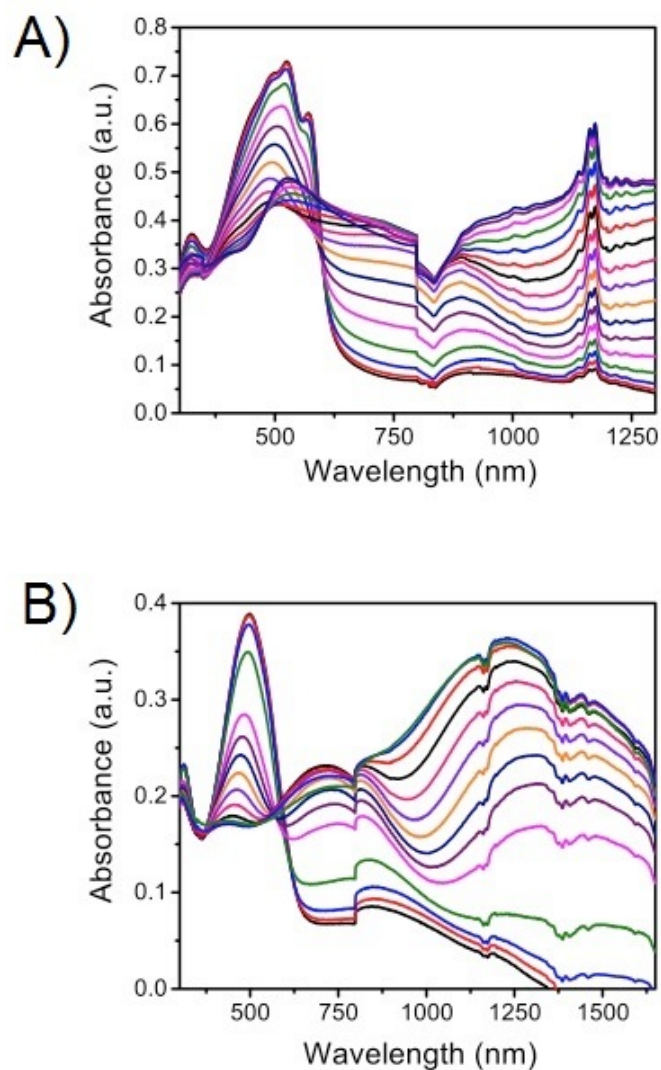


Figure 28 UV-vis-NIR spectra of PFBT (A) between 0.5 and 1.3 V and PTTBT (B) between 0.5 and 1.4 V

Reduction of neutral polymer films **PTTBT** and **PFBT** resulted in color changes since the absorption of n-doped chains enabled appearance of new colors in an accessible

potential range. **PFBT** showed highly transmissive n-doped states, **PTTBT** emerged a blue colored n-doped state, which is identical with the oxidized state color of the polymer. It is noteworthy to state that **PTTBT** has the same spectral response upon both p and n-doping. This is not likely to be seen due to the energy difference between positively and negatively charged polymer chains [8, 49] (**Figure 29**).

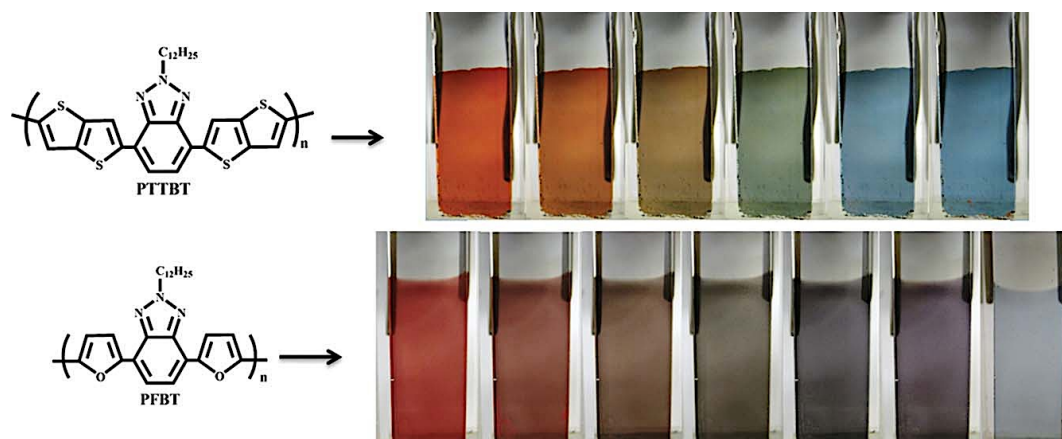


Figure 29 Chemical structures and colors of **PTTBT** and **PFBT**

3.1.4. Kinetic Studies

Switching time is defined as the time required for the polymer to attain its 95% contrast value between its neutral and fully oxidized states. In the literature, 95% of the full contrast and the corresponding switching times are used because of the insensitivity of human eye to 5% of color change. Chronoamperometry studies were carried out to monitor the changes in transmittance as a function of time while sweeping the potentials between neutral and fully oxidized states that is known as optical contrast and switching time of the polymer film at its maximum absorption wavelengths was calculated. During

the experiment, optical contrasts of the polymer films at corresponding wavelengths were recorded using a UV-vis-NIR spectrophotometer while the potentials were switched between 0.0 V and +1.4 V for **PTTBT** and 0.0 V and 1.2 V for **PFBT** within 5 s time intervals. **PTTBT** revealed 30% optical contrast at 500 nm and 60% at 1220 nm (**Figure 30**). The polymer film switched between two extreme states in 1.2 s (500 nm) and 0.8 s (1220 nm). **PFBT** exhibited lower optical contrast values in visible region compared to that of **PTTBT** due to its extant absorption at around 500 nm. In NIR region, polymer film **PFBT** showed 58% transmittance change within 1.3 s. Unlike **PTTBT**, **PFBT** was relatively unstable upon repetitive switching in visible region, which can be deduced from **Figure 30**.

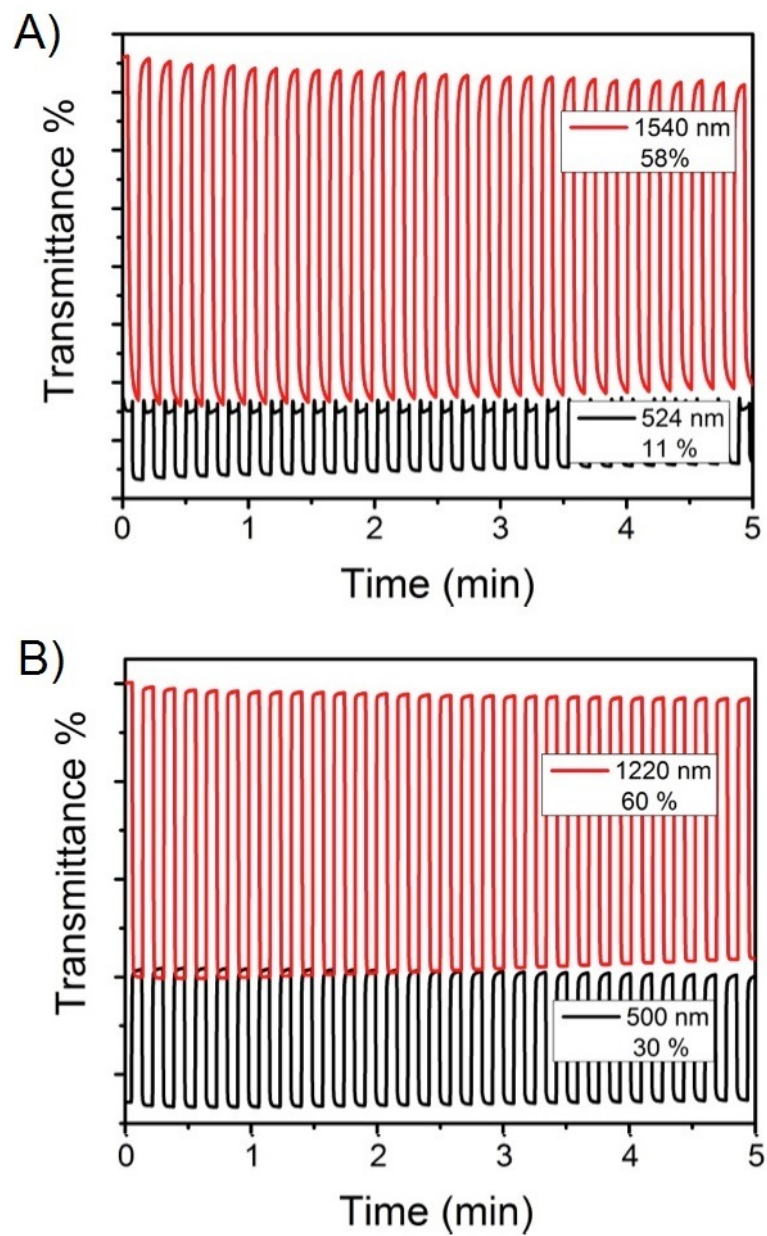


Figure 30 Percent transmittance changes of PFBT (A) and PTTBT (B) film in monomer free, 0.1 M TBAPF₆/acetonitrile solution at its maximum absorption wavelengths

3.1.5. Comparison with other benzotriazole based conjugated polymers

Structures of all BTz based conjugated polymers with different donor units are outlined in **Figure 23** and optical and electrochemical properties of conjugated polymers are summarized in **Table 1**. When oxidation potential of monomers were compared, all DAD type monomers with BTz as the acceptor unit revealed the lower oxidation potentials than those of their single donor units since the DAD monomer has an extended conjugation. However, incorporation of acceptor BTz unit has affected each monomer differently. **TTBT** possesses thieno[3,2-b]thiophene unit which provides an electron rich structure with extended conjugation and is expected to have lower monomer oxidation than that of different donor substituted BTz based monomers, it revealed the highest one among all. This is attributed to the higher resonance stabilization energy of the fused rings than that of single ring heterocycles, which lowers the HOMO and makes more difficult to extract an electron from the system [91]. Although, selenophene has lower oxidation potential than that of thiophene, their DAD monomer with BTz gets oxidized at the same potential. This indicates that interaction between donor and acceptor or their match plays the key role on electronic characteristic of resulting monomers or polymers. Keeping the acceptor unit identical (2-dodecyl-benzotriazole), donor characters or donor acceptor interactions in resulting polymers can be compared. As seen from **Table 1**, the lowest polymer oxidation was exhibited by **PBEBT** that concludes that the donating character is highest for **PBEBT** among all BTz based polymers. In the same manner, electron donating character is decreasing in the order; **PBEBT** > **PPyBT** > **PFBT** > **PHTBT** > **PTTBT** > **PTBT** ~ **PSeBT**.

Table 1 Summary of optical and electrochemical properties of benzotriazole based polymers

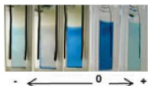
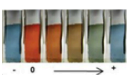
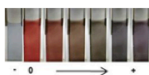
Polymer	$E_{\text{mon}}^{\text{ox}}$ (V)	$E_{\text{p-doping}}$ (V)	$E_{\text{p-dedoping}}$ (V)	$E_{\text{n-doping}}$ (V)	$E_{\text{n-dedoping}}$ (V)	λ_{max} (nm)
PBEBT	0.97	0.23	-0.04	-1.71	-1.62	618
PTBT	1.2	1	0.6	-1.6	-1.4	503
PSeBT	1.2	1	0.8	-1.7	-1.3	511
PPyBT	0.7	0.4	0.2	-1.67	-1.05	577
PHTBT	1.2	0.9	0.6	-1.97	-1.8	450
PTTBT	1.25	0.96	0.6	-1.99	-1.58	500
PFBT	1.15	0.88	0.55	-2.3	-1.5	524

Achievable colors and kinetic properties of BTz based polymers are summarized in **Table 2**. Except **PBEBT** and **PPyBT** which were blue, all other BTz based polymers were red in their neutral states with λ_{max} at around 500 nm. Visible polaronic state absorptions for all these red polymers allowed achieving multicolored electrochromic polymers and specifically **PTBT** revealed all RGB colors. Since polaronic absorptions for **PBEBT** and **PPyBT** are at lower energy regions and very slightly tailed into visible region, oxidation of these polymers resulted in highly transmissive states. However, all other BTz based polymers including **PFBT** and **PTTBT** revealed colored oxidized states. Since polaronic absorptions for **PBEBT** and **PPyBT** are at lower energy regions and very slightly tailed into visible region, oxidation of these polymers resulted in highly

transmissive states. Moreover, although most of the BTz based polymers including **PFBT** showed highly transmissive n-doped states, **PTTBT** emerged a blue colored n-doped state, which is identical with the oxidized state color of the polymer. **PFBT** switched between six colored states that are the maximum achievable color causing oxidation of single monomer.

Optical contrast of **TTBT** was competitive with other BTz based conjugated polymers. However, **PFBT** exhibited lower optical contrast that can be assigned to its extent absorption at around 500 nm. Insertion of thieno[3,2-*b*]thiophene and furan in polymer backbone resulted in fast switching time. This situation can be correlated with the ionic conductivity of the electrolyte, magnitude of the applied potential, film thickness, film morphology, and ion diffusion.

Table 2 Summary of colors and kinetic properties of benzotriazole-based polymers

Donor Unit	Colors	Optical contrast	Switching time
 R: -H or C ₆ H ₁₃		35 % 35 %	2.4 1.4
		32 %	2.4
		30 %	0.5
		53 %	1.1
		30 %	0.8
		11 %	1.7

In summary, electrochemically synthesized BTz based DAD type polymers **PTTBT** and **PFTBT** were characterized in terms of their electrochemical and spectral properties. Relatively low monomer oxidation for FBT (1.15 V) allowed formation of conjugated polymer film although furan containing monomers although their polymers tend to get overoxidized easily. Polymer oxidation and reduction characteristics for PTTBT and **PFBT** showed that both polymers have ambipolar characteristics with relatively low HOMO / LUMO energy levels. Comparison among all BTz based monomers showed that increasing electron density of donor unit is decreasing the monomer oxidation potential of the monomer to some extent where donor acceptor match is an important effect on electronic properties of DAD material. Spectroelectrochemical studies showed that stepwise oxidation of **PTTBT** and **PFBT** allow multicolored electrochromic states to be detected. Reported electrochemical and optical properties of polymers suggest that **PTTBT** and **PFBT** are great candidates for nonemissive electrochromic device applications as all BTz based conjugated polymers, which will be used as active materials in future display technology.

3.2. Dithienopyrrole and benzotriazole based conjugated polymers

Recent studies showed that incorporation of fused structures in polymer backbone resulted in enhancement of charge mobilities and intermolecular interaction. Among fused structures, bithiophene containing conjugated polymers having different heteroatoms (nitrogen, silicon, phosphorous, carbon, and germanium) exhibit promising optical and electrochemical properties. Dithienopyrrole (DTP) has been indicated as a strong donor unit for the synthesis of low energy gap conjugated systems since DTP causes decrease in the band gap of the polymers by raising HOMO energy level. Furthermore, the presence of bridging nitrogen atom contributes to enhancement of the hole-transporting properties and processability of conjugated polymers via aromatic and

aliphatic groups substituents without disturbing planarity [91-98]. Therefore, in this part we have coupled BTz unit with DTP building block to evaluate the effect of this unit on electrochromic properties in terms of optical contrast and switching time since decrease in band gap directly affect the properties of resulting polymer. Besides, thiophene and 3-hexylthiophene are inserted as the conjugated π -bridging groups. Although, little attention is given to conjugated π -bridging groups in donor-acceptor (D-A) architectures, insertion of them as a spacer plays a crucial role on properties of conjugated polymers. They contribute to the π -electron density and mediate the electronic interaction between donor and acceptor moieties. Besides, π -bridges affect the structural conformation of the polymer chains such as rigidity, planarity, and torsion angles on the backbone [87].

3.2.1. Synthetic Pathway

The synthesis of the monomer and polymers are outlined in **Figure 31**. 4,7-Dibromo-2-dodecyl-2H-benzo[d][1,2,3]triazole [74] (**2**), 4,7-bis(5-bromothiophen-2-yl)-2-dodecyl-2H-benzo[d][1,2,3]triazole (**3**) [76], 4,7-bis(5-bromo-4-hexylthiophen-2-yl)-2-dodecyl-2H-benzo[d][1,2,3]triazole [76] (**4**) were synthesized according to the previously published procedures. 4-hexyl-2,6-Bis(tributylstannyl)-4H-dithieno[3,2-b:2',3'-d]pyrrole (DTP-ditin) was synthesized from stannylation of 4-hexyl-4H-dithieno[3,2-b:2',3'-d]pyrrole (**1**) in the presence of n-BuLi and tributyltinchloride. The polymerization of DTP-ditin was carried out via a Stille polymerization with **2**, **4**, and **5** in the presence of catalytic $\text{Pd}_2(\text{PPh}_3)_2\text{Cl}_2$ to synthesize **PDTPBTz**, **PDTPTBT** and **PDTPHTBT**, respectively. Solubility of polymers is tested in common organic solvents such as toluene, THF, chloroform, and dichloromethane. All polymers showed good solubility in these solvents. Characterization of polymers is performed by ^1H NMR. Molecular weight of the polymers is determined by GPC with polystyrene standards using THF as the eluent. The **PDTPBTz**, **PDTPTBT** and **PDTPHTBT** have the number average

molecular weight (M_n) of 72.1 kDa, 3.2 and 6.3 with a polydispersity indexes (PDI) of 7.9, 6.7 and 5.1, respectively. **PDTPTBT** has a low molecular weight compared to **PDTPBTz** and **PDTPHTBT**. Insertion of thiophene ring cause the decrease in solubility and thus result low molecular weight of **PDTPTBT**. Thermogravimetric analysis (TGA) was utilized to determine the specific mass loss of the polymer. During the TGA run, the polymer film was heated from 25 °C to 900 °C at a heating rate of 10 °C/min under inert atmosphere. Decomposition temperature (Td) of the **PDTPBTz**, **PDTPTBT**, and **PDTPHTBT** are observed at 310.8 317.5 and 300 °C, respectively.

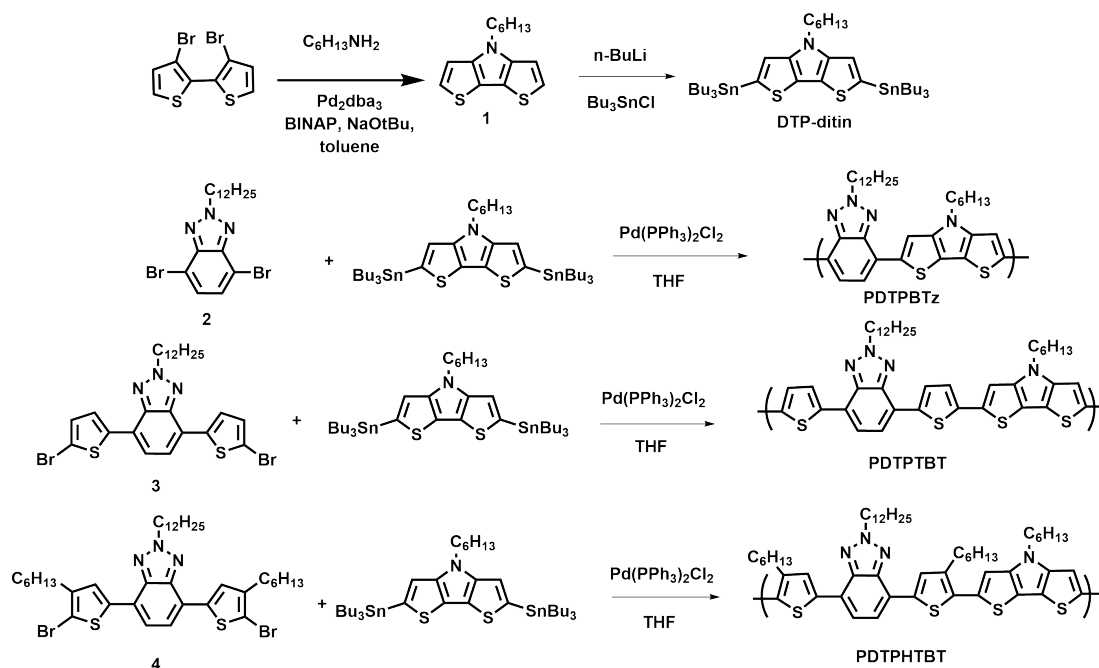


Figure 31 Synthetic pathway for benzotriazole and dithienopyrrole based polymers

3.2.2. Electronic Properties

The frontier orbital energy levels (HOMO and LUMO energy levels) of the **PDTPBTz**, **PDTPBT**, and **PDTPHTBT**, were measured using CV of polymer films. Polymers are dissolved in CHCl_3 (5 mg/mL) and spray coated onto ITO working electrode, and CV was carried out in 0.1 M of TBAPF_6 in acetonitrile solution with Ag wire pseudo reference electrode calibrated against Fc/Fc^+ . During oxidation, all polymers revealed a quasi-reversible oxidation and oxidation potentials of the polymers affected by the presence of thiophene and 3-hexylthiophene. Due to the inserting electron-rich thiophene rings in **PDTPBT** chains, polymer exhibited lower oxidation potential (0.75 V) compared to **PDTPBTz** (0.79 V). On the other hand, **PDTPHTBT** showed the highest oxidation potential of 1.14 V due to interannular rotation and corruption of planarity in polymer chains. This is consistent with the literature. N-doping properties of polymers were investigated and **PDTPBT** and **PDTPHTBT** films revealed reversible reduction couples at $-1.96/-1.72$ V and $-1.91/-1.51$ V, respectively, while **PDTPBTz** showed an irreversible reduction as seen in **Figure 32**.

Electrochemical properties of polymers are introduced in **Table 3**. As mentioned before, **PDTPBT** and **PDTPHTBT** showed reversible oxidation and reduction cycles. However, **PDTPBTz** only exhibited reversible oxidation. Therefore, LUMO energy level of **PDTPBTz** was calculated using the HOMO energy level and the optical band gap. **PDTPBTz** revealed the highest HOMO level as -4.75 eV. Incorporation of the π -bridges has important impact on both HOMO and LUMO energy levels of the polymers. Both **PDTPBT** and **PDTPHTBT** have lower HOMO energy levels, i.e. -5.19 and -5.70 eV, respectively. The exact LUMO energy level of **PDTPBT** and **PDTPHTBT** were calculated from reduction onset potential and found as -3.45 and -3.91 eV, respectively. Corresponding LUMO energy levels of **PDTPBT** and **PDTPHTBT** were determined to be -3.45 and -3.91 eV with the corresponding E_g^{ec} of 1.74 and 1.79 eV. Approximate

LUMO energy level of **PDTPBTz** is calculated as -3.03 eV. Among the polymers, **PDTPHTBT** showed the low-lying LUMO and HOMO energy levels.

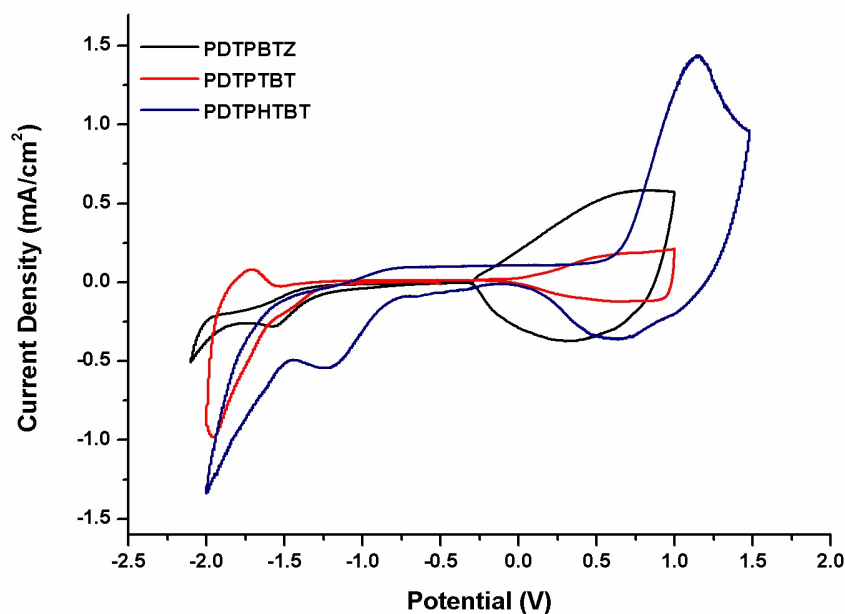


Figure 32 Cyclic voltammograms of the polymer films on ITO electrode in 0.1 M TBAPF₆, CH₃CN solution with a scan rate of 100 mV/s.

3.2.3. Optical Studies

Figure 33 shows the absorption spectra of the polymers in dichloromethane solution and in thin film. Optical data is detailed in **Table 3**. **PDTPBTz**, **PDTPBT**, and **PDTPHTBT** revealed absorption maxima due to π - π^* transitions at 500, 490, and 508 nm in solution, respectively. Generally, incorporation of π -bridge in D-A approach causes a red shift of the absorption band but this was not the case for **PDTPBT**. This can be attributed to a low molecular weight of it. Besides, polymers indicated different

bathochromic shift from solution to thin film that is the indicative of different levels of backbone planarization and interchain interaction. The values of this red shift are 44, 59, and 18 nm for **PDTPBTz**, **PDTPTBT**, and **PTPHTBT**. Among the polymers, **PTPHTBT** showed a smaller red shift from solution to thin film since hexyl units on thiophene ring that introduces unfavorable steric hindrance and prevent aggregation in thin film. **PDTPTBT** exhibited a larger red shift compared to **PDTPBTz** due to strong aggregation.

Although, HOMO and LUMO energy level of polymers differentiate, their optical band gap are very close to each other. Optical band gaps of the polymers (E_g^{opt}) were calculated by taking a tangent line from the $\pi-\pi^*$ transition and found as 1.72 eV for **PDTPBTz**, 1.70 eV for **PDTPTBT**, and 1.69 eV for **PDTPHTBT**. E_g^{opt} of the polymers are 0.04 eV and 0.1 eV lower than E_g^{ec} of **PDTPTBT** and **PDTPHTBT** respectively. The smaller difference between E_g^{opt} and E_g^{ec} for **PDTPTBT** can be explained by small exciton binding energy of it compared to **PDTPHTBT**.

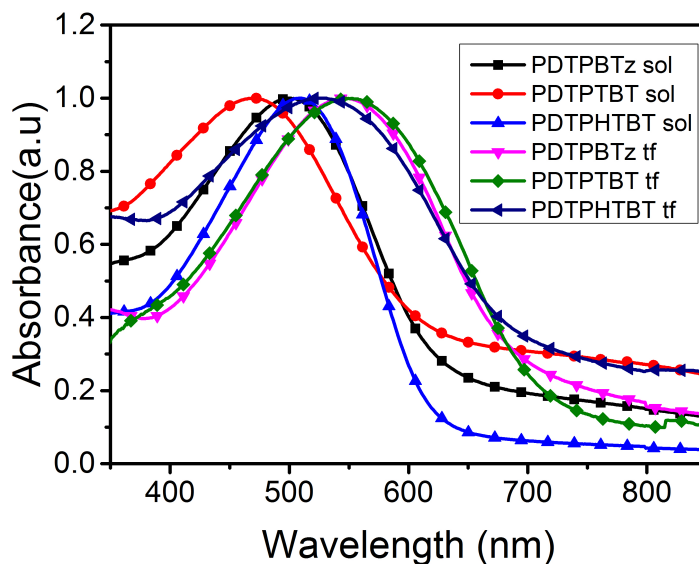


Figure 33 Absorption spectra of **PDTPBTz**, **PDTPTBT**, and **PDTPHTBT** in dichloromethane and thin film

Table 3 Summary of optical and electrochemical properties of **PDTPBTz**, **PDTPTBT** and **PDTPHTBT**

Polymers	$\lambda_{\max}^{\text{sol}}$	$\lambda_{\max}^{\text{film}}$	E_g^{opt} (eV)	HOMO (eV)	LUMO (eV)	E_g^{ec} (eV)
PDTPBTz	500	544	1.72	-4.75	-	-
PDTPTBT	490	549	1.70	-5.19	-3.45	1.74
PDTPHTBT	508	526	1.69	-5.70	-3.91	1.79

3.2.4. Spectroelectrochemical Studies

Spectroelectrochemical studies were carried out to investigate electrochromic behavior of polymers. Spray-coated polymers were subjected to stepwise oxidation while changes in their optical properties were investigated. π - π^* transitions of **PDTPBTz**, **PDTPBT**, and **PDTPHTBT** were observed at 544, 549, and 526 nm, respectively (**Figure 34**). Although, maximum absorption values of the polymers are close to each other, polymers were switched between different colors during oxidation process.

During the stepwise oxidation of polymers, the absorptions in the visible region depleted while new absorptions at around 700 and 1000 nm are intensified owing to formation of free charge carriers such as polarons and bipolarons. Polaron bands are tailed into the visible region, which was contributed to multichromism of polymer. **PDTPBTz** exhibited purple color in its neutral state and upon stepwise oxidation the visible absorption gradually decreases and black color formed as an intermediate states. **PDTPBTz** showed transmissive sky blue in its oxidized state. **PDTPBT** and **PDTPHTBT** have a red color in their neutral states and it switched between purple, brown, black, green, and blue color (oxidized state). **PDTPHTBT** exhibits orange-brown, purple, gray, greenish-blue at intermediate states and blue at oxidized state. Furthermore, **PDTPBT** and **PDTPHTBT** revealed transparent and gray color in their reduced states, respectively (**Figure 35**).

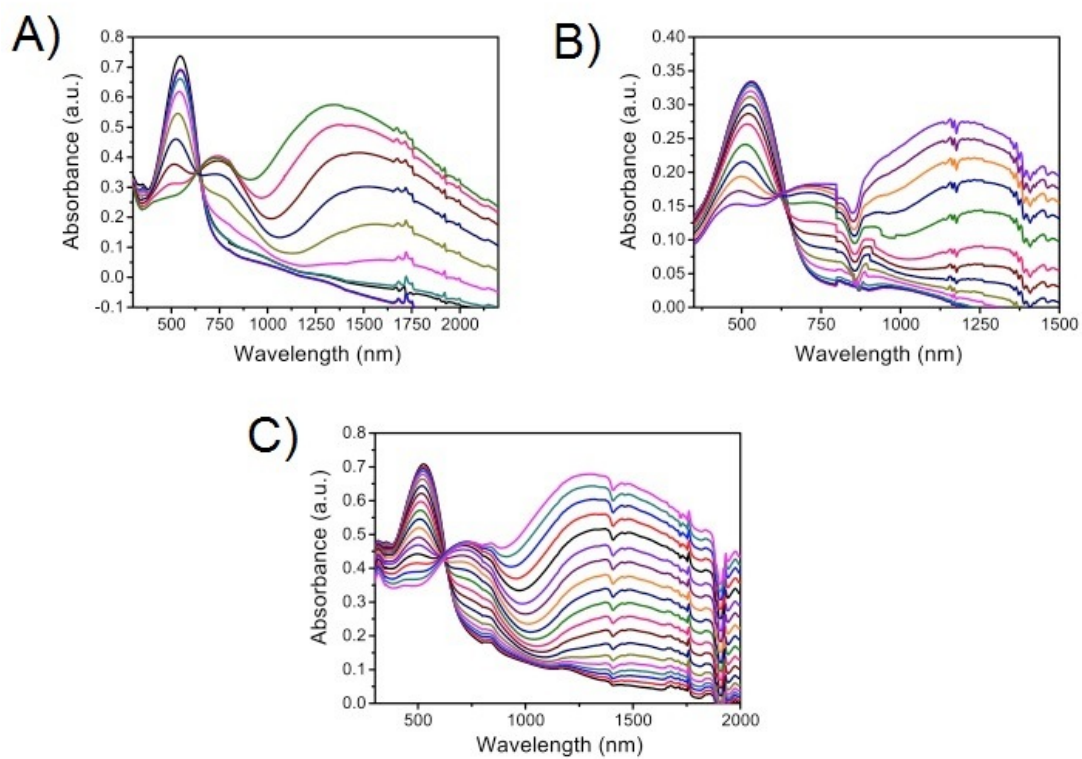


Figure 34 UV-Vis-NIR spectra of (A) **PDTPBTz** at potentials between 0.0 and 0.9 V (B) **PDTPTBT** at potentials between 0 and 0.9 V (C) **PDTPTHBT** at potentials between 0.0 and 1.6 V

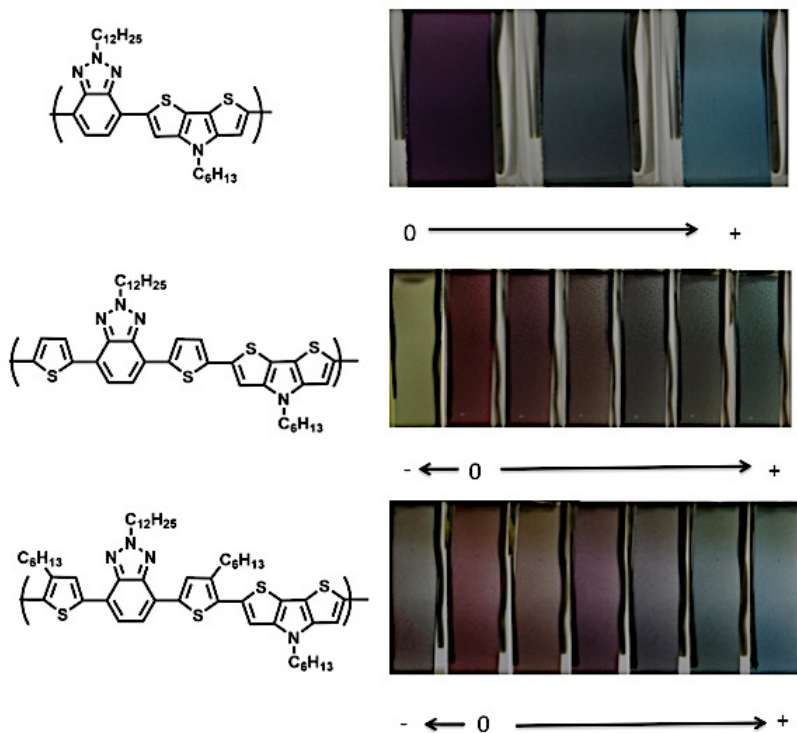


Figure 35 Colors of **PDTPBTz**, **PDTPTBT**, and **PDTPHBTz**

3.2.5. Kinetic Studies

Optical contrast and electrochromic switching times of the polymers between neutral and oxidized states are monitored in UV and visible regions by applying square-wave potential steps between their neutral and fully oxidized states (**Table 4**). The highest optical contrasts were observed for **PDTPBTz** that revealed optical contrasts of 42% at 542 nm, 26.5% at 765 nm, and 70% at 1345 nm and has an outstanding optical contrast in NIR region, which is important parameter for NIR electrochromic applications. **PDTPTBT** has satisfactory optical contrasts values in the visible and NIR regions; 27%

at 545 nm, 36% at 785 nm, and 49% at 1245 nm. Besides, **PDTPHTBT** revealed 32% contrast in UV region (530 nm) and 45% in NIR region (1330 nm) (**Figure 36**).

In addition to transmittance changes upon doping/ dedoping, switching time of the polymers is determined. **PDTPBTz** switched between two states in 0.8 s (542 nm), 2.5 s (765 nm) and 2.4 s (1345 nm). Ejection and injection of the counter ions during oxidation and reduction processes are crucial parameters playing an important role on the switching time. Therefore, **PDTPBT** has fast switching time since thiophene bridges prevent the steric interaction between the alkyl chain attached to the DTP and BTz units and create interchain spacing thus reducing steric interaction and allowing ion diffusion and dopant insertion. **PDTPBT** switched in 0.5 s (545 nm), 1.9 s (1245 nm), and 0.5 s at 1245 nm. Besides, **PDTPHTBT** showed slow switching time of 1.8s (530 nm) and 2.9 s (1330 nm) compared to **PDTPBTz** and **PDTPBT**. This can be attributed to steric hindrance created by hexyl unit on 3-hexylthiophene.

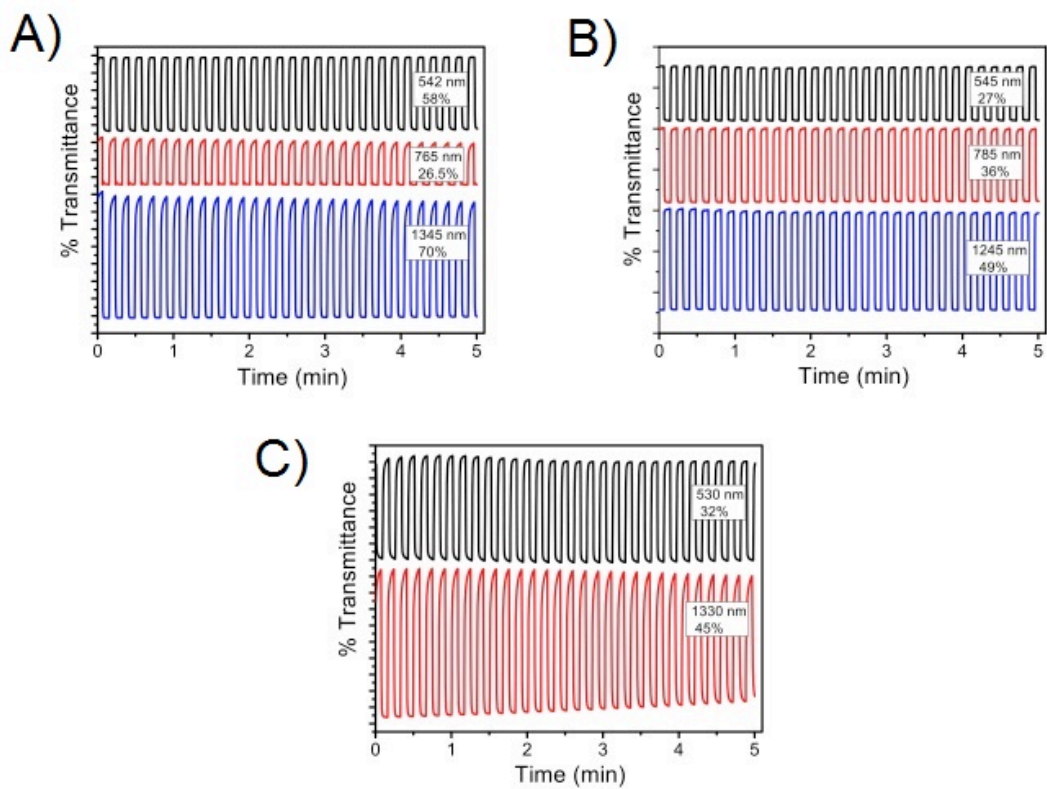


Figure 36 Percent transmittance changes of **PDTPBTz (A)**, **PDTPTBT (B)** and **PDTPTHBT (C)** film in monomer free, 0.1 M TBAPF₆/acetonitrile solution at its maximum absorption wavelengths

Table 4 Optical contrast and switching times of the polymers

Polymers	Optical Contrast ($\Delta T\%$)	Switching times (s)
PDTPBTz	42% (542 nm)	0.8
	26.5% (765 nm)	2.5
	70% (1345 nm)	2.4
PDTPBT	27% (545 nm)	0.5
	36% (785 nm)	1.9
	49% (1245 nm)	0.5
PDTPHTBT	32% (530 nm)	1.8
	45% (1330 nm)	2.9

In summary, a series of polymers namely **PDTPBTz**, **PDTPBT**, and **PDTPHTBT** were synthesized via Stille coupling reaction. Thiophene and 3-hexylthiophene were incorporated as the π -bridging units between BTz and DTP. Optical properties, i.e. maximum absorption in thin film and electrochemical properties, i.e, HOMO-LUMO energy alignment were also affected from presence of as π -bridging units. π -bridging units affected the switching times and optical contrast. Steric effect created or reduced by π -bridging units affected switching times and optical contrast. All three polymers showed moderate optical contrasts in visible region and **PDTPBTz** showed 70% optical contrast in NIR region. **PDTPBT** exhibited fast switching time since thiophene creates an interspace which making ejection and injection of the counter ions during oxidation and reduction processes easy.

3.3. Benzodithiophene and benzotriazole based conjugated polymers

The choice of different π -bridges influence the degree of aromaticity, the planarity of the backbone, and the electron density of conjugated polymer. Thus it dictates polymer optical absorption, energy level alignment, charge transport, and interchain interactions. Therefore, recently, modification of π -bridges in DA approach becomes an important strategy either to control photovoltaic performance or to control all these properties [87].

Chalcolophene derivatives are commonly utilized π -bridges in DA architecture. Among them, thiophene derivatives are predominantly used. However, other chalcolophene derivatives, i.e furan, selenophene and tellurephene, less explored compared to thiophene. These derivatives showed different electronic, optical, and physical properties. Electronegativity of chalcogens are different, which impacts donation of electrons into five membered ring and their dipole moment. Furan has highest dipole moment thus resulting high solubility of it in polar solvent. Thus affect the molecular weight polymers that were synthesized with this building block. Molecular weight determines the film quality of active layer that is significant for efficient charge generation and collection for OSCs. Furan not only affects molecular weight but also stabilizes HOMO energy level resulting higher band gap compared to thiophene due to low aromaticity of it. However, low-lying HOMO energy level enhances V_{OC} of solar cell compared to thiophene containing conjugated polymers. Polythiophene and polyfuran exhibit similar hole mobilities as a consequence of similar quinoid character. Another interesting property of furan is its production from natural sources. Hence, it is counted as “green building block” that makes this building block suitable for large scale and low cost applications [99-101]

In addition to chalcolophene derivatives, fused aromatic structures have gained much attention as π -bridges. Among them, thieno[3,2-*b*]thiophene showed interesting optical and electrochemical properties due to its centrosymmetric, coplanar and rigid structure.

First of all, it provides red shifted absorption, lowered band gap and increased charge mobilities compared to thiophene containing polymers due to high delocalization of π - electrons and better intermolecular π -stacking interactions [102-87]. Therefore, in this part of thesis, thieno[3,2-*b*]thiophene and furan are utilized as π -bridges in benzotriazole and benzodithiophene bearing DA polymers for electrochromic and photovoltaic applications

3.3.1. Synthetic Pathway

Synthetic pathway for **PTTBTBDT** and **PFBTBDT** is outlined in **Figure 37**. By keeping in mind that modification of the alkyl side chains on a polymer backbone not only change the physical properties such as solubility but also affect intramolecular interactions and optoelectronic characteristics, such as light absorptivity and charge transport behavior. We functionalized benzotriazole with branched alkyl chain to ensure the solubility of polymers [103-105]. Synthesis of 4,7-dibromo-2-(2-octyldodecyl)-2H-benzo[d][1,2,3]triazole (**1**) was performed according to previously published procedure. 4,7-bis(5-bromothiopheno[3,2-*b*]thiophen-2-yl)-2-(2-octyldodecyl)-2H-benzo[d][1,2,3]triazole (TTBTBT-Br) and 4,7-bis(5-bromofuran-2-yl)-2-(2-octyldodecyl)-2H-benzo[d][1,2,3]triazole (FBT-Br) were prepared in two steps. In the first step, stille cross-coupling between **1** and tributyl(thiopheno[3,2-*b*]thiophen-2-yl)stannane (**2**) or between **1** and tributyl(furan-2-yl)stannane (**3**) was performed with a Pd(PPh₃)₂Cl₂ catalyst. In the second step, bromination was done with NBS to synthesize TTBTBT-Br and FBT-Br in moderate yields. Polymerization reactions of TTBTBT-Br and FBT-Br were performed with 2,6-bis(trimethylstannyl)-4,8-bis(2-ethylhexyloxy)benzo[1,2-*b*:4,5-*b'*]dithiophene in the presence of catalytic Pd₂dba₃ and a ligand P(*o*-tolyl) to synthesize **PTTBTBDT** and **PFBTBDT**, respectively. After purification of polymers, solubility of them was tested in common organic solvents such as THF, chloroform, chlorobenzene and 1,2-dichlorobenzene. **PFBTBDT** is readily

soluble in these solvents. Although, branched alkyl chain is anchored on BTz moiety, **PTTBTBDT** suffered from solubility and it showed limited solubility in hot chloroform, chlorobenzene and dichlorobenzene. Thermogravimetric analysis (TGA) and differential scanning calorimetry (DSC) were used to assess the thermal stability and thermal transitions of polymers. Both polymers showed no significant degradation up to 300°C. DSC scan indicated that polymers didn't show any thermal transition. Molecular weight of the polymers is determined by GPC with polystyrene standards using chloroform as the eluent.

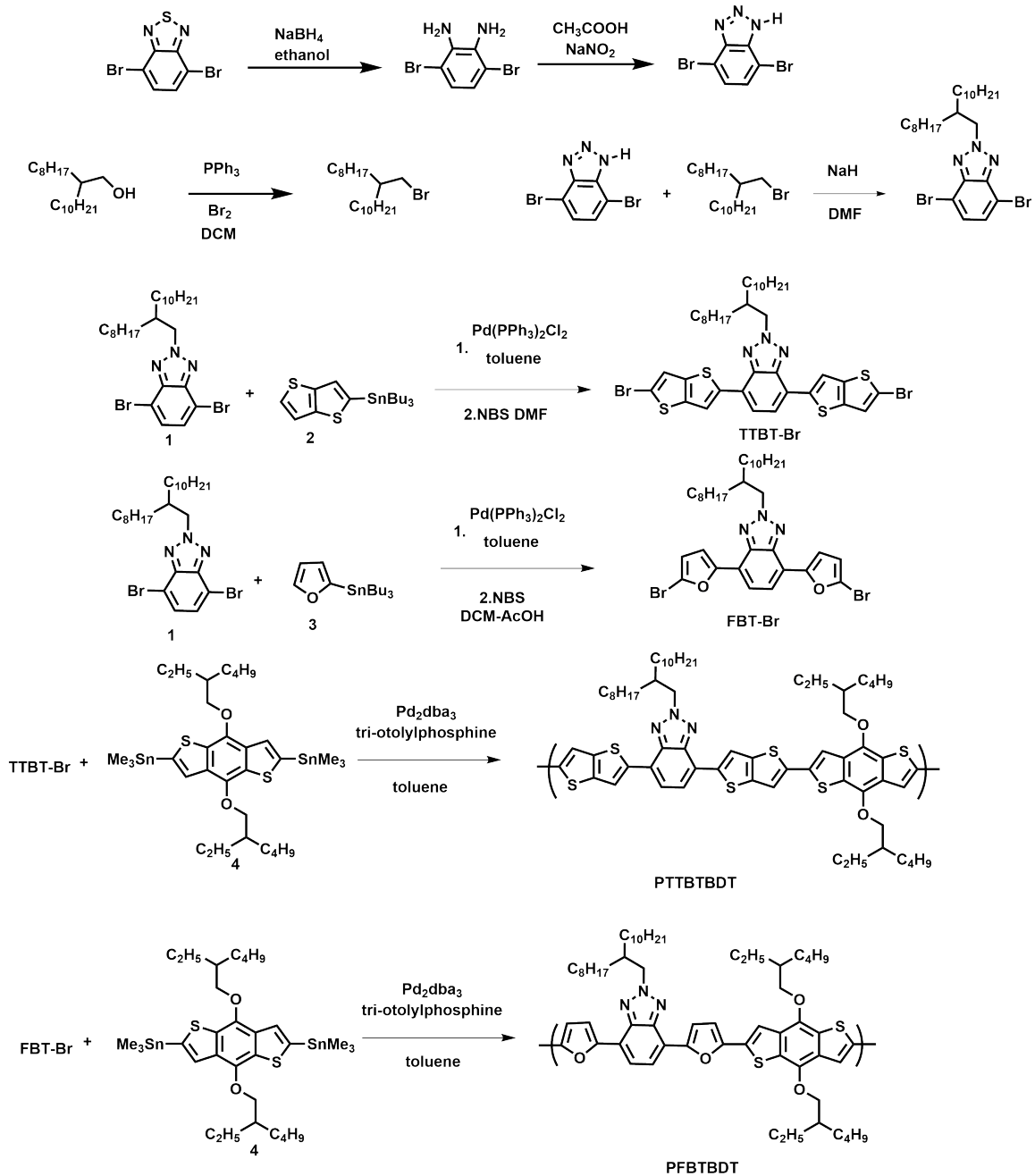


Figure 37 Synthetic pathways of **PTTBTBDT** and **PFBTBDT**

3.3.2. Electronic Properties

Evaluation of frontier orbitals is essential in order to evaluate polymers potential for organic solar cell applications. Therefore, HOMO and LUMO energy level as well as their oxidation and reduction potential are investigated with CV and cyclic voltamograms of polymers are outlined in **Figure 38** and relevant data are presented in **Table 5**. **PTTBTBDT** showed reversible oxidation and reduction peak. Oxidation potential of **PTTBTBDT** are observed at 0.69/0.96 V with a reversible dedoping peak at 0.60 and 0.89 V. Reduction potential of **PTTBTBDT** is observed at 1.84 V with a reversible dedoping peak at 1.67 V. HOMO and LUMO energy level **PTTBTBDT** are calculated from $\text{HOMO} = -(4.75 - \text{Fc} + E_{\text{ox}}^{\text{onset}})$, $\text{LUMO} = -(4.75 - \text{Fc} + E_{\text{red}}^{\text{onset}})$ equations and found as -4.96 and -3.11 eV, respectively. **PFBTBDT** showed only reversible oxidation. Oxidation potential of **PFBTBDT** is observed at 1.03 V with a reversible dedoping peak at 1.08 and 0.84 V. HOMO energy level of **PFBTBDT** is calculated as -5.09 eV. It showed lower HOMO energy level compared to **PTTBTBDT**. LUMO energy level of **PFBTBDT** is calculated from HOMO energy level and optical band gap and found as -3.04 eV. Both polymers have suitable HOMO energy level to favor higher V_{OC} values in polymer: PCBM OSCs and suitable LUMO energy level for photoinduced charge transfer.

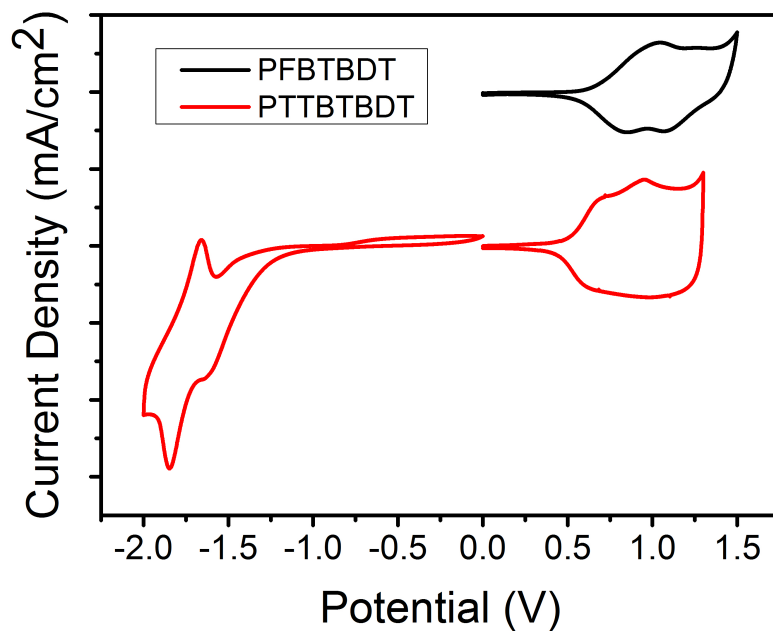


Figure 38 Cyclic voltammograms of the **PTTBTBDT** and **PFBTBDT** on ITO electrode in 0.1 M TBAPF₆, CH₃CN solution with a scan rate of 100 mV/s ((Fc/Fc⁺ redox couple was used as internal standard)

The scan rate dependence of peak currents was examined in an electrolyte solution (Figure 39). A linear relationship between the peak current and scan rate illustrates that the electrochemical processes were reversible and non-diffusion-controlled.

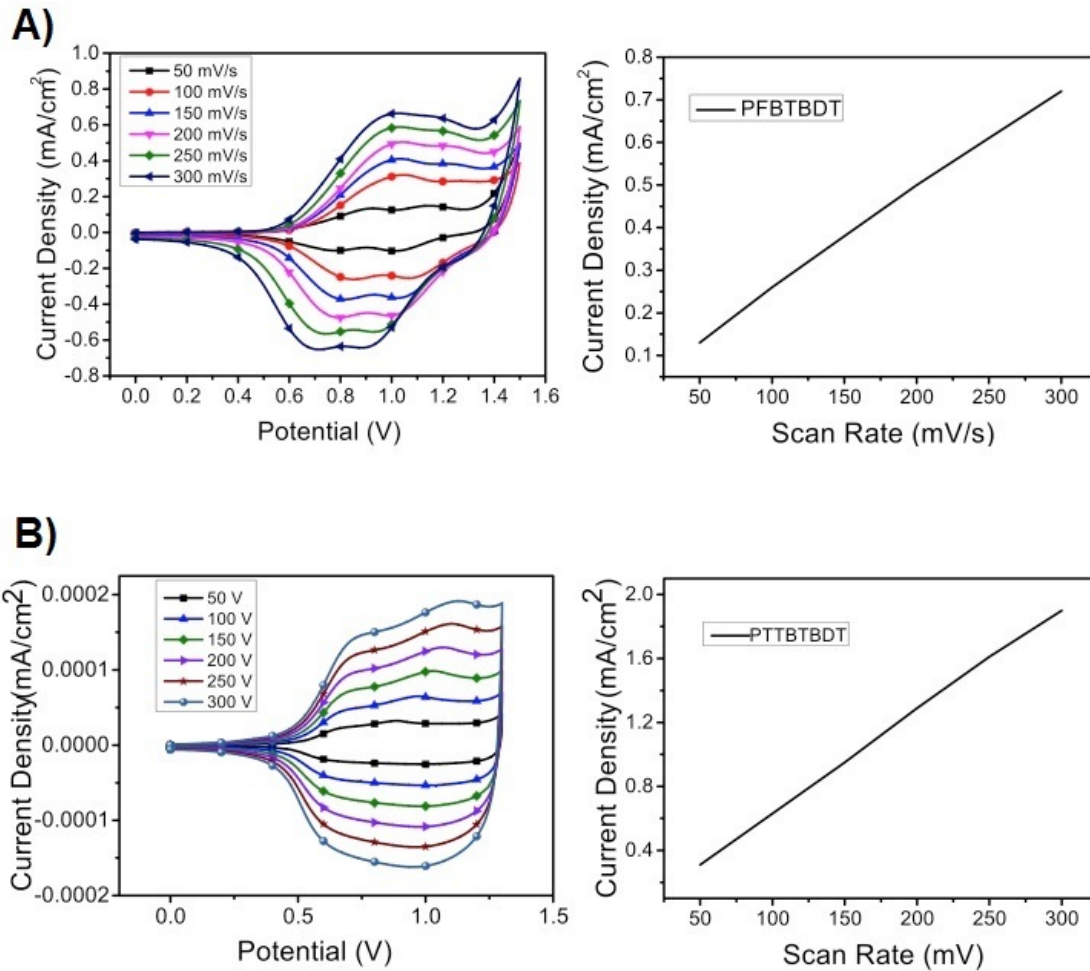


Figure 39 Cyclic voltammograms of A) **PFBTBDT** B) **PTTBTBDT** in 0.1 M TBABF₆/ACN at scan rates of 50, 100, 150, 200, 250, and 300 mV/s

3.3.3. Optical Properties

The absorption profiles and light harvesting potential of polymers were investigated by UV-Vis spectroscopy in dilute chlorobenzene solution and thin films. The UV-Vis absorption spectra of polymer in solution and film are depicted in Figure 40 and the results are summarized in **Table 5**. Both polymers exhibited different behavior in

solution and thin film absorption. **PFBTBDT** showed absorption maximum at 508 nm that is assigned to π - π^* transition. It showed 12 nm bathochromic shifts from solution to thin film that is indicative of chain planarization and strong aggregation of polymer in thin film. In addition to this, it showed a vibronic shoulder in thin film as a consequence of stronger interchain π - π stacking of the polymer chains in thin film. **PTTBTBDT** showed two absorption peaks in solution at around 547/588 nm and it did not show any red shift from solution to thin film although intensity of peak at longer wavelength is changed. The absence of red shift can be attributed to substantial aggregation in solution. However, the intensity change from solution to thin film can be ascribed the enhanced conjugation length and intermolecular interaction between polymer chains in the solid state as a result of molecular organization in the thin film to form more ordered structures. E_g^{opt} of polymers were calculated from onset of π - π^* transitions in thin film and **PTTBTBDT** possess smaller E_g^{opt} of 1.93 eV compared to **PFBTBDT** (2.05 eV) due to strong electron donating ability of thieno[3,2-*b*]thiophene.

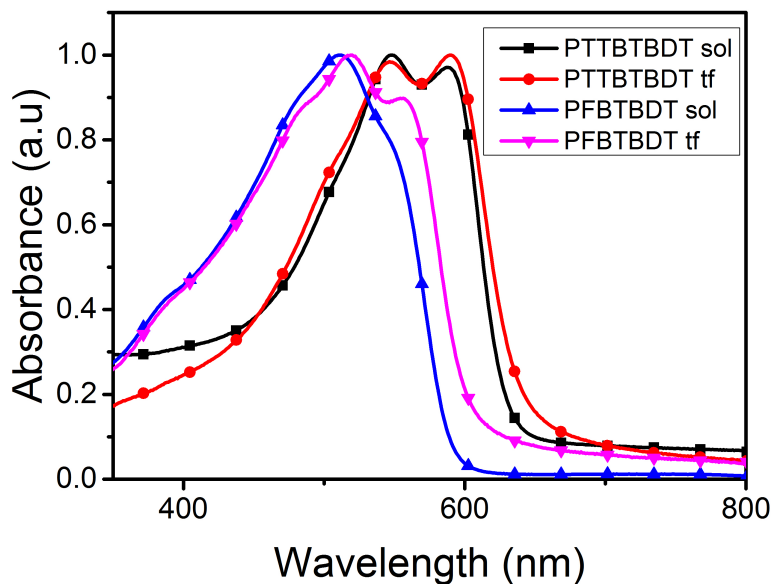


Figure 40 Absorption spectra of **PFBTBDT** and **PTTBTBDT** in chlorobenzene solution and in thin film

Table 5 Summary of optical and electrochemical properties of **PFBTBDT** and **PTTBTBDT**

Polymers	$\lambda_{\max}^{\text{sol}}$	$\lambda_{\max}^{\text{film}}$	E_g^{opt} (eV)	HOMO (eV)	LUMO (eV)	E_g^{ec} (eV)
PFBTBDT	508	520	2.05	-5.09	-3.04*	-
PTTBTBDT	547/588	544/590	1.93	-4.96	-3.11	1.85

- LUMO was calculated from optical band gap

3.3.4. Spectroelectrochemistry

Figure 41 shows spectroelectrochemistry of **PTTBTBDT** and **PFBTBDT**. $\pi-\pi^*$ transitions of **PTTBTBDT**, and **PFBTBDT** were observed at 544/590 and 520 nm, respectively. **PTTBTBDT** showed red-shifted absorption compared to **PFBTBDT** due to stronger electron donating nature of thieno[3,2-*b*]thiophene than furan.

PTTBTBDT showed purple color in its neutral state and oxidation of polymer resulted new absorptions at around 815 and 1000 nm that were intensified due to formation of free charge carriers such as polarons and bipolarons. **PTTBTBDT** switched between purple and blue at neutral and bleaching state. Partial oxidation of it resulted in grey color. Besides, polymer showed light green in its reduced state. **PFBTBDT** exhibited red color in its neutral state and upon stepwise oxidation the visible absorption gradually decreases and grey color formed as an intermediate states due to creation of polaron and bipolaron. **PFBTBDT** showed transmissive sky blue in its oxidized state. Both polymers showed multichromism due to tailoring of polaron bands in visible region.

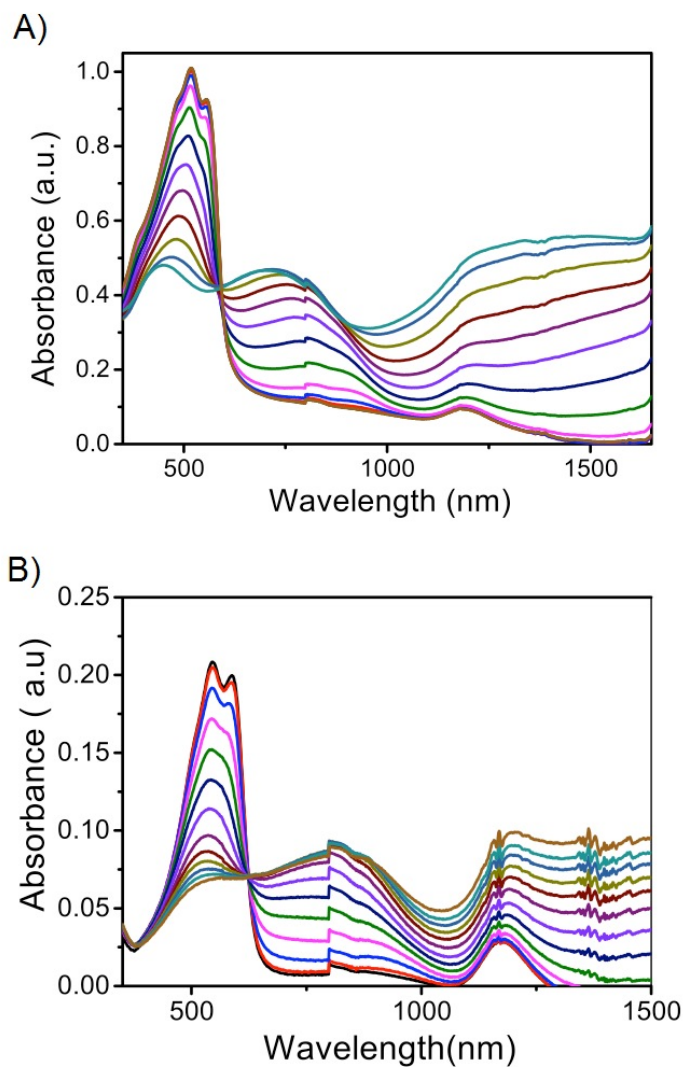


Figure 41 UV–Vis–NIR spectra of (A) PFBTBDT (B) PTTBTBDT

3.3.5. Kinetic Studies

Optical contrast and electrochromic switching times of the polymers were determined by sweeping potential between neutral and oxidized state with a switching time interval of 5 s in 0.1 M TBAPF₆/ACN at two different wavelengths (Figure 42). Synopsis of optical

contrast and switching times are summarized in **Table 6**. Both polymers showed moderate optical contrast and fast switching times at their dominated wavelengths. **PTTBTBDT** possesses 18% and 28% optical contrast with switching times of 0.2 s at 545 and 1520 nm, respectively. Optical contrast of **PFBTBDT** was 15% and 29% at 520 and 1240 nm. Switching time of **PFBTBDT** was 0.4 and 0.2s at 545 and 1520nm.

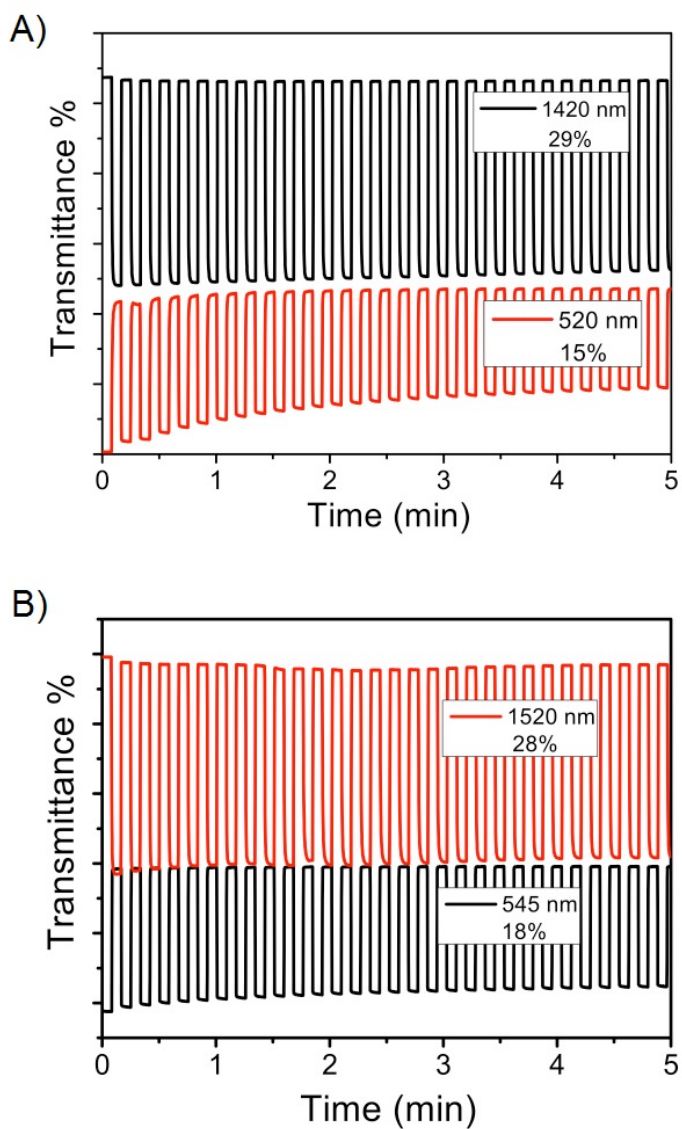


Figure 42 Percent transmittance changes of **PFBTBDT (A)**, **PTTBTBDT (B)** film in monomer free, 0.1 M TBAPF₆/acetonitrile solution at its maximum absorption wavelengths

Table 6 Summary of optical contrast and switching times of **PFBTBDT** and **PTTBTBDT**

Polymers	Optical Contrast ($\Delta T\%$)	Switching times (s)
PFBTBDT	15% (520 nm)	0.4
	29% (1240 nm)	0.2
PTTBTBDT	18% (545 nm)	0.2
	28% (785 nm)	0.2

3.3.6. Photovoltaic Properties

Although, both polymers possess suitable absorption profiles and energy levels for OSC fabrication, **PTTBTBDT** didn't show good film forming ability and solubility thus cause poor photovoltaic performance. Therefore, only photovoltaic properties of **PFBTBDT** were studied. Fabrication of organic solar cell of **PFBTBDT** performed with conventional configuration of ITO/PEDOT:PSS/polymer:PC₇₁BM/Ca/Al to evaluate photovoltaic performance of **PFBTBDT**. PC₇₁BM was selected as an acceptor due to its stronger absorption in visible region compared to PC₆₁BM. PEDOT: PSS is inserted as hole transport layer in this device configuration in order to smooth the ITO electrode and increase the work function of ITO to collect hole effectively [38]. Photovoltaic cell were prepared and tested under 100 mW/cm² AM1.5G illumination. Optimization studies of OSC were performed by investigating effect of polymer: PC₇₁BM ratios, film thicknesses, additives, and thermal annealing.

Device fabrication of **PFBTBDT** was performed with low-vapor-pressure solvent that is o-dichlorobenzene (DCB). It was selected because of its good solvation properties and

low evaporation rates allow time for polymer chain organization to form suitable BHJ film morphology [106]. Weight ratio of **PFBTBDT** to PC₇₁BM is changed from 1:1 to 1:4. The current density-voltage (J-V) characteristics of OSCs are depicted in Figure 43 and photovoltaic parameters are presented in **Table 7**. The optimized weight ratio of **PFBTBDT** to PC₇₁BM is 1:3. Devices fabricated from the **PFBTBDT**: PC₇₁BM ratio of 1:1, 1:2, 1:3 and 1:4 gave PCEs of 1.66%, 1.51%, 2.98%, and 2.22%, respectively. V_{OC} theoretically is equal to the difference in HOMO energy level of donor and LUMO energy level of the acceptor. Although, some losses in V_{OC} is observed due to interfacial electron-hole pairs located on the DA heterointerface (Charge transfer state complexes), vacuum level misalignment, poor dielectric properties, and disorder-induced changes in the hole and electron quasi-Fermi levels, the V_{OC} 's of the polymer are in the range of 0.72-0.73 V [107]. This means that HOMO energy level of donor and LUMO energy level of the acceptor are the main factor for determination of V_{OC} . J_{SC} and FF were significantly affected from active layer composition. The best device gave a PCE of 2.98 %, with V_{oc} of 0.74 V, J_{sc} of 6.31 mA cm⁻², and FF of 55%.

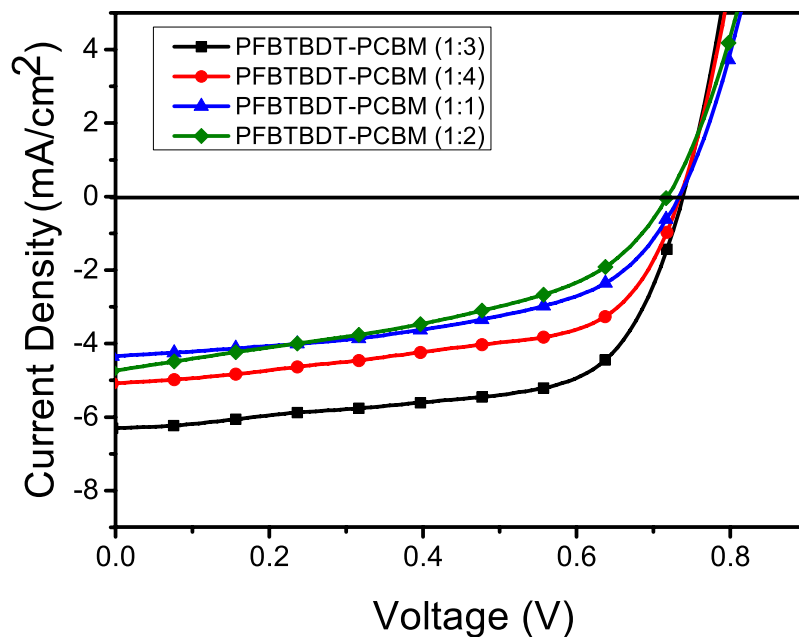


Figure 43 J-V characteristic of conventional device based on different ratio of **PFBTBDT: PC₇₁BM**

Table 7 Photovoltaic performance of **PFBTBDT** with PC₇₁BM in different weight composition

BHJ PFBTBT: PC₇₁BM	V_{OC} (V)	J_{sc} (mA/cm²)	FF	PCE (%)
1:1	0.73	4.36	52	1.66
1:2	0.72	4.75	44	1.51
1:3	0.74	6.31	64	2.98
1:4	0.73	5.07	60	2.22

Further optimization studies such as thermal annealing, polar solvent treatment (methanol), and processive additives were performed to improve performance of OSCs. However, as shown in Figure 44, any optimization study improved photovoltaic performance. Interestingly, methanol treatment enhanced J_{SC} from 6.31 mA/cm^2 to 7.71 mA/cm^2 . However, decrease in FF resulted low PCE. Relevant photovoltaic data are summarized in **Table 8**

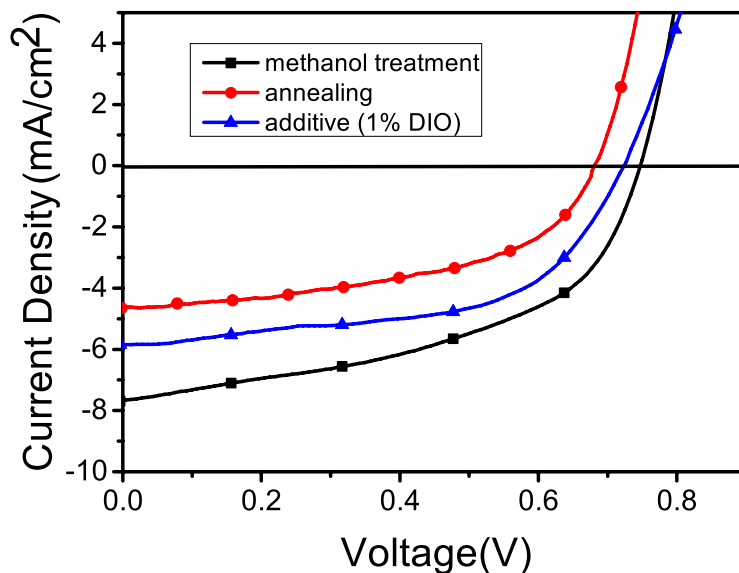


Figure 44 J-V characteristic of conventional device based on different ratio of **PFBTBDT: PC₇₁BM**

Table 8 Summary of the performance of OSCs optimization studies

BHJ PFBTBT: PC₇₁BM	V_{OC} (V)	J_{sc} (mA/cm²)	FF	PCE (%)
methanol treatment	0.75	7.70	49	2.82
annealing	0.68	4.31	54	1.61
Additive (1% DIO)	0.72	5.89	55	2.35

IPCE is defined as the ratio of photocurrent to the incident photons, which are converted to carriers collected at the electrodes under short circuit conditions. Therefore, the integration of an IPCE spectrum is proportional to the short circuit current [30]. Hence, incident photon to current efficiency (IPCE) spectra of the **PFBTBDT: PC₇₁BM** based OSCs were investigated to verify the change of J_{sc}, and showed in Figure 45. Photocurrent response of both systems started from 340 nm and ended at 700 nm that is consistent with absorption spectra of blends. Both **PFBTBDT** and PC₇₁BM made contribution to photon to electron conversion. It has a photoresponse with highest IPCE of 16%.

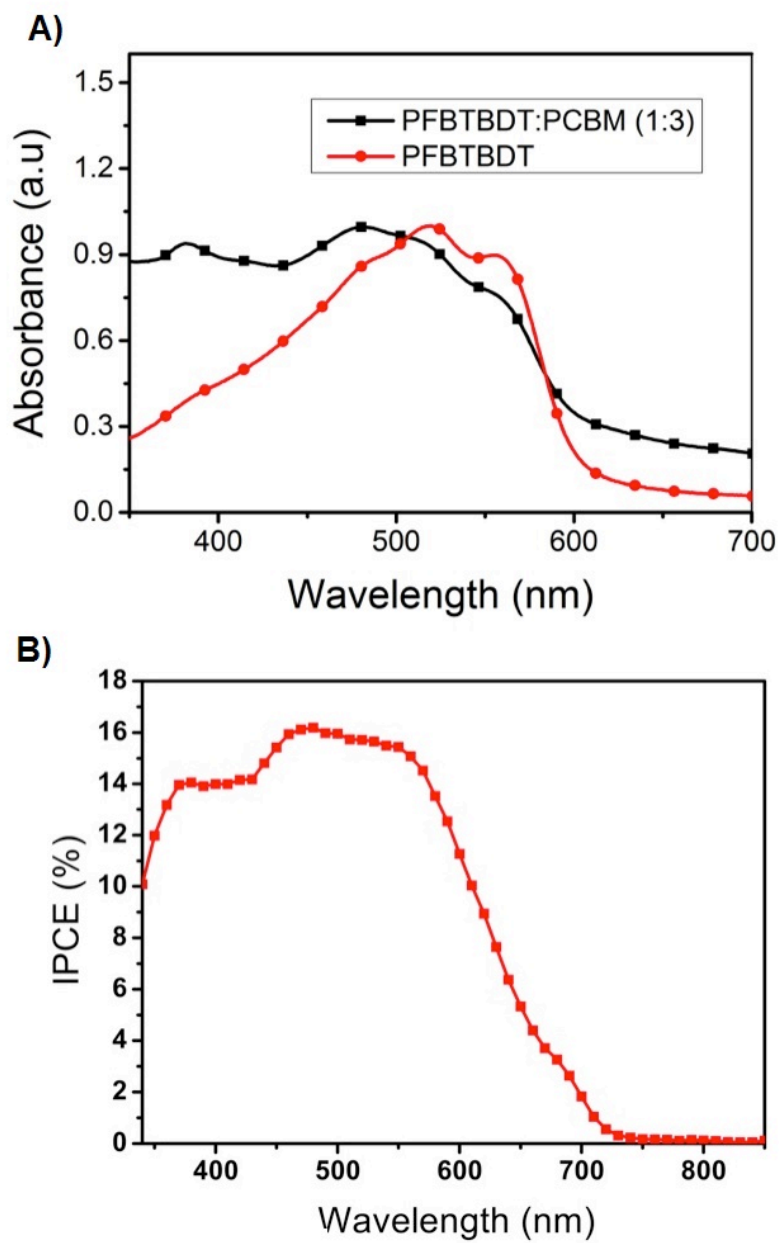


Figure 45 Absorption (A) and (B) incident to photon conversion efficiency (IPCE) spectra of **PFBTBDT:PC₇₁BM (1:3)**

3.3.7. Morphology

Photovoltaic performance of polymer is directly related to morphology so we studied atomic force microscopy (AFM) and transmission electron microscopy (TEM) to gain deeper insight into film morphologies of **PFBTBDT**: PC₇₁BM (1:3) blends with and without methanol treatment. AFM images are depicted in Figure 46. Morphology of active layer was not affected from methanol treatment in AFM images. It is expected that PC₇₁BM would penetrate into the active layer to form more interconnected and smooth surface in the presence of methanol treatment. Therefore, we analyzed surface roughness to understand the difference in J_{SC} . The blend film without methanol treatment exhibited relatively course phase separation with a root-mean-square (RMS) of 7.38 nm. This value decreased to 5.15 nm with methanol treatment. This relatively smooth surface could be the reason for enhancement of J_{SC} [101].

In addition to AFM, we studied TEM images of **PFBTBDT**: PC₇₁BM blend films with and without methanol treatment to elucidate PCBM and polymer rich domains. The dark areas in the TEM images are attributed to PCBM rich domains since it causes more effective scattering compared to polymer due to its high electron density. It is important to note taking that both blend films showed larger domains, which limits device performance.

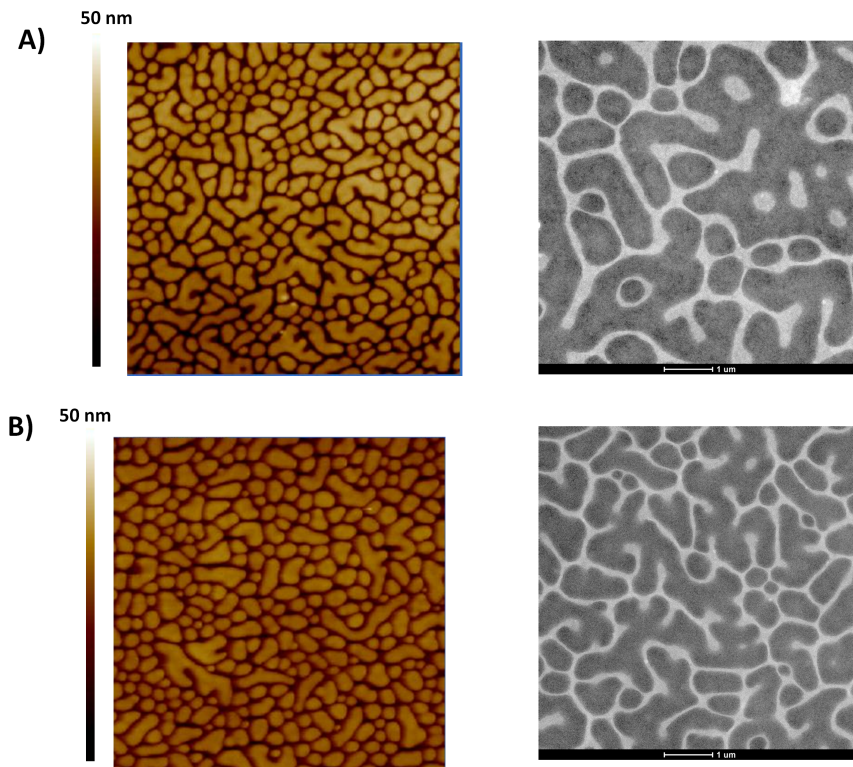


Figure 46 AFM and TEM images of **PFBTBDT:PC₇₁BM (1:3)** with (B) and without methanol treatment (A)

3.3.8. SCLC Mobilities

The space charge limited current (SCLC) model were examined from current density-voltage characteristics (J–V curve) under dark and mobility was calculated with Child's law under the trap free SCLCs situation

$$J_{SCL} = \frac{9\epsilon_r\theta\epsilon_0\mu V^2}{8L^3}$$

Where J is the current, μ_0 is the zero-field mobility, ϵ_0 is the permittivity of free space, ϵ_r is the relative permittivity of the material, V is the effective voltage, and L is the thickness of the active layer

SCLC graph is shown in Figure 47 and hole mobilities are presented in **Table 9**. The average hole mobilities for the blend are correlated with device performance and highest hole mobility was found as $1.37 \times 10^{-3} \text{cm}^2 \text{V}^{-1} \text{s}^{-1}$.

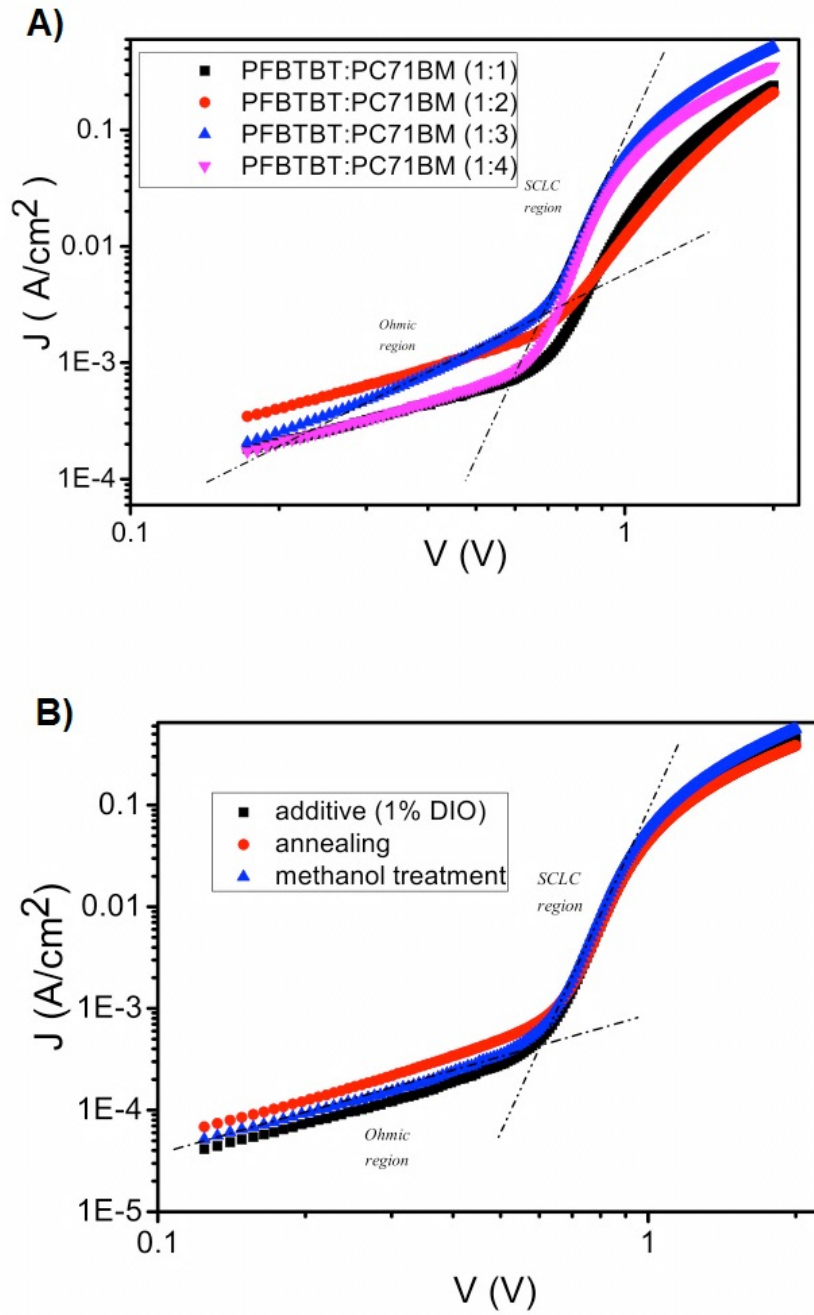


Figure 47 SCLC mobilities of PFBTBDT: PC₇₁BM

Table 9 Summary of SCLC mobilities of **PFBTBDT**: PC₇₁BM blends

BHJ PFBTBT: PC₇₁BM	μ_h(cm²/V.s)
1:1	2.48x10 ⁻⁴
1:2	1.29x10 ⁻⁴
1:3	1.37x10 ⁻³
1:4	1.21x10 ⁻³
methanol treatment	9.40 x10 ⁻⁴
annealing	6.5 x10 ⁻⁴
additive (1% DIO)	8.2x 10 ⁻⁴

In summary, benzodithiophene was coupled with benzotriazole for electrochromic and optoelectronic applications. Thieno[3,2-*b*]thiophene and furan was inserted as π -bridging units. **PTTBTBDT** had red-shifted absorption profile and **PFBTBDT** has low-lying HOMO energy level. Besides both polymers showed multichromism fast switching time, and moderate optical contrast in electrochromic applications. OSC fabrication of **PFBTBT** was performed with conventional device configuration and optimization studies like different polymer: PCBM blend ratio, annealing, solvent, methanol treatment, and additive were performed. Polymer showed 2.98% PCE with **PFBTBDT**: PCBM blend ratio (1:3). Morphological findings were performed to elucidate the factors affecting performance. It was found that high RMS roughness and larger domains could be the reason for limiting the performance of solar cell.

3.4. Indacenodithiophene/selenophene and Naphthalene Diimide n-Type Copolymers for Efficient All-Polymer Solar Cells

In this part of the thesis, copolymerization of NDI was performed with ladder indacenodithiophene (IDT) and indacenodiselenophene (IDSe). IDT and IDSe based less-crystalline polymers are found to possess merits of good processability and non-sensitive phase behaviors to enable good PCE over simple processing [77,108]. Additionally, such ladder type units with rigid and planer structure allow optimizing the absorption coefficients and reorganizational energies of resulting polymers. Incorporation of heteroatom, like Se into ladder structure further engineers the aromaticity of polymeric repeating unit.

Fabrication of solar cell was performed with PTB7 and PBDTTT-E-T since PTBx based p-type semiconductor is suitable for all polymer solar cells due to their high charge mobilities, suitable absorption profiles and attractive photovoltaic properties. Furthermore, syntheses of two-dimensional polymers (2D-polymers) such as PBDTTT-E-T via structural modifications can be possible. Increasing dimensionality of polymer resulted in red-shifted absorption profile, enhanced hole mobility, and improved photovoltaic properties [109]. Besides, this type of polymers yield good compatibility with n-type conjugated polymers.

3.4.1. Synthesis of PIDTNDI and PIDSeNDI

Syntheses of **PIDTNDI** and **PIDSeNDI** were performed by Stille coupling of NDI with IDT-ditin and IDSe-ditin respectively in the presence of $\text{Pd}_2(\text{dba})_3$ and o-tolylphosphine (Figure 48). The molecular weights (MW) of these n-type polymers are measured by gel permeation chromatography (GPC) using monodispersed polystyrene as the standard and o-dichlorobenzene (DCB) as the eluent. The **PIDTNDI** and **PIDSeNDI** have the number average molecular weight (M_n) of 34.2 kDa and 57.2 kDa, with polydispersity indexes (PDI) of 1.88 and 2.07, respectively. Choice of processing solvent for solar cell fabrication and solution-based processing affects the kinetics and thermodynamics of

BHJ film formation so solubility of polymers was tested in common organic solvents. They were readily soluble in common organic solvents like tetrahydrofuran, toluene, chloroform, dichlorobenzene (DCB), and chlorobenzene (CB).

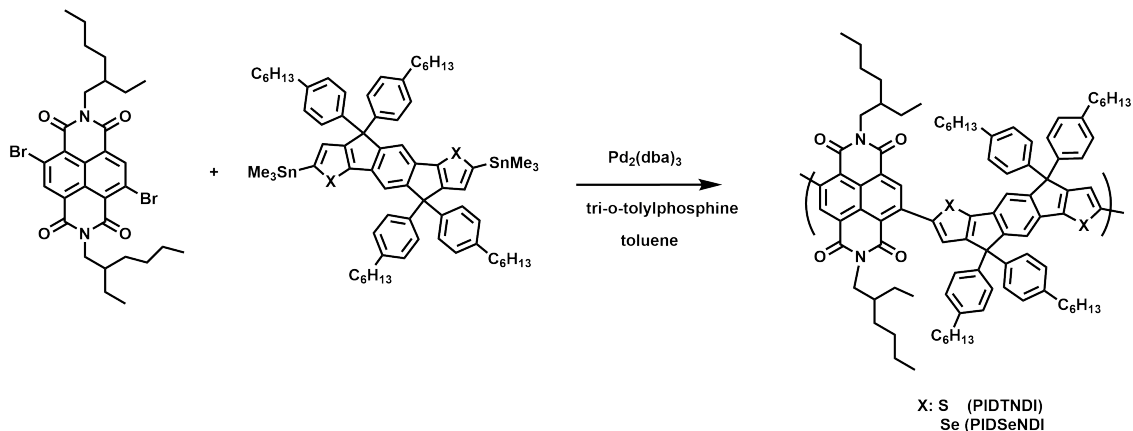


Figure 48 Synthetic pathways for **PIDTNDI** and **PIDSeNDI**

3.4.2. Electronic properties of PIDTNDI and PIDSeNDI

Proper alignment of the highest occupied molecular orbital (HOMO) and the LUMO energy levels is critical since alignment of HOMO/LUMO energy levels of acceptor units relative to donor affects photoinduced charge transfer and effective charge separation. Therefore, redox behaviors of polymers were investigated by cyclic voltammetry (CV). Polymer first dissolved in chloroform (5 mg/mL) and drop-casted on ITO electrode. Then CV was performed in three-electrode cell consisting of an ITO-coated glass slide as the working electrode, Pt wire as the counter electrode, and Ag wire as the pseudo reference electrode calibrated against Fc/Fc^+ . 0.1 M Bu_4NPF_6 (TBAPF₆) was used as the supporting electrolytes. Oxidation and reduction voltamograms of

polymers showed in Figure 49 and electrochemical properties of polymers were summarized in **Table 9**. Both polymers showed reversible p-doping/n-doping process in cathodic and anodic scans. Oxidation potentials of **PIDTNDI** and **PIDSeNDI** were observed at 1.20 and 1.09 V respectively. Reduction of the **PIDTNDI** was achieved at -0.75/-1.17 V and the reversible dedoping peaks lie at -0.59/ -1.03 V. The reduction peaks were slightly shifted for **PIDSeNDI**, the reduction was observed at relatively higher potentials -0.83 / -1.19 V with a reversible dedoping peaks at -0.67/ -1.09 V. Relative HOMO and LUMO energy levels of **PIDTNDI** and **PIDSeNDI** were calculated from oxidation and reduction onsets and found -5.62/-3.87 and -5.55/-3.79 eV respectively with an electrochemical band gap of 1.75 and 1.76 eV respectively.

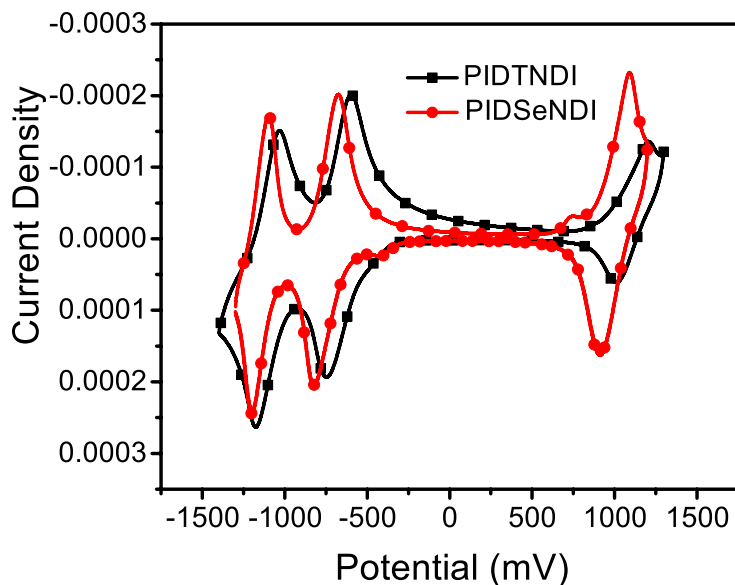


Figure 49 Cyclic voltammogram of **PIDTNDI** and **PIDSeNDI** on ITO electrode in a 0.1 M $\text{Bu}_4\text{NPF}_6/\text{ACN}$ solution with a scan rate of 100 mV s^{-1}

3.4.3. Optical Properties of PIDTNDI and PIDSeNDI

In addition to proper energy alignments, the absorption band and optical band gap (E_g^{opt}) of the acceptor material should be considered since extension of absorption to near-IR region could be possible by decreasing optical band gap. Optical properties of polymers were investigated in thin film and dilute CB solution and displayed in Figure 50. Relevant data are summarized in **Table 10**. Both polymers showed dual absorption peaks at low energy and high energy that can be assigned to π - π^* transition and intramolecular charge transfer (ICT) inherent to the donor-acceptor system respectively. The maximum absorption of **PIDTNDI** and **PIDSeNDI** in solution observed at 394/700 and 402/714 nm respectively. The ICT absorption band of the polymer films of **PIDTNDI** and **PIDSeNDI** showed 34 and 43 nm red shift relative to their solution. Besides, it is noteworthy to state that intensity of absorption peak was also changed from solution to thin film state that can be assigned to the increased conjugation length and intermolecular interaction between polymer chains in the solid state that is the result of molecular organization in the thin film to form more ordered structures **PIDTNDI** and **PIDSeNDI** exhibited an E_g^{opt} of 1.49 and 1.47 eV respectively.

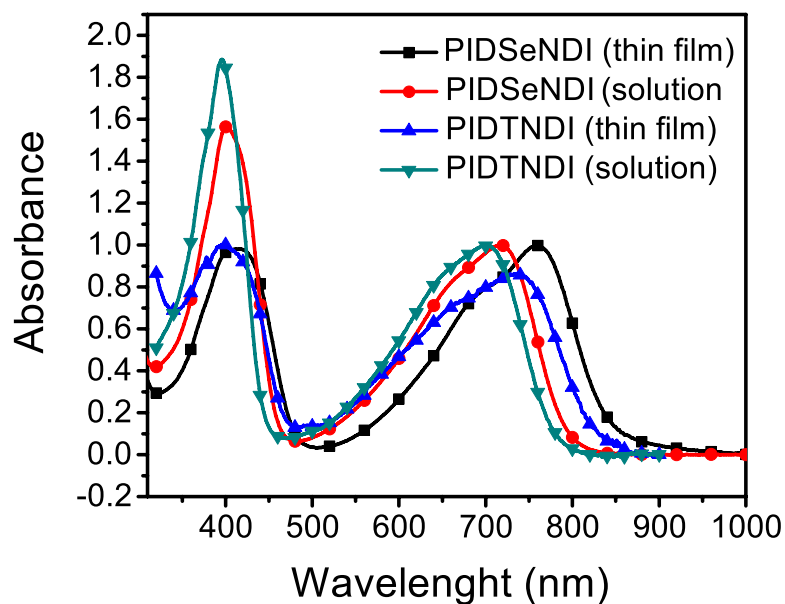


Figure 50 Absorption spectra of **PIDSeNDI** and **PIDTNDI** in chlorobenzene and thin film

Table 10 Molecular weight, optical and electrochemical properties

Polymers	Mn (kDa)	PDI	$\lambda_{\max}^{\text{sol}}$	$\lambda_{\max}^{\text{film}}$	E_g^{opt} (eV)	LUMO (eV)	HOMO (eV)	E_g^{ec} (eV)
PIDTNDI	34.2	1.88	700	734	1.49	-3.87	-5.62	1.75
PIDSeNDI	57.2	2.07	714	757	1.47	-3.79	-5.55	1.76

3.4.4. OFET mobilities of PIDTNDI and PIDSeNDI

Electron transporting properties of **PIDSeNDI** and **PIDTNDI** were studied with organic field effect transistors (OFETs) by bottom gate top contact configuration. Mobilities of **PIDTNDI** and **PIDSeNDI** are presented in **Table 11**. **PIDTNDI** showed electron mobility of $0.0089 \text{ cm}^2/(\text{V s})$ with an on/off ratio of $1.3 \cdot 10^5$. **PIDSeNDI** showed higher electron mobility compared to **PIDTNDI** and it showed comparable electron mobility to PC₆₀BM ($0.09 \text{ cm}^2/(\text{V s})$) with good electrical-stability. Field-effect electron mobilities of **PIDSeNDI** were found $0.028 \text{ cm}^2/(\text{V s})$ with an on/off ratio of $3 \cdot 10^5$ (). This improvement likely originates from Se-Se interactions due to the larger and more polarizable Se atom [110]. Both materials seem suitable electron mobilities to enhance good charge transport and efficient charge collection at the electrodes.

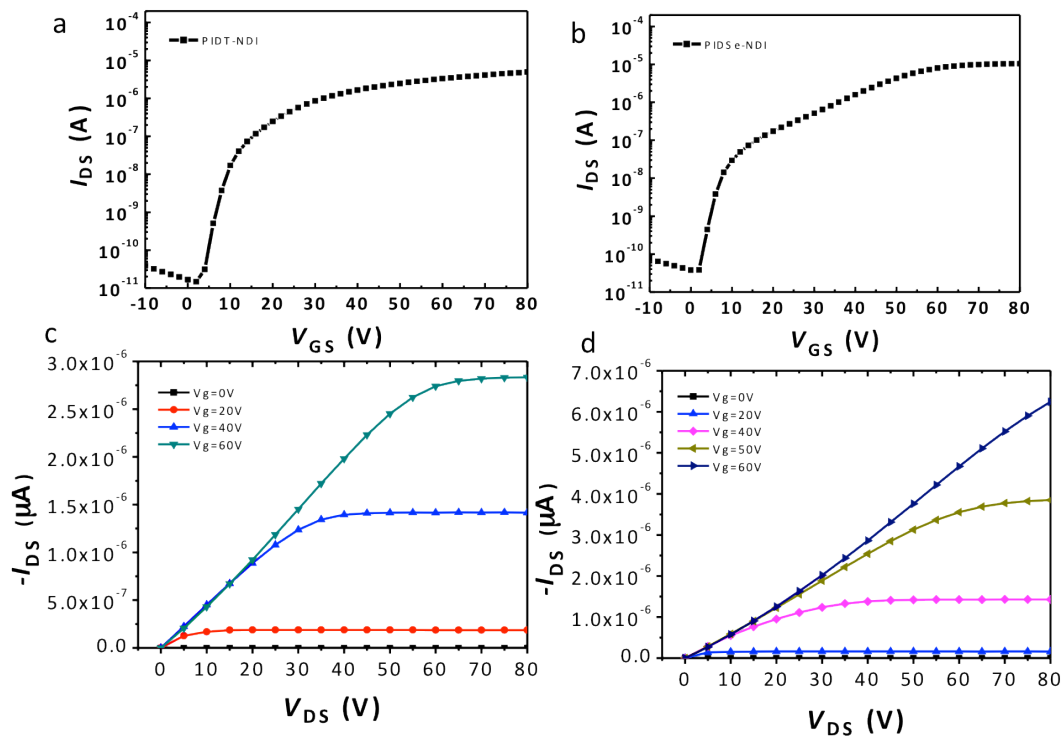


Figure 51 Typical transfer curves of **PIDTNDI** and **PIDSeNDI** based electron only devices

Table 11 Organic Field-Effect Transistor (OFET) mobilities of **PIDTNDI** and **PIDSeNDI**

Polymers	μ_e (cm ² /V.s)	I _{on} /I _{off}
PIDTNDI	0.0083	1.3 10 ⁵
PIDSeNDI	0.028	3 10 ⁵

3.4.5. Fabrication of BHJ OSCs

The inverted structure device configuration of ITO/ZnO/blend/MoO₃/Ag has been chosen for fabrication of all polymer solar cells and, chemical structures of p-type materials and representative energy levels of p-type and n-type materials are depicted on Figure 52. Inverted device configuration was selected due to higher performance and stability that achieved by the removal of susceptible low-work-function metals, preferable vertical phase separation, and favorable distribution of optical field.

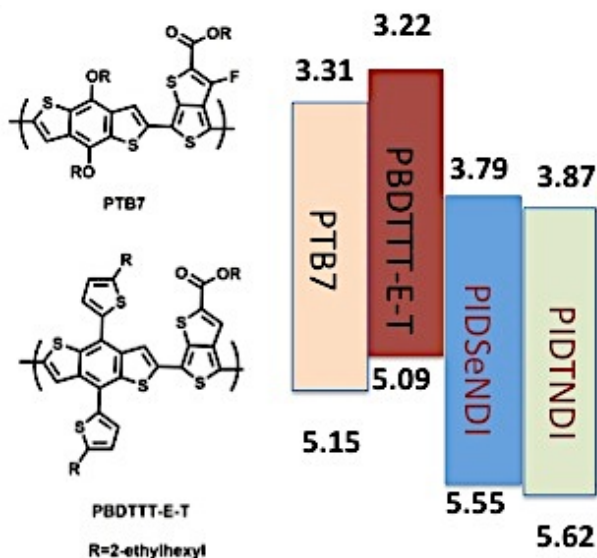


Figure 52 Chemical structures of p-type materials and representative energy levels of p-type and n-type materials

Choice of p-type material was done taking into account of LUMO/LUMO and HOMO/HOMO offsets of donors and acceptors as well as absorption profile. LUMO/LUMO offset should be 0.12-0.3 eV for photoinduced charge transfer and HOMO/ HOMO offset has to be 0.2- 0.3 eV or larger to refine holes on donor units.

Both PTB7 and PBDTTT-E-T seem suitable energy levels for solar cell fabrication. Therefore, as an active layer PTB7 and PBDTTT-E-T mixed with **PIDTNDI** and **PIDSeNDI**, spin coated from dichlorobenzene (DCB) with different composition and the optimal composition was found 1:1 after the fabrication of solar cell from different blend compositions. Neither changing the composition of p-type nor n-type material resulted the increase in PCE of solar cell both system. The current density-voltage (J-V) characteristics of OSCs with different donors are depicted in Figure 53. Corresponding photovoltaic parameters of the devices are summarized in **Table 12**.

PTB7/n-type based solar cell showed relatively lower PCE than device based on PBDTTT-E-T/n-type polymers. The highest PCE was the same for both system with small changes in V_{OC} , J_{SC} and FF. PCE was found 0.51 % with $V_{OC} = 0.88$ V, $J_{SC} = 1.71$ mA/cm², and FF = 0.34 for **PIDSeNDI** and with $V_{OC} = 0.89$ V, $J_{SC} = 1.88$ mA/cm², and FF = 0.31 for **PIDTNDI**. Modification of molecular structure of p-type material by increasing the dimensionality of BDT core with incorporation of thiophene group caused increase in photovoltaic performance.

V_{OC} values of the PSCs based on PBDTTT-E-T was slightly lower than those of PTB7. On the other hand, main differences observed in J_{SC} and increased from 1.71 to 6.17 for **PIDSeNDI** and from 1.88 to 6.21 for **PIDTNDI**. PCEs of the systems were slightly different. The highest PCE was found 2.13 % with $V_{OC} = 0.83$ V, $J_{SC} = 6.21$ mA/cm², and FF = 0.41 for **PIDTNDI**:PBDTTT-E-T. PCE of **PIDSeNDI**:PBDTTT-E-T was 2.02 with $V_{OC} = 0.84$ V, $J_{SC} = 6.17$ mA/cm², and FF = 0.39. Device performance seems sensitive to nature p-type polymers rather than n-type polymers. Therefore, **PIDSeNDI** was selected as a model due to its high-lying HOMO energy level.

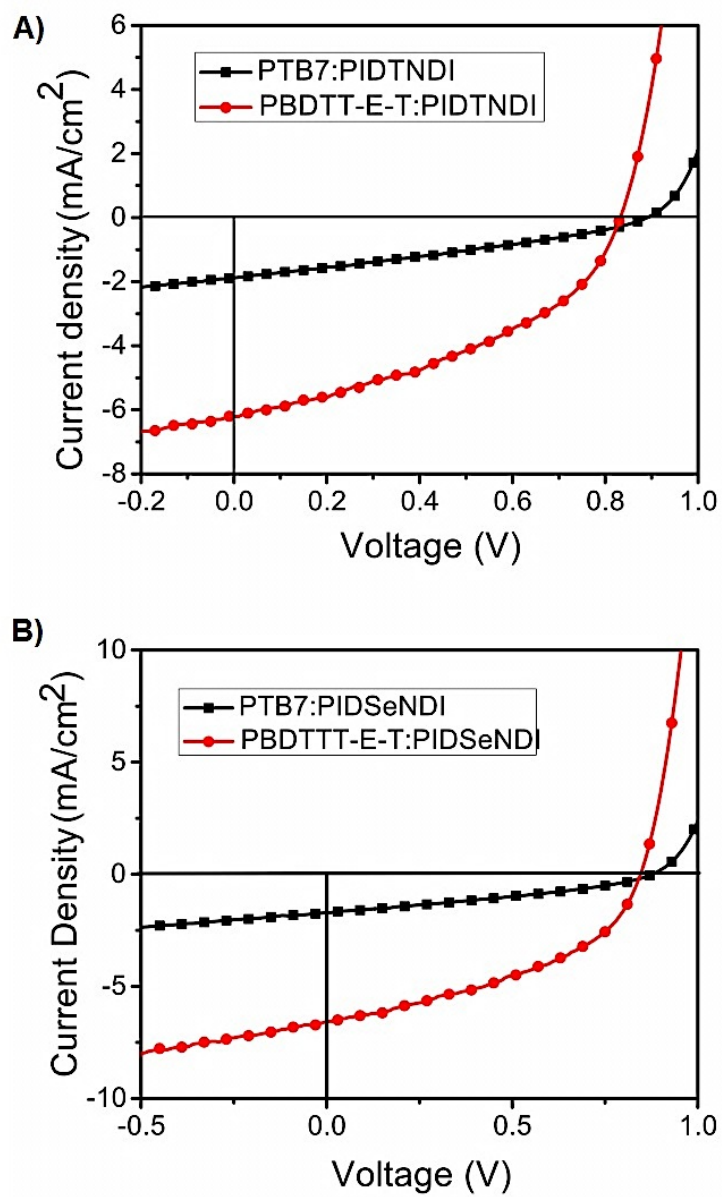


Figure 53 Current density-voltage (J-V) characteristics of all-polymer BHJ solar cells with two different donors

Table 12 Photovoltaic characteristics of all polymer solar cells based on **PIDTNDI** and **PIDSeNDI**

BHJ		J_{SC} (mA/cm²)	FF	PCE (%)
PTB7: PIDTNDI	0.89	1.88	0.31	0.51
PBDTTT-E-T: PIDTNDI	0.83	6.21	0.41	2.13
PTB7: PIDSeNDI	0.88	1.71	0.34	0.51
PBDTTT-E-T: PIDSeNDI	0.84	6.17	0.39	2.02

To verify the change of J_{SC} , the external quantum efficiency (EQE) spectra of the PTB7: **PIDSeNDI** and PBDTTT-E-T: **PIDSeNDI** based OSCs were investigated (Figure 54). To be consistent with absorption spectra of blends, photocurrent response of both systems started from 340 nm and ended at 800 nm. Both **PIDSeNDI** and PTB7 or PBDTTT-E-T made contribution to photon to electron conversion. PTB7: **PIDSeNDI** and PBDTTT-E-T: **PIDSeNDI** EQE curves have similar shapes, but PBDTTT-E-T: **PIDSeNDI** system has a higher photoresponse with highest EQE of 27% at 640 nm than that of PTB7: **PIDSeNDI** device (EQE is around 8%). The J_{SC} values calculated from the EQE curves under the standard AM 1.5 G condition match well with the values obtained from J-V measurement.

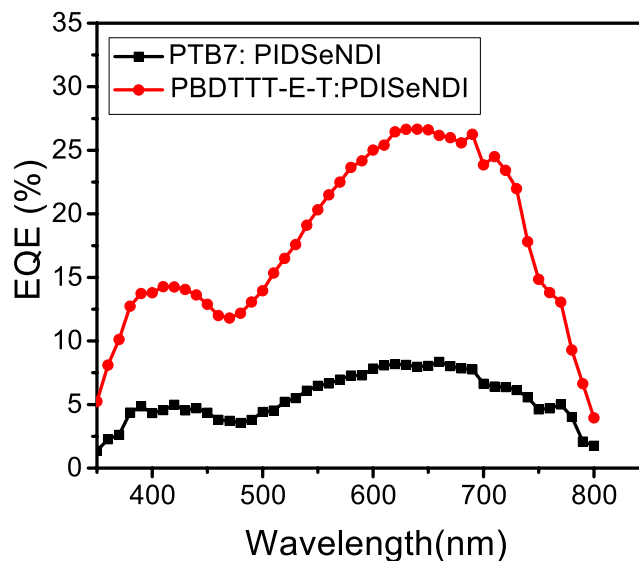


Figure 54 External quantum efficiency (EQE) spectra of all-polymer BHJ OSCs of **PIDSeNDI: PTB7**, **PIDSeNDI: PBDTT-E-T**

3.4.6. Morphology

Morphological findings could be the main reason for the difference in the performance of solar cell. Therefore, we studied AFM to gain deeper insight into film morphologies of different blends and AFM images were depicted in Figure 55. Blend of PBDTTT-E-T: **PIDSeNDI** showed relatively larger aggregates and higher rough surface compared to PBTB7: **PIDSeNDI**. Larger domains could be the indication of phase-separated morphology and enlarged D/A interfacial areas that enhance exciton separation and free charge carriers. These different morphologies can be directly related to molecular structure of p-type polymers. PBDTTT-E-T has a 2D structure that facilitates aggregation leading to larger domains.

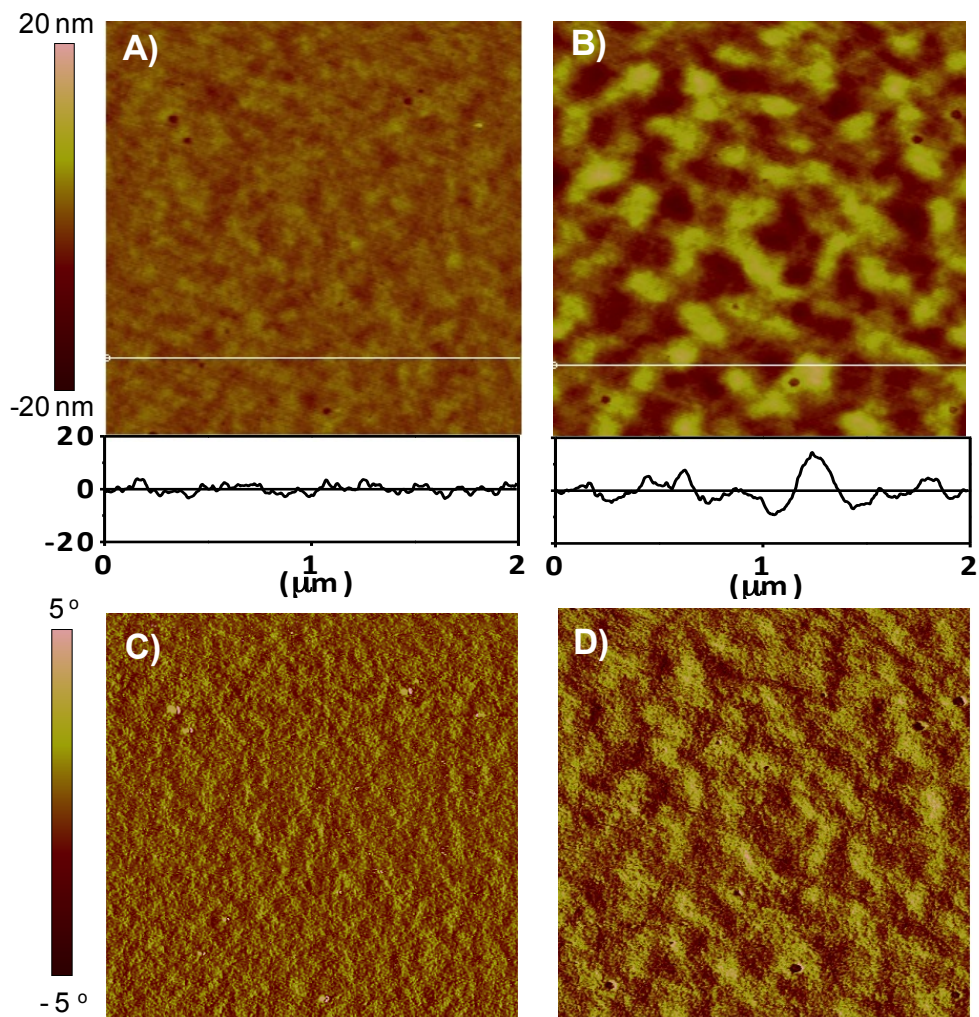


Figure 55 AFM face and height images of PTB7: **PIDSeNDI** (A,C) and PBDTTT-E-T: **PIDSeNDI** (B,D)

3.4.7. SCLC Mobilities

Space charge limited currents have been tested in electron-only devices with a configuration of ITO/Al/BHJ/Ca/Al and hole-only devices with a configuration of ITO/PEDOT: PSS/BHJ/MoO₃/Ag. The mobilities were determined by fitting the dark

current to the model of a single carrier SCLC current with field dependent mobility, which is described as

$$J = \frac{9\varepsilon_r\varepsilon_0\mu_0V^2}{8L^3} \exp\left(\beta\frac{V}{L}\right)$$

Where J is the current, μ_0 is the zero-field mobility, ε_0 is the permittivity of free space, ε_r is the relative permittivity of the material, V is the effective voltage, and L is the thickness of the active layer.

SCLC graph is shown in Figure 56 and electron and hole mobilities are presented in **Table 13**. The average hole and electron mobilities for the blend of PBT7: **PIDSeNDI** are found to be $2.73 \times 10^{-3} \text{ cm}^2/\text{V.s}$ and $2.30 \times 10^{-7} \text{ cm}^2/\text{V.s}$, respectively. The blend of PBDTTT-E-T: **PIDSeNDI** exhibited enhanced charge transport with a hole mobility of $2.66 \times 10^{-3} \text{ cm}^2/\text{V.s}$ and electron mobility of $4.66 \times 10^{-7} \text{ cm}^2/\text{V.s}$. The slightly improved charge transport would lead to an enhancement in the J_{SC} of PBDTTT-E-T: **PIDSeNDI** based OSC. Nevertheless, the measured low electron mobilities in these systems are the primary reason to determine the low overall performance.

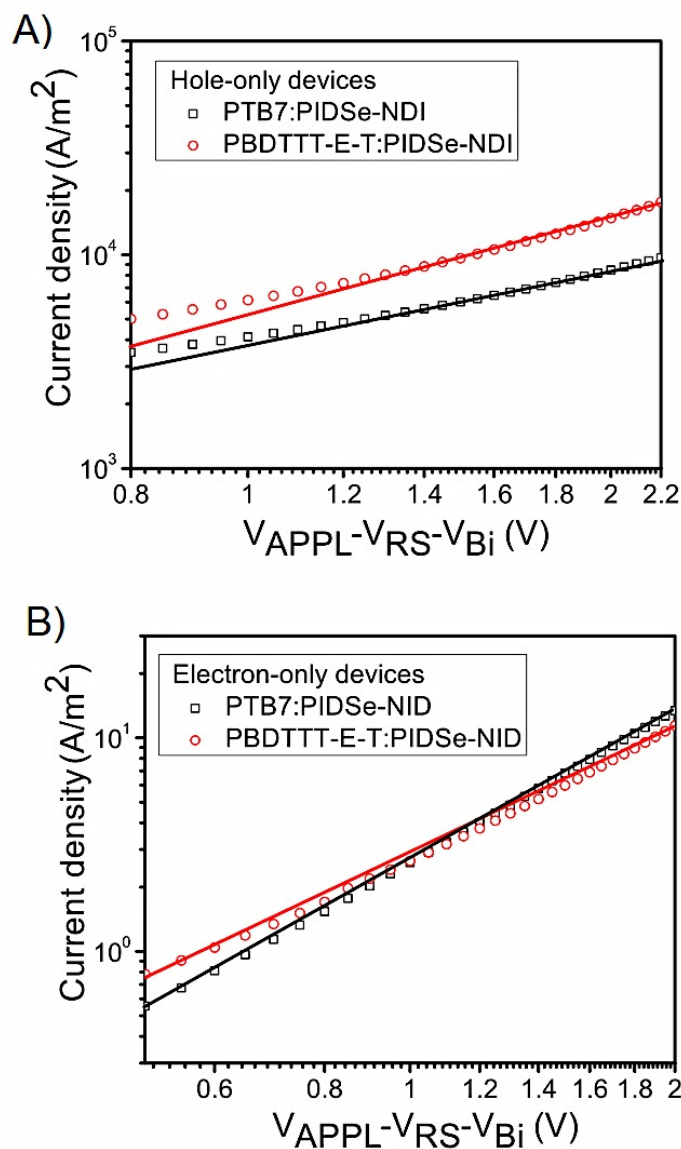


Figure 56 J-V characteristics under dark for hole-only and electron-only devices consisting of PTB7: **PIDSeNDI** and PBDTTT-E-T: **PIDSeNDI** BHJ films. The bias (V) is corrected for built-in voltage, V_{Bi} , arising from different in the work function of the contacts, and the voltage drop due to substrate series resistance (V_{RS}), such that $V=V_{APPL}-V_{RS}-V_{Bi}$. (V_{APPL} is the applied voltage). The solid lines represent the fitting curves.

Table 13 SCLC mobilities of PTB7: **PIDSeNDI** and PBDTTT-E-T: **PIDSeNDI** BHJ films

Polymers: PIDSeNDI	$\mu_h(\text{cm}^2/\text{V.s})$	$\mu_e(\text{cm}^2/\text{V.s})$	μ_e/μ_h
PBT7: PIDSeNDI	2.73×10^{-3}	2.30×10^{-7}	0.84×10^{-4}
PBDTTT-E-T: PIDSeNDI	2.66×10^{-3}	4.66×10^{-7}	1.75×10^{-4}

3.4.8. Light intensity dependence of J_{sc} and V_{oc}

Fill factors (FF) of devices fabricated from **PIDSeNDI** are low. This depressed FF can be explained by carrier recombination that causes in both reduced carrier lifetime and low extractable current. As stated before, there are two types of recombination process (i.e monomolecular and bimolecular) observed under short circuit and open voltage conditions. Bimolecular recombination is known as the recombination of free electron and holes in bulk heterojunction layer and observed at open voltage condition since the built-in potential is cancelled out and photo-generated carriers remain and accumulate inside the device

At short circuit condition, charges are separated and swept out prior to recombination due to built-in voltage. Therefore, bimolecular recombination is rare. Trap-assisted monomolecular recombination is observed in this condition. Therefore, light intensity dependence of J_{sc} provides information about recombination mechanism. Short circuit voltage causes a linear dependence on the light intensity with a slope of close to 1 in the absence of biomolecular recombination so deviation from 1 is correlated to biomolecular recombination, space charge effects, and variations in mobility of hole and electron [111].

The dependence of J_{SC} on the light intensity in PTB7 blend has a slope of 0.92, which is close to unity. The nearly linear dependence indicates that bimolecular recombination is weak. However, the slope decreases to 0.87 for the device based on PBDTTT-E-T blend. The deviation of slope from 1 is typically attributed to the bimolecular recombination, space charge effects, and variations in mobility between the two carriers. As shown in Figure 57, the low electron/hole mobility ratios (10^{-4} - 10^{-3}) in these system indicate that space charge effects and unbalanced charge transport should be responsible for the deviation of slope from unity to the decreased slope, which may be responsible for the relatively low FF in the OSCs [112].

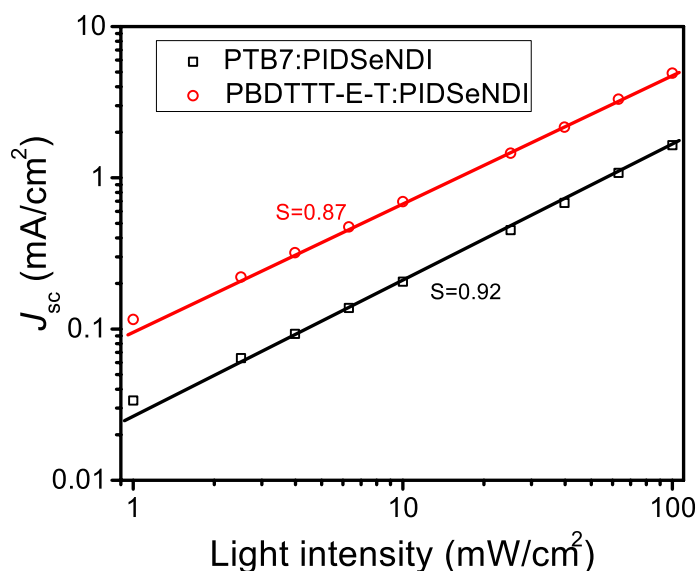


Figure 57 Light intensity dependence of J_{SC} in BHJ (1: 1) with inverted configuration

At open circuit condition, charges are accumulated inside the device since the current is zero and the built-in potential is cancelled out within the cell. Therefore, bimolecular recombination is overwhelmed over monomolecular recombination. V_{OC} is defined according to following equation:

$$q \cdot V_{OC} = \Delta E_{DA} - k_B \cdot T \cdot \ln \left(\frac{J_{sc}}{J_0} + 1 \right)$$

where, the first term is the effective band gap, which is energy difference between $E_{HOMO,D}$ and $E_{LUMO,A}$, the second term represent disorder-induced V_{OC} loss, and the third term present carrier recombination induced V_{OC} loss.

Therefore, examination of the light intensity dependence of V_{OC} provides information about recombination process. At low light intensities V_{OC} rapidly increases until a certain point after which V_{OC} turns over and enters a partially saturated regime. Typically for trap-free operation, OSCs devices exhibit a linear dependence of V_{OC} on light intensity when plotted on a linear-log plot. The slope of the V_{OC} versus the natural logarithm of the light intensity gives kT/q for bimolecular recombination [112]. However, electron trapping, and a sub-linear dependence are generally observed for all polymer solar cells. Therefore, bimolecular recombination dominates at open circuit condition for PBDTTT-E-T: **PIDSeNDI** device and monomolecular trap-assistant recombination is also observed. Moreover, the stronger dependence of V_{OC} on light intensity in PTB7: **PIDSeNDI** devices indicates that more pronounced recombination occurs from electron trapping compared to PBDTTT-E-T: **PIDSeNDI** (Figure 58).

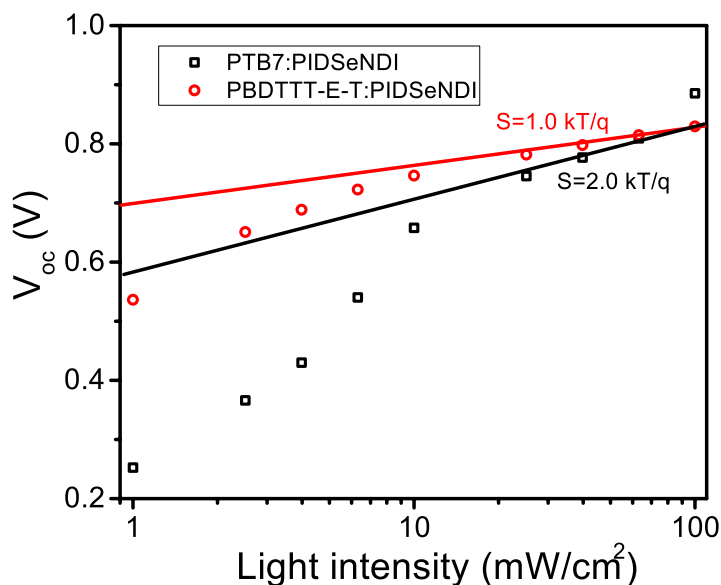


Figure 58 Light intensity dependence of V_{OC} in BHJ (1:1) with inverted configuration

In summary, we developed n-type conjugated polymers namely **PIDSeNDI** and **PIDTNDI** for all-polymer solar cell applications. The corresponding all-polymer OSCs found that PCEs changed from 0.51%-2.02% for **PIDSeNDI** and 0.51% to 2.13% for **PIDTNDI** devices blended with PTB7 and PBDTTT-E-T respectively. The morphology and phase domains of all-polymer blends dramatically affect their device performances. Light intensity dependence of J_{SC} and V_{OC} was performed to understand the charge recombination kinetics, which suggests both strong bimolecular and trap-assisted recombination are the main cause of the low performance in the studied low performance all-polymer solar cells.

CHAPTER 4

CONCLUSION

P-type conjugated polymers containing different donor units and BTz acceptor units were prepared via electrochemical and chemical methods. Electrochemical, spectroelectrochemical, and kinetic studies of polymers were studied in order to probe the electrochemical, and electrochromic properties. Polymers were exhibited promising electrochromic properties in terms of optical contrast and switching times.

Electrochemically synthesized BTz based DAD type polymers **PTTBT** and **PFTBT** were characterized in terms of their electrochemical and spectral properties. Relatively low monomer oxidation for FBT (1.15 V) allowed formation of conjugated polymer film although furan containing monomers although their polymers tend to get overoxidized easily. Polymer oxidation and reduction characteristics for PTTBT and PFBT showed that both polymers have ambipolar characteristics with relatively low HOMO / LUMO energy levels. Comparison among all BTz based monomers showed that increasing electron density of donor unit is decreasing the monomer oxidation potential of the monomer to some extent where donor acceptor match is an important effect on electronic properties of DAD material. Spectroelectrochemical studies showed that stepwise oxidation of **PTTBT** and **PFBT** allow detection of multicolored electrochromic states. Reported electrochemical and optical properties of polymers suggest that **PTTBT** and **PFBT** are great candidates for nonemissive electrochromic device applications as all BTz based conjugated polymers, which may be used as active

materials in future display technology.

Dithienopyrrole (DTP) was utilized another donor unit to probe its effect on optical and electrochemical properties of benzotriazole based conjugated polymers. Therefore, a series of polymers namely **PDTPBTz**, **PDTPBT**, and **PDTPHTBT** were synthesized via Stille coupling reaction. Thiophene and 3-hexylthiophene were incorporated as π -bridging units between BTz and DTP. Optical properties, i.e. maximum absorption in thin film and electrochemical properties, i.e. HOMO-LUMO energy alignment were also affected from presence of the π -bridging units. π -bridging units affected the switching times and optical contrast. Steric effect created or reduced by π -bridging units affected switching times and optical contrast. All three polymers showed moderate optical contrast in visible region and **PDTPBTz** showed 70% optical contrast in NIR region. **PDTPBT** exhibited fast switching time since thiophene creates an interspace making ejection and injection of the counter ions during oxidation and reduction processes easy.

Benzodithiophene was coupled with benzotriazole for electrochromic and optoelectronic applications. Thieno[3,2-*b*]thiophene and furan was inserted as π -bridging units. **PTTBTBDT** had red-shifted absorption profile and **PFBTBDT** has low-lying HOMO energy level. Besides both polymers showed multichromism, fast switching time, and moderate optical contrast in electrochromic applications. OSC fabrication of **PFBTBFT** was performed with conventional device configuration and optimization studies like different polymer: PCBM blend ratio, annealing, solvent, methanol treatment, and additives were performed. Polymer showed 2.98% PCE with 1:3 **PFBTBF**: PCBM blend ratio. Morphological findings were performed to elucidate the factors affecting performance. It was found that high RMS roughness and larger domains could be the reason for limiting the performance of solar cell.

We also developed n-type conjugated polymers namely **PIDSeNDI** and **PIDTNDI** for all- polymer solar cell applications. The corresponding all-polymer OSCs and found that PCEs changed from 0.51%-2.02% for **PIDSeNDI** and 0.51% to 2.13% for **PIDTNDI**

devices blended with PTB7 and PBDTTT-E-T respectively. The morphology and phase domains of all-polymer blends dramatically affect their device performances. Light intensity dependence of J_{SC} and V_{OC} was performed to understand the charge recombination kinetics, which suggests both strong bimolecular and trap-assisted recombination are the main cause of the low performance in the studied low performance all-polymer solar cells.

REFERENCES

1. H. Letheby, *J. Chem. Soc.* 1862, 15, 161
2. G. Natta, G. Mazzanti, P. Corradini, *Atti. Acad. Naz. Lincei Rend. CI. Sci. Fis. Mat. Natur.* 1958, 25, 3
3. H. Shirakawa, E. J. Louis, A. G. MacDiarmid, C. K. Chiang, A. J. Heeger, *J. Chem. Soc. Chem. Commun.* 1977, 578
4. C. K. Chiang, Y. W. Park, A. J. Heeger, H. Shirakawa, E. J. Louis, A. G. MacDiarmid, *Phys. Rev. Lett.* 1977, 39, 1098
5. A. F. Diaz, K. K. Kanazawa, G. P. Gardini, *J. Chem. Soc. Chem. Commun.* 1979, 635
6. J. Heinze, B. A. Frontana-Uribe, S. Ludwigs, *Chem. Rev.* 2010, 110, 4724
7. L. Dami, *Intelligent Macromolecules for Smart Devices From Materials Synthesis to Device Applications*, Springer-Verlag London Limited, 2004
8. J. L. Bredas, G. B. Street, *Acc. Chem. Res.* 1985, 18, 309
9. B. D. Malhotra, *Handbook of Polymers in Electronics*, United Kingdom, Rapra Technology Limited, 2002
10. J. A. Pople, S. H. Walmsley, *Molecular Physics* 1962, 5, 15
11. T. A. Skotheim, J. R. Reynolds, *Handbook of Conducting Polymers Third Edition, Conjugated polymers, theory, synthesis, properties, and characterization*, CRC Press Taylor & Francis Group, 2007
12. D. Emin, T. Holstein, *Physical Review Letters*, 1976, 36, 323
13. K. Müllen, J. R. Reynolds, T. Masuda, *Conjugated Polymers: A Practical Guide to Synthesis*, Cambridge, GBR: Royal Society of Chemistry, 2013
14. N. Miyaoura, K. Yamada, A. Suzuki, *Tetrahedron Lett.* 1979, 20, 3437

15. F. A. Carey, R.J. Sudberg, *Advanced Organic Chemistry, Part B: Reactions and Synthesis*, New York, NY: Springer, 2001
16. D. Milstein, J. K. Stille, *J. Am. Chem. Soc.* 1978, 100, 3636
17. M. Kosugi, K. Sasazawa, Y. Shimizu, T. Migita, *Chem. Lett.* 1977, 6, 301
18. S. Sadki, P. Schottland, N. Brodie, G. Sabouraud, *Chem. Soc. Rev.* 2000, 29, 283
19. J. Roncali, *J. Mater. Chem.* 1999, 9, 1875
20. P. Bamfield, *Chromic Phenomena The Technological Applications of Colour Chemistry*, Cambridge, Royal Society of Chemistry, 2001
21. J. L. Bré das, *J. Chem. Phys.* 1985, 82, 3808
22. F. C. Krebs, *Polymer Photovoltaics*, Bellingham, Wash.: SPIE Press, 2008
23. A. Luque, S. Hegedus, *Handbook of Photovoltaic Science and Engineering*, Chichester, Wiley, 2003
24. S.-S. Sun, N. S. Sariciftci *Organic Photovoltaics*, Boca Raton, FL: Taylor& Francis, 2005
25. R. Po, M. Maggini, N. Camaioni, *J. Phys. Chem. C* 2010, 114, 695
26. S. Günes, H. Neugebauer, N. S. Sariciftci, *Chem. Rev.* 2007, 107, 1324
27. Y. Li, *Accounts of Chemical Research*, 2012, 45, 723
28. P. Heremans, D. Cheyys, B. P. Rand, *Acc. Chem. Res.* 2009, 42, 1740
29. M. Pagliaro, G. Palmisano, R. Ciriminna, 2008, Weinheim, Wiley-VCH
30. W.C.H, Choy, *Organic solar cells*. London: Springer, 2013
31. V. A. Trukhanov, V. V. Bruevich, D. Y. Paraschuk, *Sci. Rep.* 2015, 5, 11478
32. A. J. Heeger, *Adv. Mater.* 2014, 26, 10
33. P. Heremans, D. Cheyys, B. P. Rand, *Acc. Chem. Res.* 2009, 42, 1740
34. L. J. A. Koster, V. D. Mihailetschi, P. W. M. Blom, *Appl. Phys. Lett.* 2006, 88, 052104
35. C. W. Tang, *Appl. Phys. Lett.* 1986, 48, 183
36. B. Qi, J. Wang, *J. Mater. Chem.* 2012, 22, 24315
37. C. J. Brabec, A. Cravino, D. Meissner, N. S. Sariciftci, T. Fromherz, M. T. Rispens, L. Sanchez, J. C. Hummelen, *Adv. Funct. Mater.* 2001, 11, 374.

38. H. Ma, H.-L. Yip, F. Huang, A. K.-Y. Jen, *Adv. Funct. Mater.* 2010, 20, 1371
39. C. J. Brabec, A. Cravino, D. Meissner, N. S. Sariciftci, T. Fromherz, M. T. Rispens, L. Sanchez, J. C. Hummelen, *Adv. Funct. Mater.* 2001, 11, 374.
40. M. C. Scharber, D. Muhlbacher, M. Koppe, P. Denk, C. Waldauf, A. J. Heeger, C. J. Brabec, *Adv. Mater.* 2006, 18, 789
41. X. Guo, N. Zhou, S. J. Lou, J. Smith, D. B. Tice, J. W. Hennek, R. P. Ortiz, J. T. L. Navarrete, S. Li, J. Strzalka, L. X. Chen, R. P. H. Chang, A. Facchetti, T. J. Marks, *Nature Photonics* 2013, 7, 825
42. C. W. Tang, *Appl. Phys. Lett.* 1986, 48, 183
43. J. Roncali, *Chem. Rev.* 1997, 97, 173
44. M. Kertesz, C. H. Choi, S. Yang, *Chem. Rev.* 2005, 105, 3448
45. J.L. Brédas, *J. Chem. Phys.* 1985, 82, 3808
46. Y.-J. Cheng, S.-H. Yang, C.-S. Hsu, *Chem. Rev.* 2009, 109, 5868
47. E. E. Havinga, W. ten Hoeve, H. Wynberg, *Synth. Met.* 1993, 55, 299
48. Z.-G. Zhang, J. Wang, *J. Mater. Chem.* 2012, 22, 4178
49. A. Balan, D. Baran, L. Toppare, *Polym. Chem.* 2011, 2, 1029
50. S. C. Price, A. C. Stuart, L. Yang, H. Zhou, W. You, *J. Am. Chem. Soc.* 2011, 133, 4625
51. J. Min, Z.-G. Zhang, S. Zhang, M. Zhang, J. Zhang, Y. Li, *Macromolecules* 2011, 44, 7632
52. R. L. Uy, L. Yan, W. Li, W. You, *Macromolecules* 2014, 47, 2289
53. K. Wang, Y. Zhao, W. Tang, Z.-G. Zhang, Q. Fu, Y. Li, *Org. Electron.* 2014, 15, 818
54. O. Erlik, N. A. Unlu, G. Hizalan, S. O. Hacioglu, S. Comez, E. D. Yildiz, L. Toppare, A. Cirpan, *J. Polym. Sci., Part A: Polym. Chem.* 2015, 53, 1541
55. H. Unay, N. A. Unlu, G. Hizalan, S. O. Hacioglu, D. E. Yildiz, L. Toppare, A. Cirpan, *J. Polym. Sci., Part A: Polym. Chem.* 2015, 53, 528
56. L. Zhang, C. He, J. Chen, P. Yuan, L. Huang, C. Zhang, W. Cai, Z. Liu, Y. Cao, *Macromolecules* 2010, 43, 9771

57. T. Liu, A. Troisi, *Adv. Mater.* 2013, 25, 1038
58. A. Facchetti, *Mater. Today*, 2013,16, 123
59. E. Ahmed, G. Ren, F. S. Kim, E. C. Hollenbeck, S. A. Jenekhe, *Chem. Mater.* 2011, 23, 4563
60. J. W. Jung, J. W. Jo, C.-C. Chueh, F. Liu, W. H. Jo, T. P. Russell, A. K.-Y. Jen, *Adv. Mater.* 2015, 27, 3310
61. A. Luzio, D. Fazzi, D. Natali, E. Giussani, K.-J. Baeg, Z. Chen, Y.-Y. Noh, A. Facchetti, M. Caironi, *Adv. Funct. Mater.* 2014, 24, 1151.
62. R. Kim, P. S. K. Amegadze, H. -J. Yun, Y. -Y. Noh, S. -K. Kwon, Y. -H. Kim, *Adv. Funct. Mater.* 2013, 23, 5719
63. N. Zhou, H. Lin, S. J. Lou, X. Yu, P. Guo, E. F. Manley, S. Loser, P. Hartnett, H. Huang, M. R. Wasielewski, L. X. Chen, R. P. H. Chang, A. Facchetti, T. J. Marks, *Adv. Energy Mater.* 2014, 4, 1.
64. E. Zhou, J. Cong, Q. Wei, K. Tajima, C. Yang, K. Hashimoto, *Angew. Chem. Int. Ed.* 2011, 50, 2799.
65. T. Earmme, Y.-J. Hwang, N.M. Murari, S. Subramaniyan, S.A. Jenekhe, *J. Am. Chem. Soc.*, 2013, 135, 14960.
66. D. Mori, H. Benten, I. Okada, H. Ohkita, S. Ito, *Adv. Energy Mater.* 2014, 4, 1301006
67. C. R. McNeill, N. C. Greenham, *Adv. Mater.* 2009, 21, 3840
68. M. Schubert, D. Dolfen, J. Frisch, S. Roland, R. Steyrleuthner, B. Stiller, Z. Chen, U. Scherf, N. Koch, A. Facchetti, D. Neher, *Adv. Energy Mater.* 2012, 2, 369.
69. E. Zhou, J. Cong, K. Hashimoto, K. Tajima, *Adv. Mater.* 2013, 25, 6991
70. J. Zaumseil, H. Sirringhaus, *Chem. Rev.* 2007, 107, 1296
71. S. R Sandler, *Polymer Synthesis and Characterization*, Sandiego, Academic Press, 1988
72. P. Monk, R. Mortimer, D. Rosseinsky, *Electrochromism*, Weinheim, VCH, 1995

73. E. Lavion, *J. Electroanal Chem.* 39, 1972,1
74. A. Balan, D. Baran, G. Gunbas, A. Durmus, F. Özyurt, L. Toppare *Chem. Commun* 2009, 6768
75. D. Prim, G. Kirsch, *J. Chem. Soc. Perkin Trans 1* 1994, 18, 2603
76. E. Kaya, A. Balan, D. Baran, A. Cirpan, L. Toppare, *Organic Electronics* 2011, 12, 202
77. J. J. Intemann, K. Yao, H.-L. Yip, Y.-X. Xu, Y.-X. Li, P.-W. Liang, F.-Z. Ding, X. Li, A.K.-Y. Jen, *Chem. Mater.* 2013, 25, 3188
78. A. Balan, G. Gunbas, A. Durmus, L. Toppare *Chem. Mater.* 2008, 20, 7510
79. G. A. Çetin, A. Balan, A. Durmus, G. Gunbas, L. Toppare *Org. Electron.* 2009, 10, 34
80. D. Baran, A. Balan, B. M. Esteban, H. Neugebauer, N. S. Sariciftci, L. Toppare *Macromol. Chem. Phys.* 2010, 211, 2602
81. D. Baran, A. Balan, S. Celebi, B. M. Esteban, H. Neugebauer, N. S. Sariciftci, L. Toppare, *Chem. Mater.* 2010, 22, 2978
82. P. Merino, T. Tejero, J. I. Delso, R. Matute *Curr. Org. Chem.* 2007, 11, 1076
83. J. K. Politis, J. C. Nemes, M. D. Curtis *J. Am. Chem. Soc.* 2001, 123, 2537
84. S. Glenis, M. Benz, E. LeGoff, J. L. Schindler, C. R. Kannewurf, M.G. Kanatzidis *J. Am. Chem. Soc.* 1993, 115, 12519
85. H. Bronstein, Z. Chen, R. S. Ashraf, W. Zhang, J. Du, J. R. Durrant, P. S. Tuladhar, K. Song, S. E. Watkins, Y. Geerts, M. M. Wienk, R. A. J. Janssen, T. Anthopoulos, H. Sirringhaus, M. Heeney, I. McCulloch, *J. Am. Chem. Soc.* 2011, 133, 3272
86. Y. Li, C.-Y. Chang, Y. Chen, Y. Song, C.-Z. Li, H.-L. Yip, A. K.-Y. Jen, C. Li *J. Mater. Chem. C* 2013, 1, 7526
87. D. Gedefaw, M. Tassarolo, W. Zhuang, R. Kroon, E. Wang, M. Bolognesi, M. Seri, M. Muccinib, M. R. Andersson, *Polym. Chem.* 2014, 5, 2083
88. J. R. Reynolds, A. D. Child, *Macromolecules* 1993, 26, 2095

89. A. Galal, E.T. Lewis, O. Y. Ataman, H. Zimmer, H.; H. B. Jr. Mark J. Polym. Sci. Part A: Polym. Chem. 1989, 27, 1891
90. I. McCulloch, M. Heeney, C. Bailey, K. Genevicius, I. Mac-Donald, M. Shkunov, D. Sparrowe, S. Tierney, R. Wagner, W. Zhang, M. L. Chabinye, R. J. Kline, M. D. McGehee, M. F. Toney, M. F. Nat. Mater. 2006, 5, 328
91. D. R. Bai, T. Baumgartner Organometallics 2010, 29, 3289
92. K. Ogawa, S. C. Rasmussen, Macromolecules 2006, 39, 1771
93. J. Liu, R. Zhang, G. Sauve', T. Kowalewski, R. D. McCullough, J. Am. Chem. Soc. 2008, 130, 13167
94. X. Zhang, T. T. Steckler, R. R. Dasari, S. Ohira, W. J. Potscavage, J. S. P. Tiwari, S. Coppée, S. Ellinger, S. Barlow, J. -L. Brédas, B. Kippelen, J. R. Reynolds, S. R. Marder, J. Mater. Chem. 2010, 20, 123
95. W. Vanormelingen, K. V. Bergh, T. Verbiest, G. Koeckelberghs, Macromolecules 2008, 41, 5582
96. T. T. Steckler, X. Zhang, J. Hwang, R. Honeyager, S. Ohira, X.- H. Zhang, A. Grant, S. Ellinger, S. A. Odom, D. Sweat, D. B. Tanner, A. G. Rinzler, S. Barlow, J. -L. Brédas, B. Kippelen, S. R. Marder, J. R. Reynolds, J. Am. Chem. Soc. 2009, 131, 2824
97. W. Yue, Y. Zhao, S. Shao, H. Tian, Z. Xie, Y. Gengi, F. Wang, J. Mater. Chem. 2009, 19, 2199
98. S. Zhang, Y. Guo, H. Fan, Y. Liu, H. -Y. Chen, G. Yang, X. Zhan, Y. Liu, Y. Li, Y. Yang, J. Polym. Sci.: Part A: Poly. Chem. 2009, 47, 5498.
99. M. Jeffries-EL, B. M. Kobilka, B. J. Hale, Macromolecules, 2014, 47, 7253
100. A. T. Yiu, P. M. Beaujuge, O. P. Lee, C. H. Woo, M. F. Toney, J. M. J. Fréchet J. Am. Chem.Soc. 2012, 134, 2180
101. Y. Wang, Y. Liu, S. Chen, R. Peng, Z. Ge, Chem. Mater. 2013, 25, 3196
102. X. Guo, M. Zhang, L. Huo, F. Xu, Y. Wu, J. Hou, J. Mater. Chem. 2012, 22, 21024

103. S. Ko, E. T. Hoke, L. Pandey, S. Hong, R. Mondal, C. Risko, Y. Yi, R. Noriega, M. D. McGehee, J.-L. Brédas, A. Salleo, Z. Bao, *J. Am. Chem. Soc.* 2012, 134, 5222
104. I. Meager, R. S. Ashraf, S. Mollinger, B. C. Schroeder, H. Bronstein, D. Beatrup, M. S. Vezie, T. Kirchartz, A. Salleo, J. Nelson, I. McCulloch, *J. Am. Chem. Soc.* 2013, 135, 11537
105. H. Huang, N. Zhou, R. P. Ortiz, Z. Chen, S. Loser, S. Zhang, X. Guo, J. Casado, J. T. López Navarrete, X. Yu, A. Facchetti, T. J. Marks, *Adv. Funct. Mater.* 2014, 24, 2782
106. X. Guo, N. Zhou, S. J. Lou, J. W. Hennek, R. P. Ortiz, M. R. Butler, P.-L. T. Boudreault, J. Strzalka, P. O. Morin, M. Leclerc, J. T. L. Navarrete, M. A. Ratner, L. X. Chen, R. P. H. Chang, A. Facchetti, T. J. Marks, *J. Am. Chem. Soc.* 2012, 134, 18427
107. J. J. Intemann, K. Yao, F. Ding, Y. Xu, X. Xin, X. Li, A. K.-Y. Jen, *Adv. Funct. Mater.* 2015, 25, 4889
108. (a) Y.-X. Xu, C.-C. Chueh, H.-L. Yip, F.-Z. Ding, Y.-X. Li, C.-Z. Li, X. Li, W.-C. Chen, A.K.-Y. Jen, *Adv. Mater.* 2012, 24, 6356; (b) J. Roncali, *Macromol. Rapid Commun.* 2007, 28, 1761; (c) D. Hertel, U. Scherf, H. Bäessler, *Adv. Mater.* 1998, 10, 1119; (d) Y.-L. Chen, C.-Y. Chang, Y.-J. Cheng, C.-S. Hsu, *Chem. Mater.* 2012, 24, 3964; (e) J.-S. Wu, Y.-J. Cheng, T.-Y. Lin, C.-Y. Chang, P.-I. Shih, C.-S. Hsu, *Adv. Funct. Mater.* 2012, 22, 1711
109. L. Huo, S. Zhang, X. Guo, F. Xu, Y. Li, J. Hou, *Angew. Chem. Int. Ed.*, 2011, 50, 9697
110. J. S. Ha, K. H. Kim, D. H. Choi, *J. Am. Chem. Soc.* 2011, 133, 10364
111. A. K. K. Kyaw, D. H. Wang, V. Gupta, W. L. Leong, L. Ke, G.C. Bazan, A. J. Heeger, *ACS Nano* 2013, 7, 4569
112. A. Loiudice, A. Rizzo, M. Biasiucci, G. Gigli, *J. Phys. Chem. Lett.* 2012, 3, 1908.

APPENDICES

NMR DATA

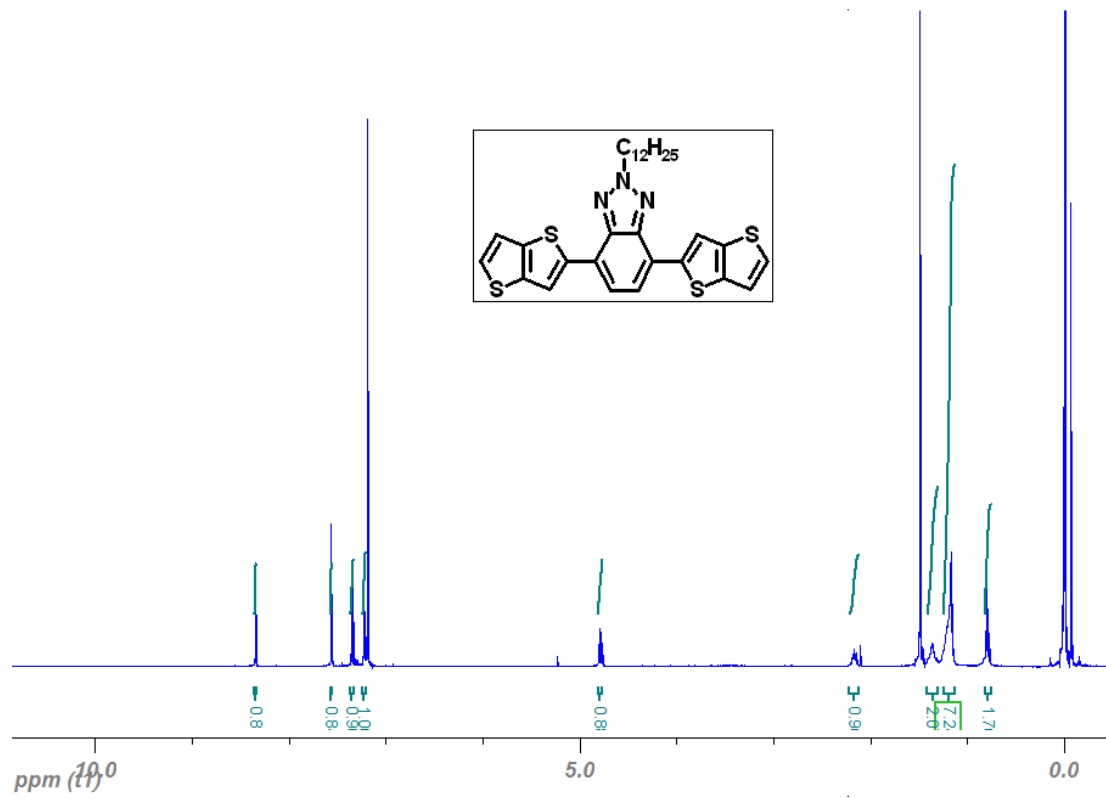


Figure 59 ^1H NMR of 2-(dodecyl)-4,7-bis(thieno[3,2-b]thiophen-2-yl)-2H-benzo[d][1,2,3]triazole

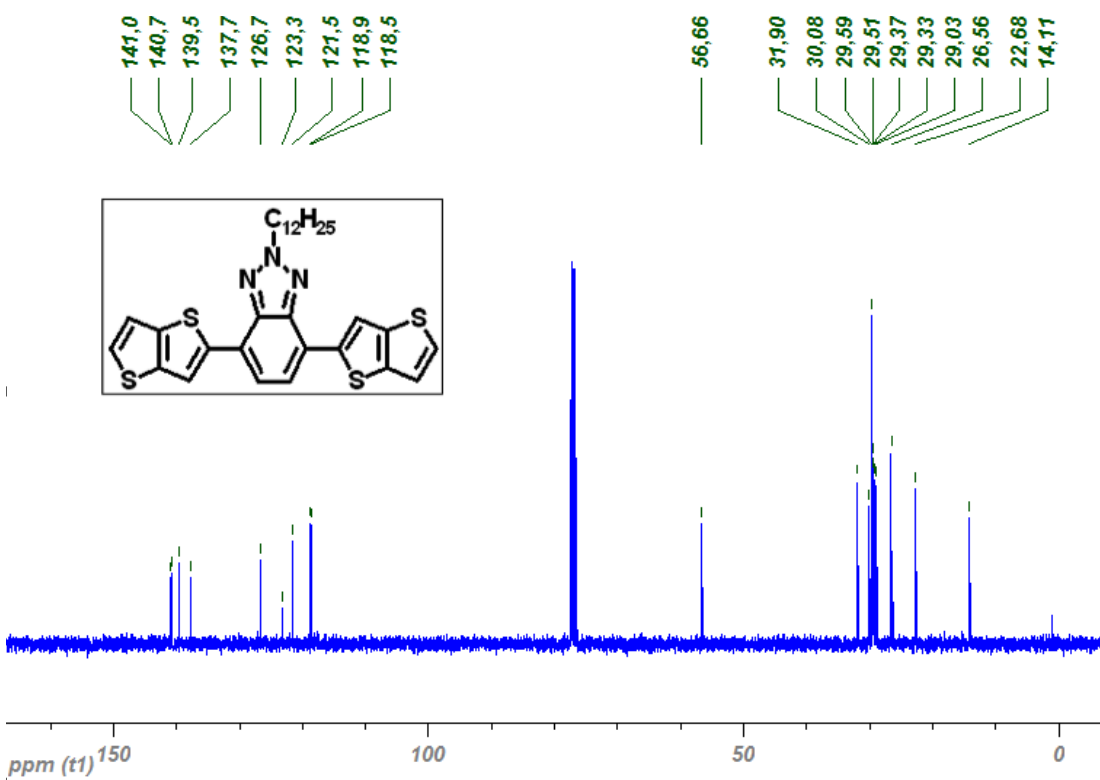


Figure 60 ^{13}C NMR of 2-(dodecyl)-4,7-bis(thieno[3,2-b]thiophen-2-yl)-2H-benzo[d][1,2,3]triazole

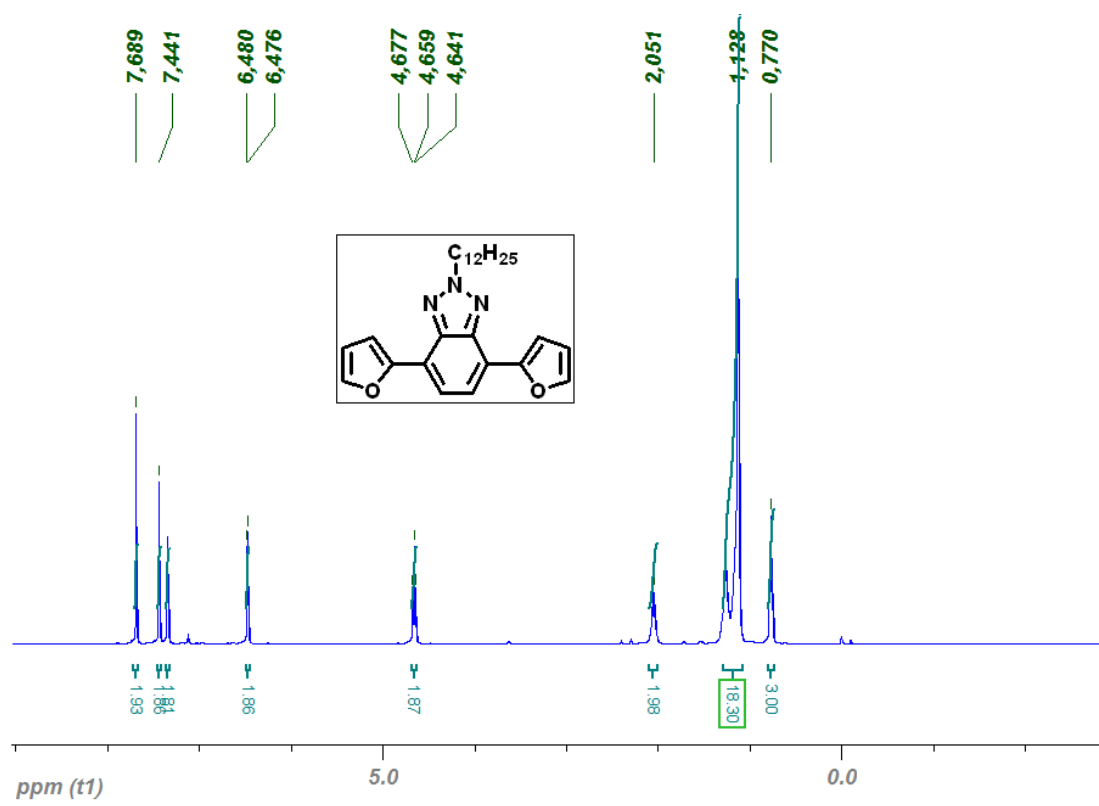


Figure 61 ¹H NMR of 2-Dodecyl-4,7-di(furan-2-yl)-2Hbenzo[d][1,2,3]triazole

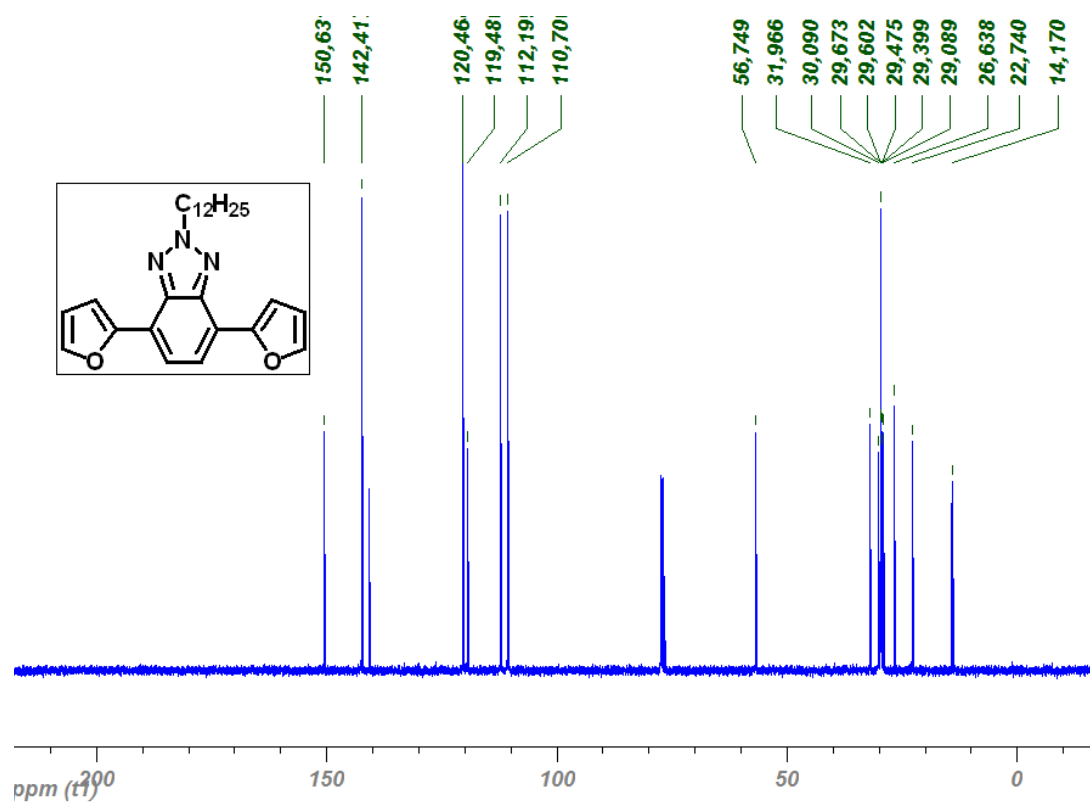
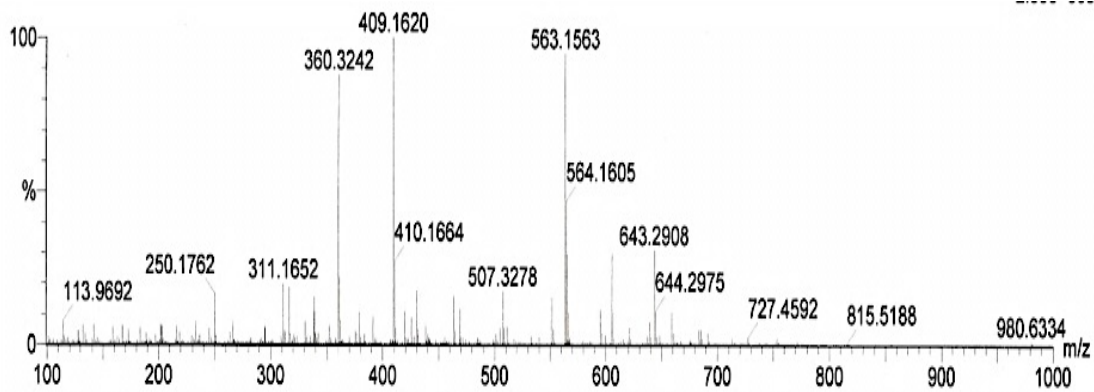


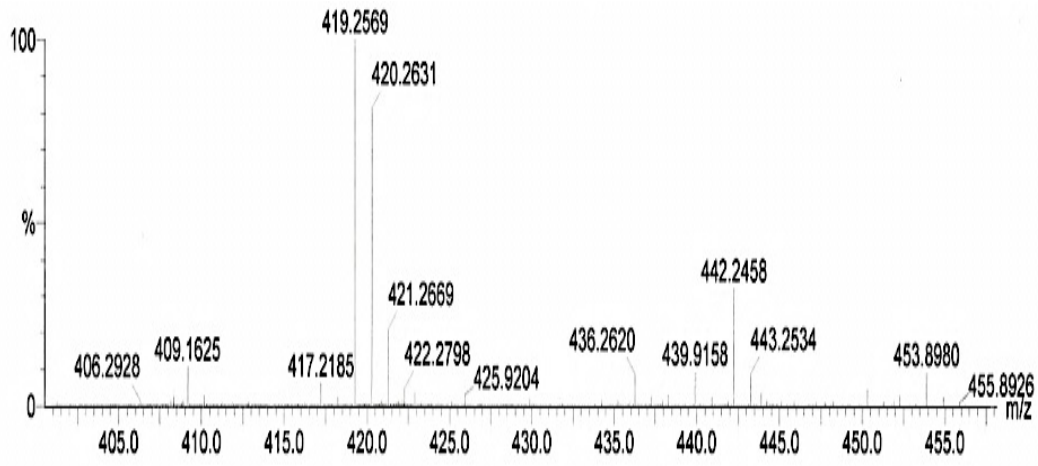
Figure 62 ^{13}C NMR of 2-Dodecyl-4,7-di(furan-2-yl)-2Hbenzo[d][1,2,3]triazole



Minimum: -1.5
 Maximum: 100.0 100.0 100.0

Mass	Calc. Mass	mDa	PPM	DBE	i-FIT	i-FIT (Norm)	Formula
563.1563	563.1557	0.6	1.1	16.0	623.4	1.0	C30 H33 N3 S4
	563.1533	3.0	5.3	13.0	624.4	2.0	C28 H34 N3 Na S4
	563.1683	-12.0	-21.3	15.5	623.0	0.7	C31 H35 N2 S4

Figure 63 HRMS of 2-(dodecyl)-4,7-bis(thieno[3,2-b]thiophen-2-yl)-2H-benzo[d][1,2,3]triazole



Minimum:								
Maximum:		100.0	100.0	100.0				
Mass	Calc. Mass	mDa	PPM	DBE	i-FIT	i-FIT (Norm)	Formula	
419.2569	419.2573	-0.4	-1.0	12.0	859.7	0.0	C26 H33 N3 O2	

Figure 64 HRMS of 2-(dodecyl)-4,7-bis(thieno[3,2-b]thiophen-2-yl)-2H-benzo[d][1,2,3]triazole

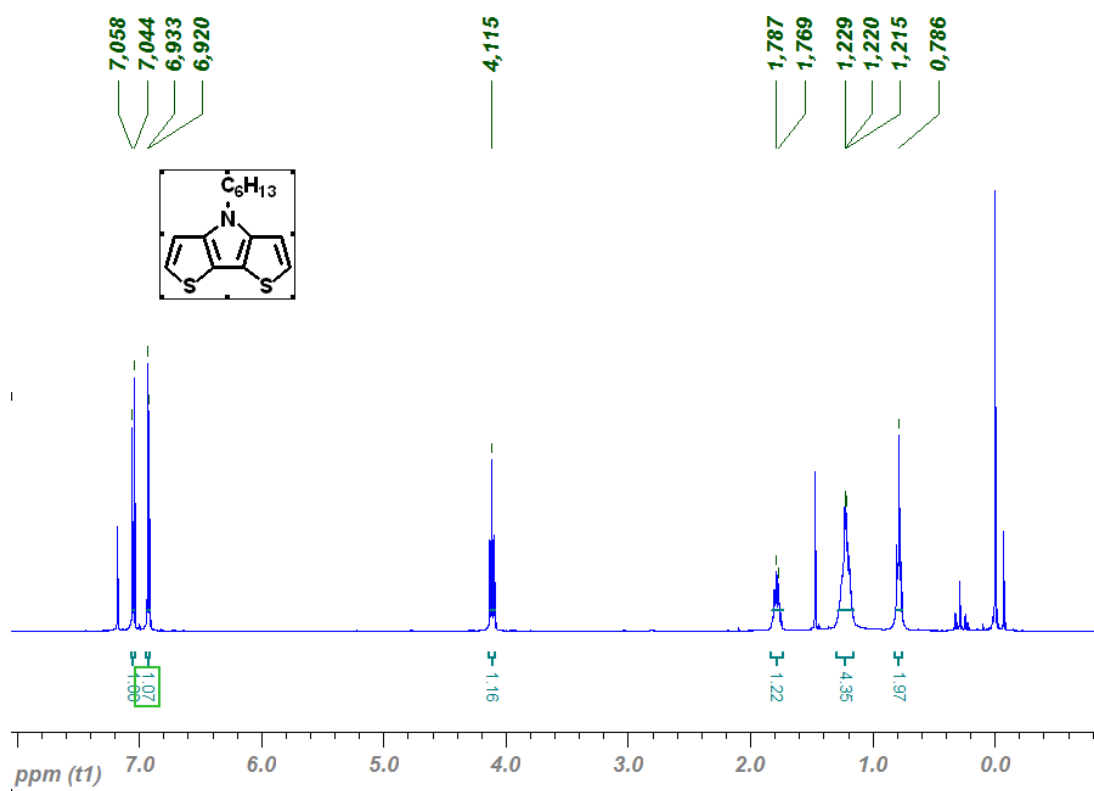


Figure 65 ^1H NMR of 4-hexyl-4H-dithieno[3,2-b:2',3'-d]pyrrole

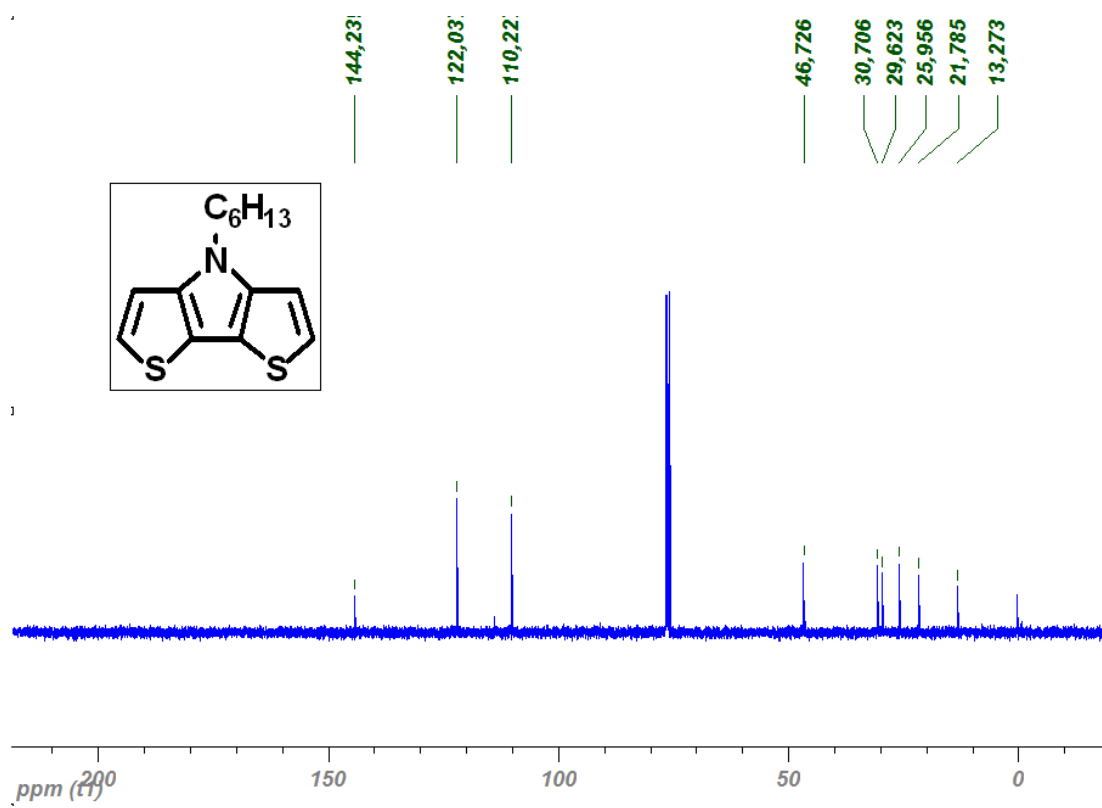


Figure 66 ^{13}C NMR of 4-hexyl-4H-dithieno[3,2-b:2',3'-d]pyrrole

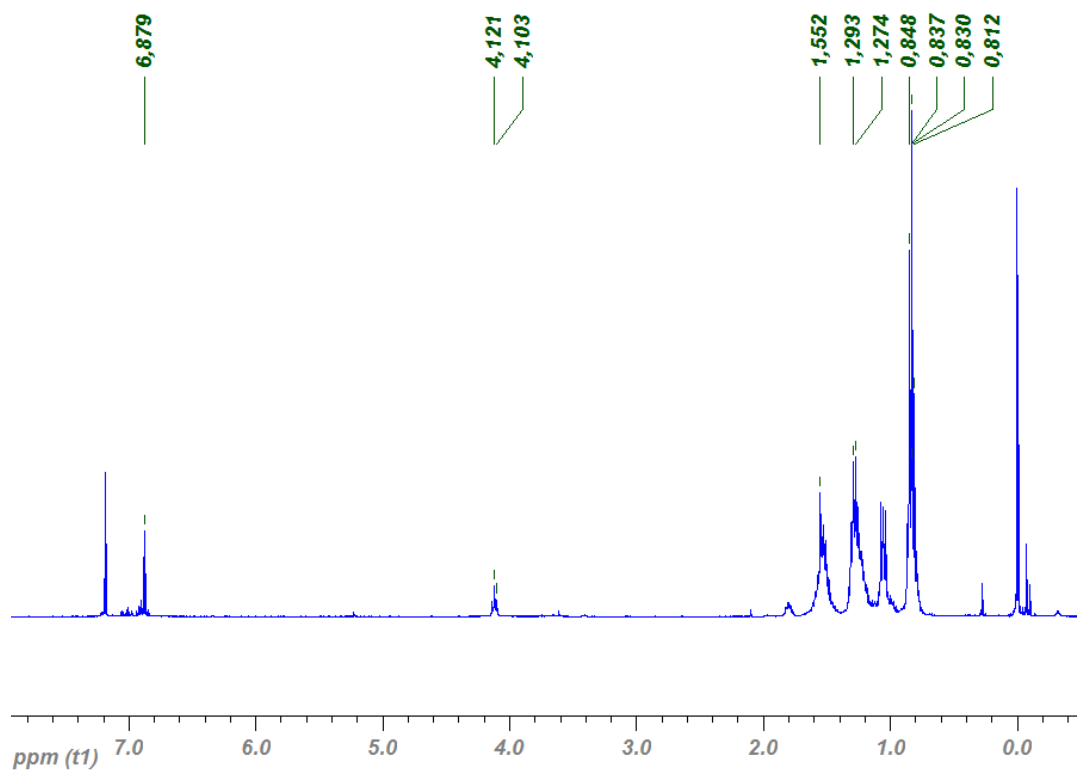


Figure 67 ^1H NMR of 4-hexyl-2,6-bis(tributylstannyl)-4H-dithieno[3,2-b:2',3'-d]pyrrole

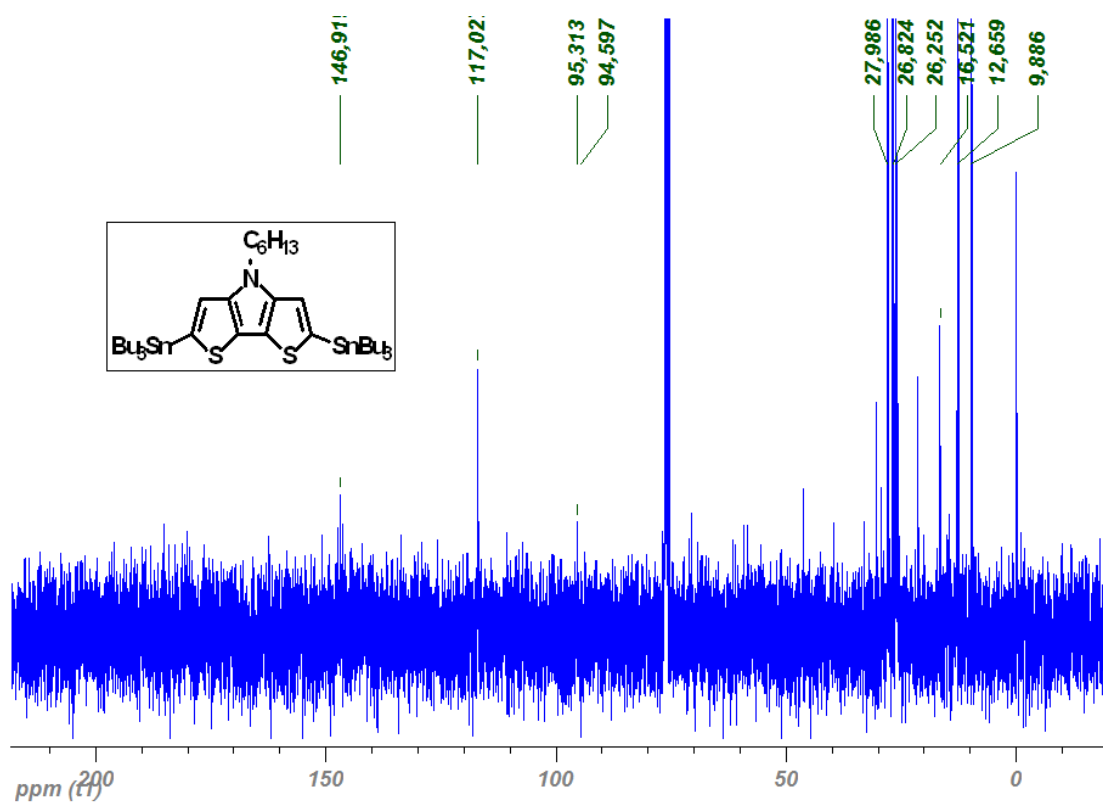


Figure 68 ^{13}C NMR of 4-hexyl-2,6-bis(tributylstannyl)-4H-dithieno[3,2-b:2',3'-d]pyrrole

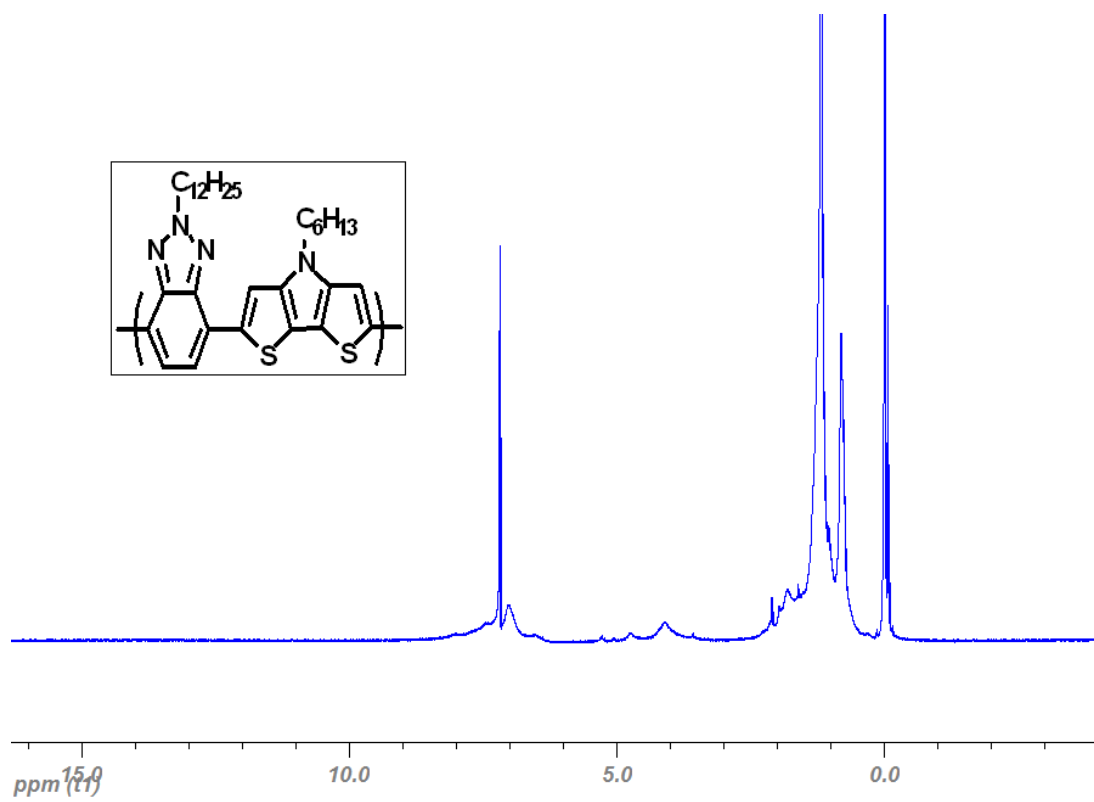


Figure 69 ^1H NMR of PDTPBTz

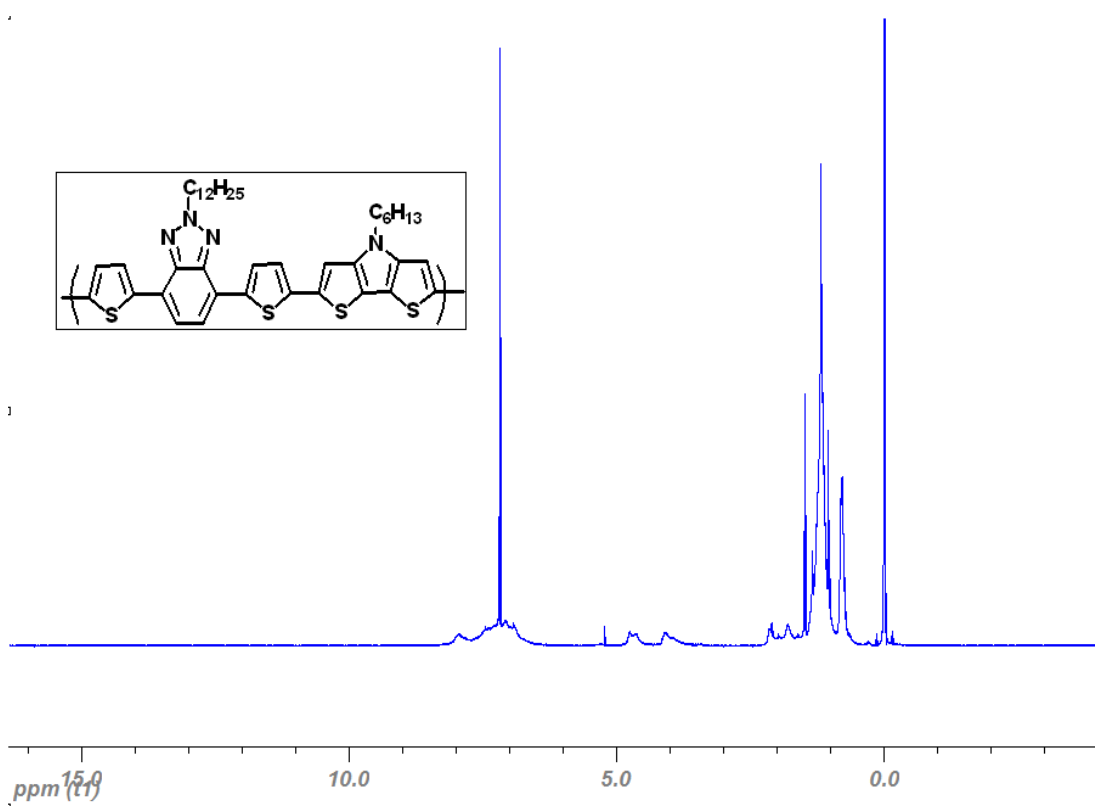


Figure 70 ^1H NMR of PDTPTBT

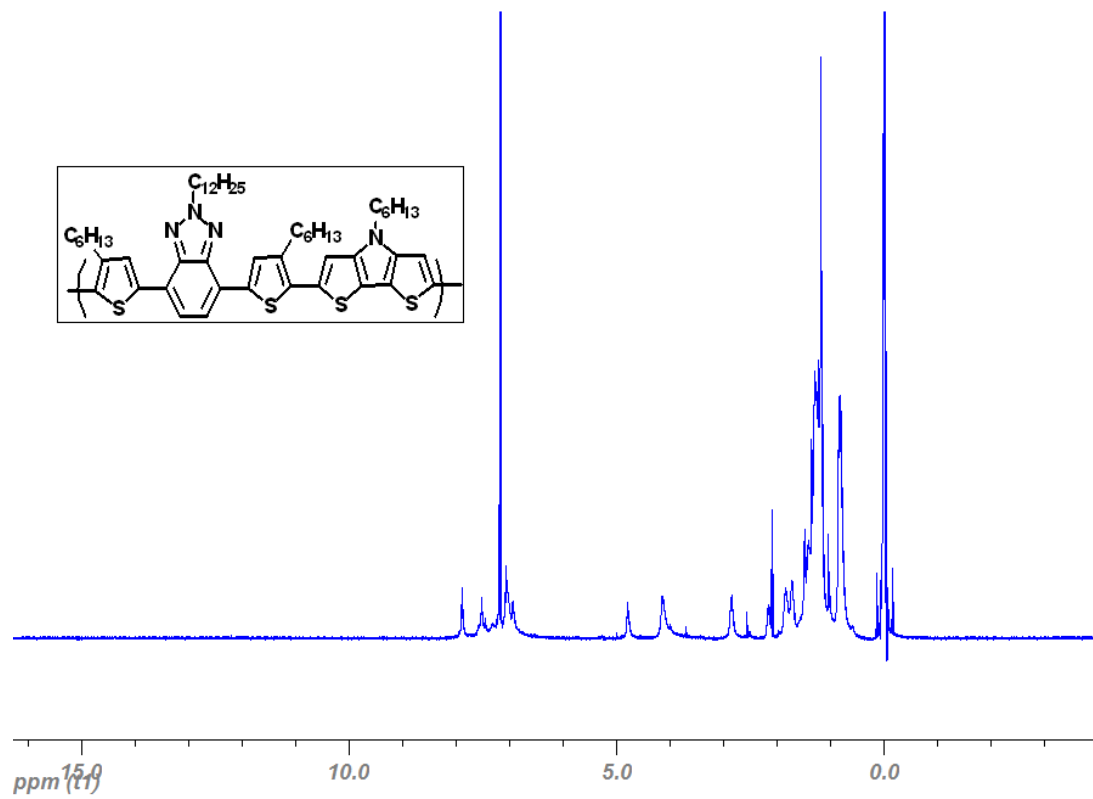


Figure 71 ^1H NMR of PDTPTBT

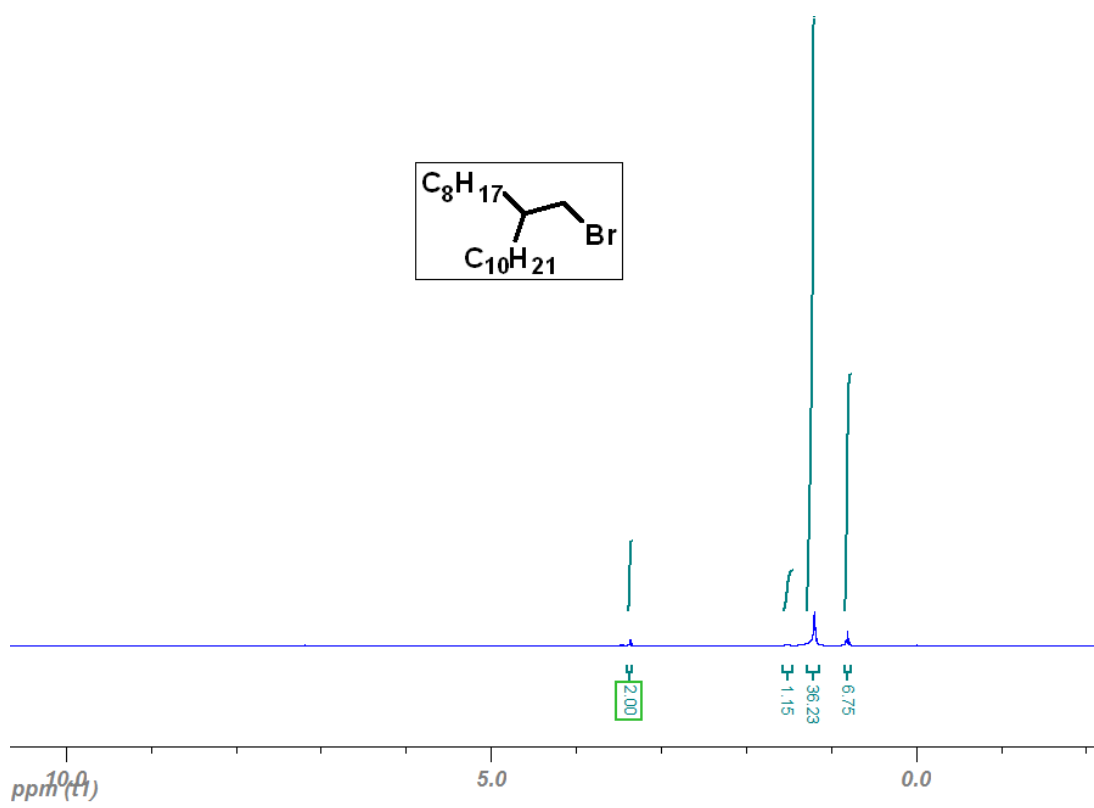


Figure 72 1H NMR of 2-(Bromomethyl)nonadecane

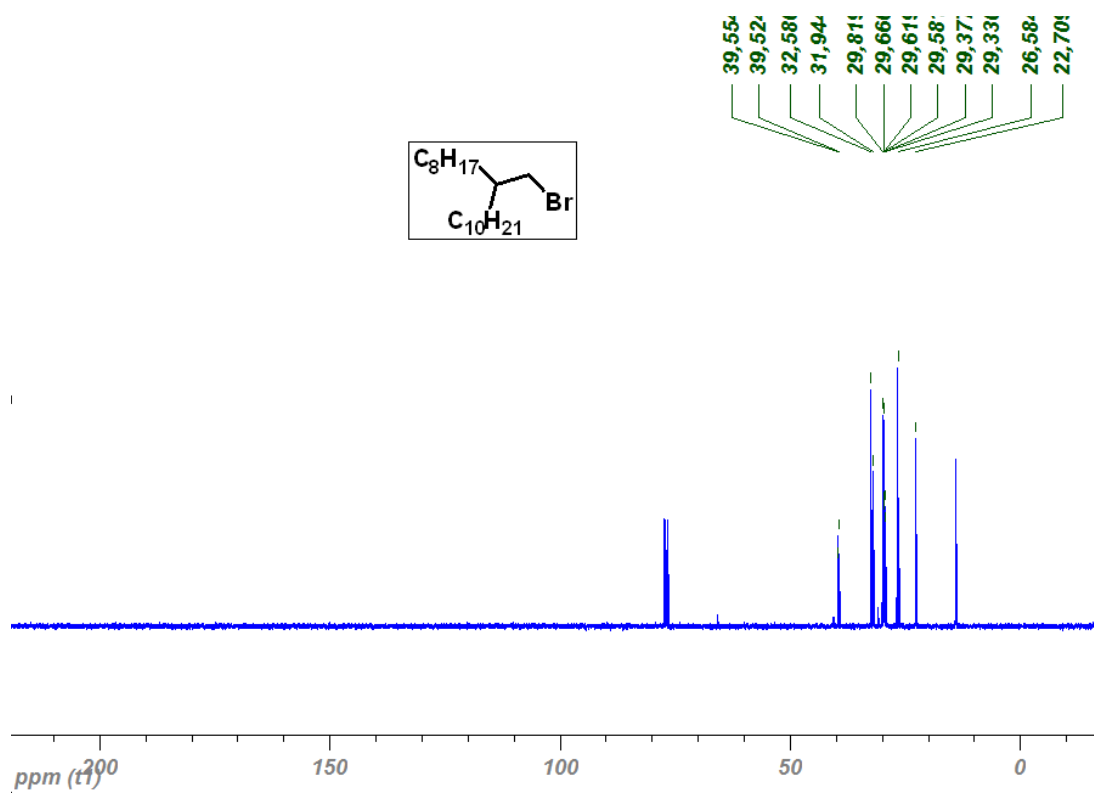


Figure 73 ^{13}C NMR of 2-(Bromomethyl)nonadecane

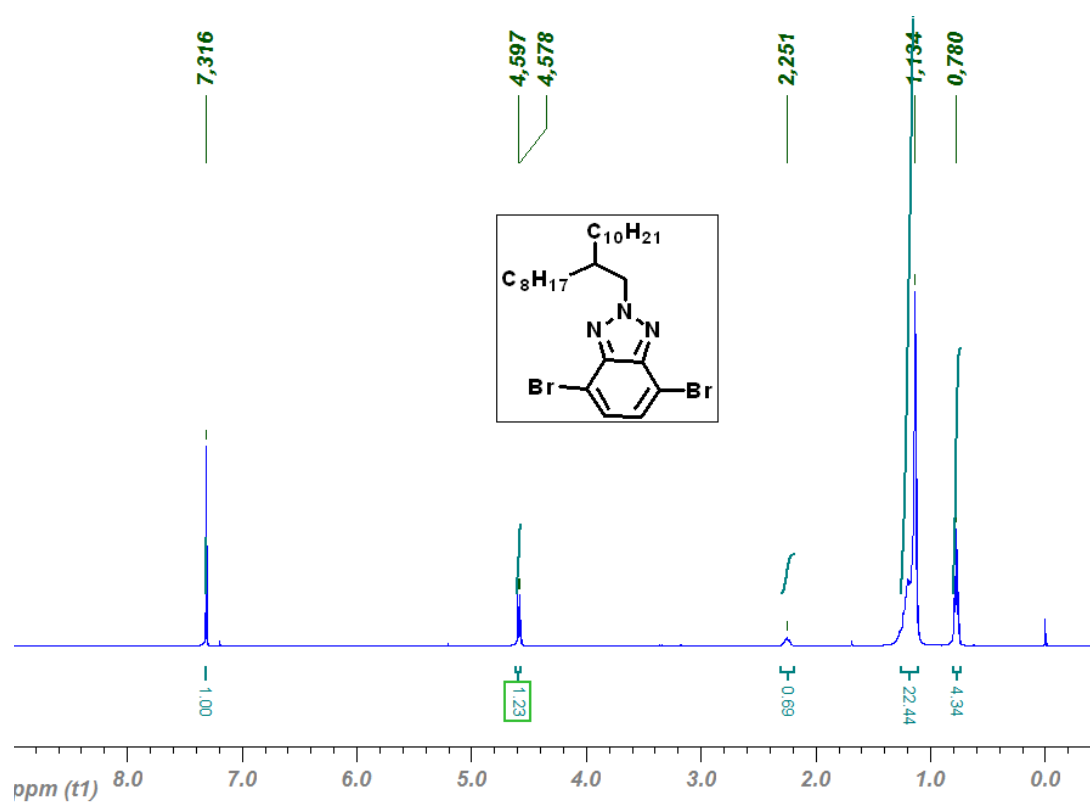


Figure 74 ^1H NMR of 4,7-Dibromo-2-(2-octyldodecyl)-2H-benzo[d][1,2,3] triazole

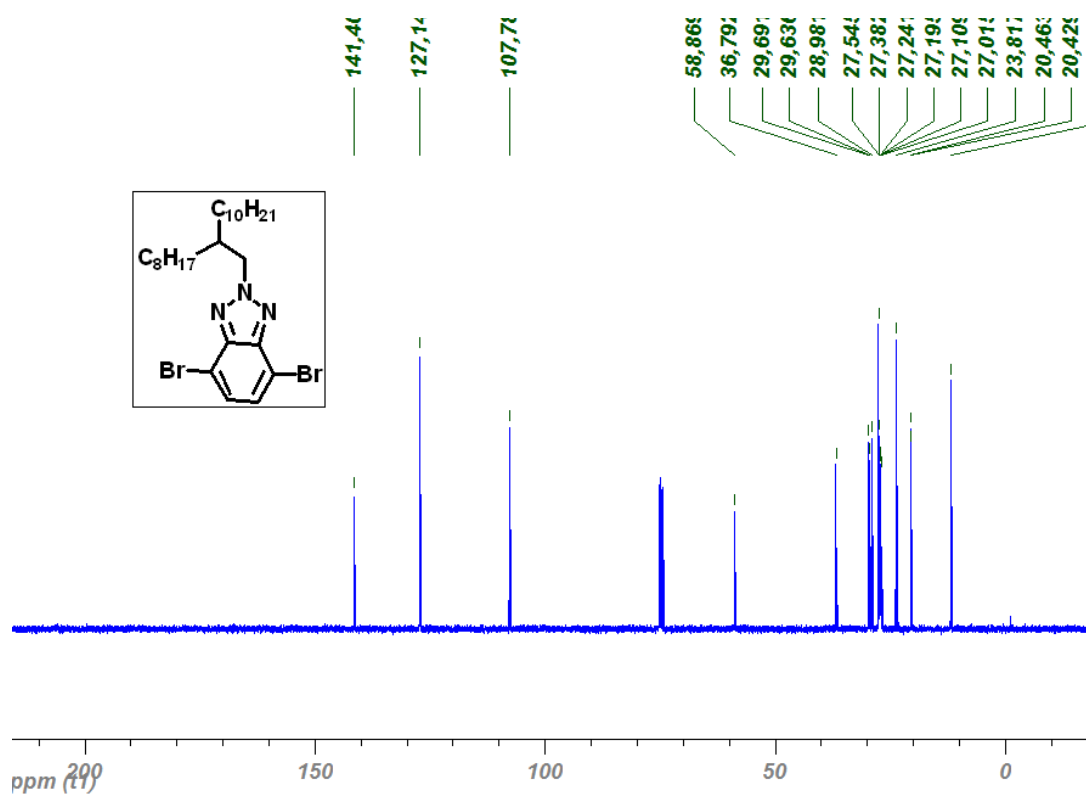


Figure 75 ^{13}C NMR of 4,7-Dibromo-2-(2-octyldodecyl)-2H-benzo[d][1,2,3] triazole

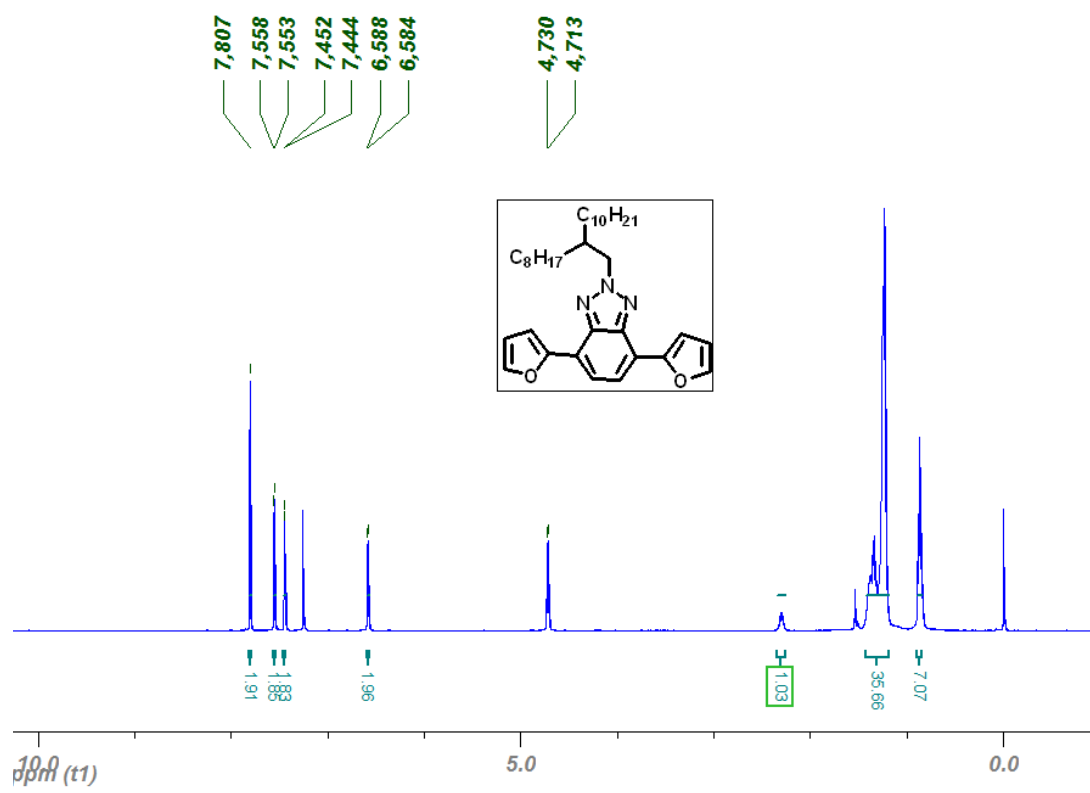


Figure 76 ^1H NMR of 4,7-di(furan-2-yl)-2-(2-(octyldodecyl)-2H-benzo[d][1,2,3]triazole

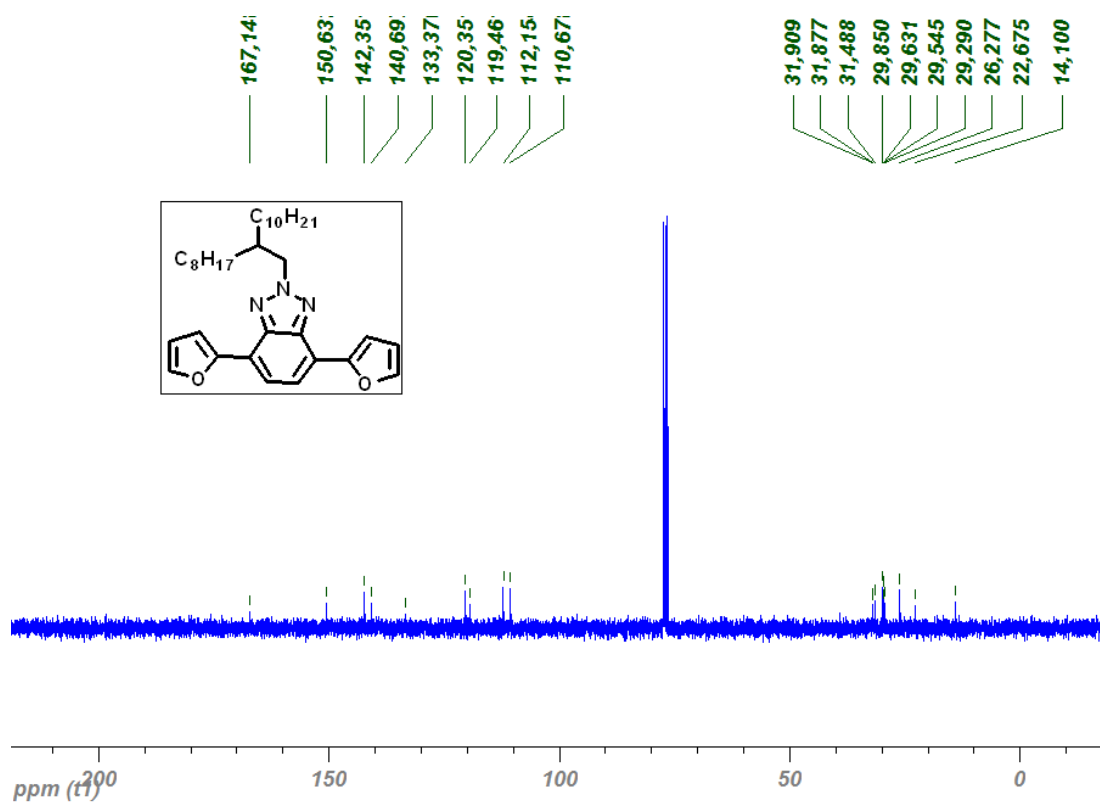


Figure 77 ^{13}C NMR of 4,7-di(furan-2-yl)-2-(2-octyldodecyl)-2H-benzo[d][1,2,3]triazole

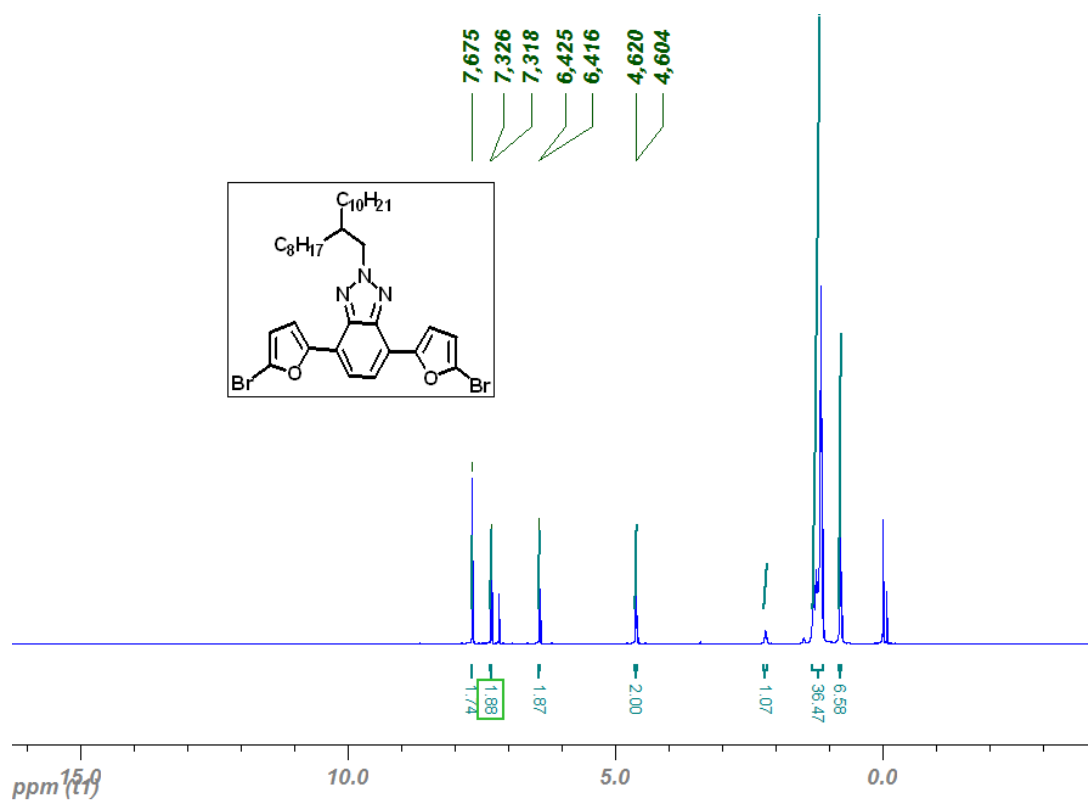


Figure 78 ¹H NMR of 4,7-bis(5-bromofuran-2-yl)-2-(2-octyldodecyl)-2H-benzo[d][1,2,3]triazole

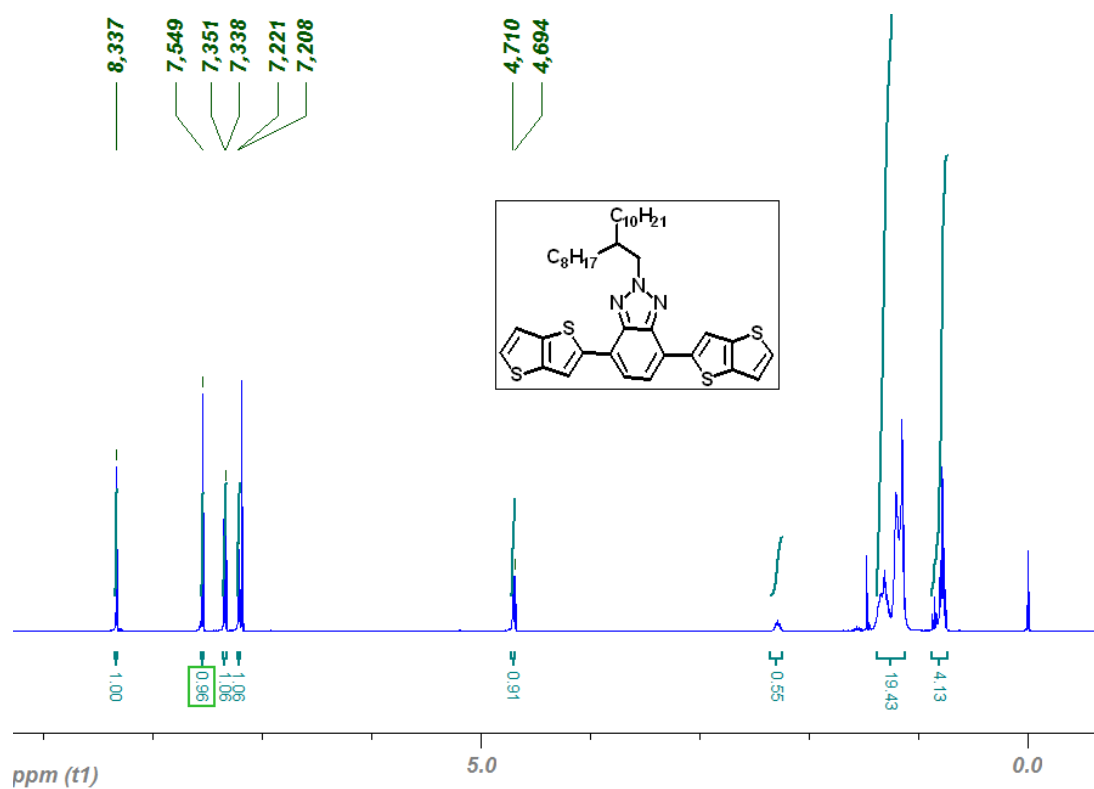


Figure 79 ¹H NMR of 2-(2-(2-octyldodecyl)-4,7-bis(thieno[3,2-*b*]thiophen-2-yl)-2H-benzo[d][1,2,3]triazole

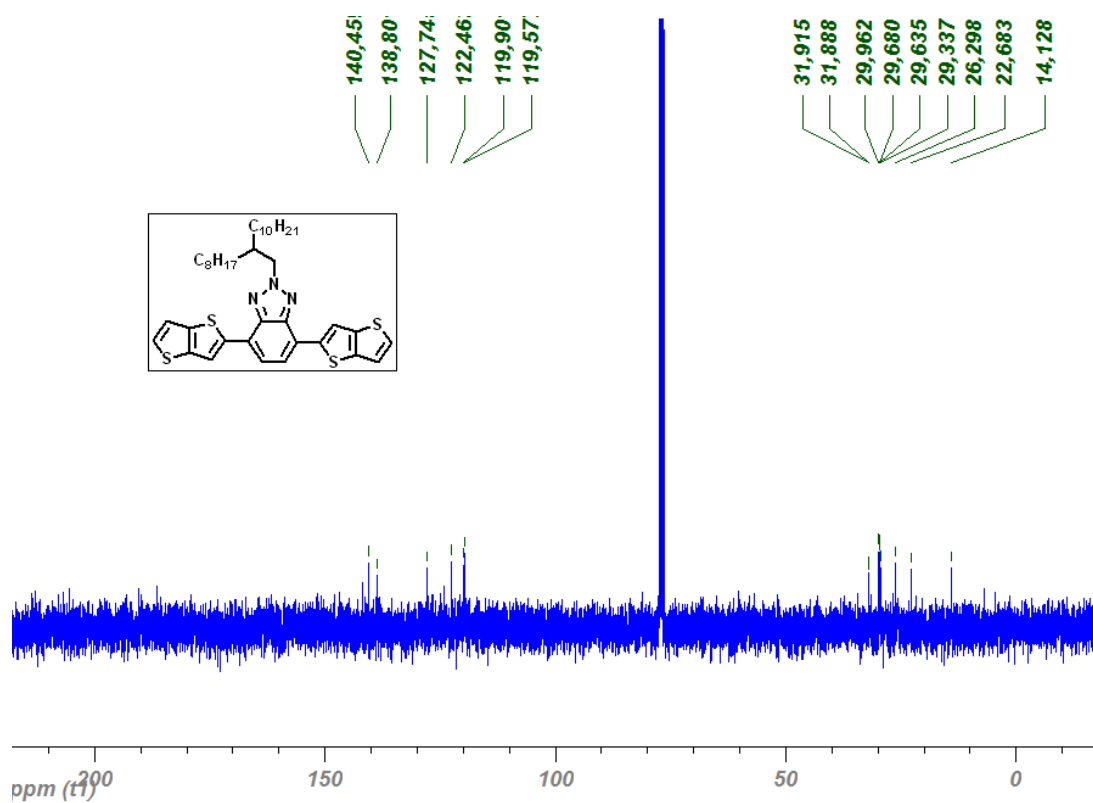


Figure 80 ^{13}C NMR of 2-(2-(2-octyldodecyl)-4,7-bis(thieno[3,2-b]thiophen-2-yl)-2H-benzo[d][1,2,3]triazole

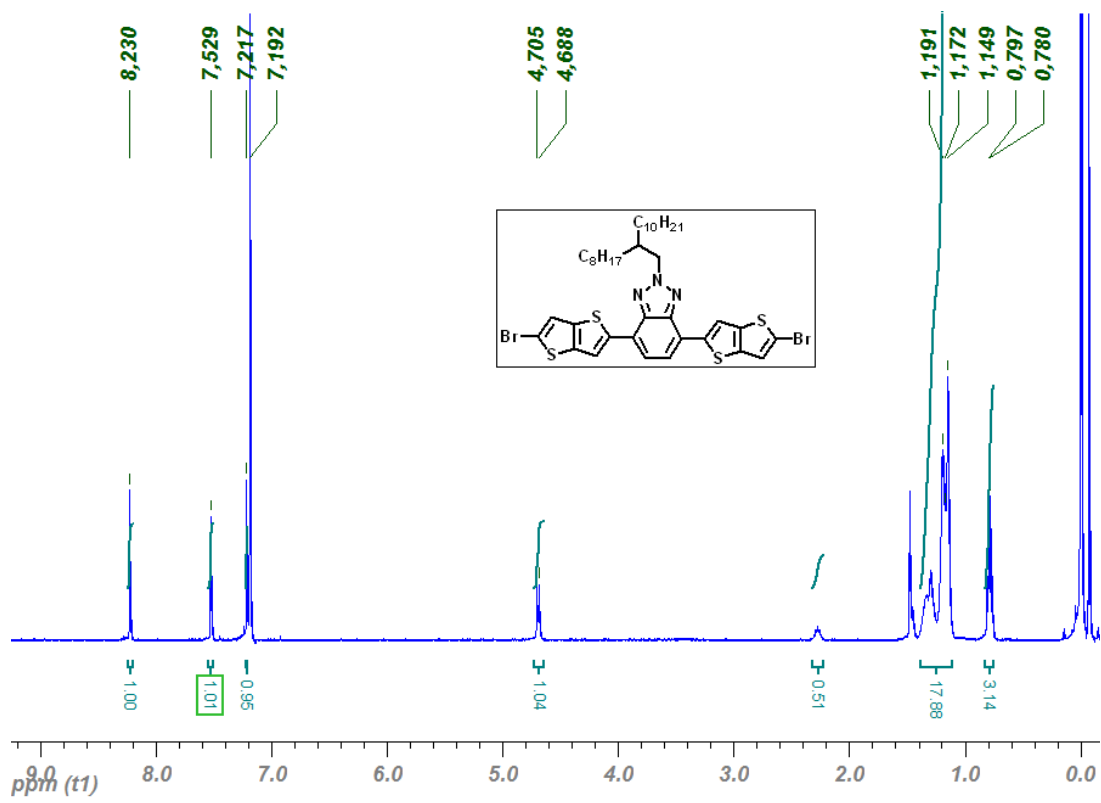


Figure 81 ^1H NMR of 4,7-bis(5-bromothieno[3,2-b]thiophen-2-yl)-2-(2-octyldodecyl)-2H benzo[d][1,2,3]triazole

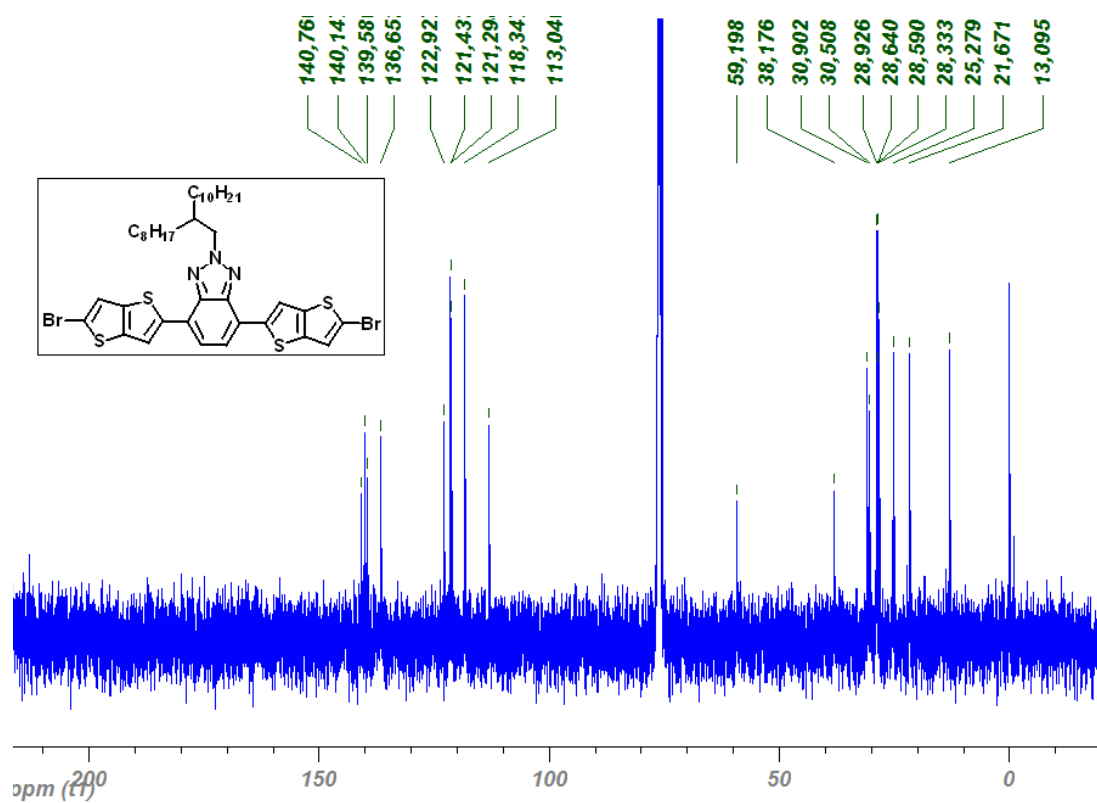


Figure 82 ^{13}C NMR of 4,7-bis(5-bromothieno[3,2-b]thiophen-2-yl)-2-(2-octyldodecyl)-2H benzo[d][1,2,3]triazole

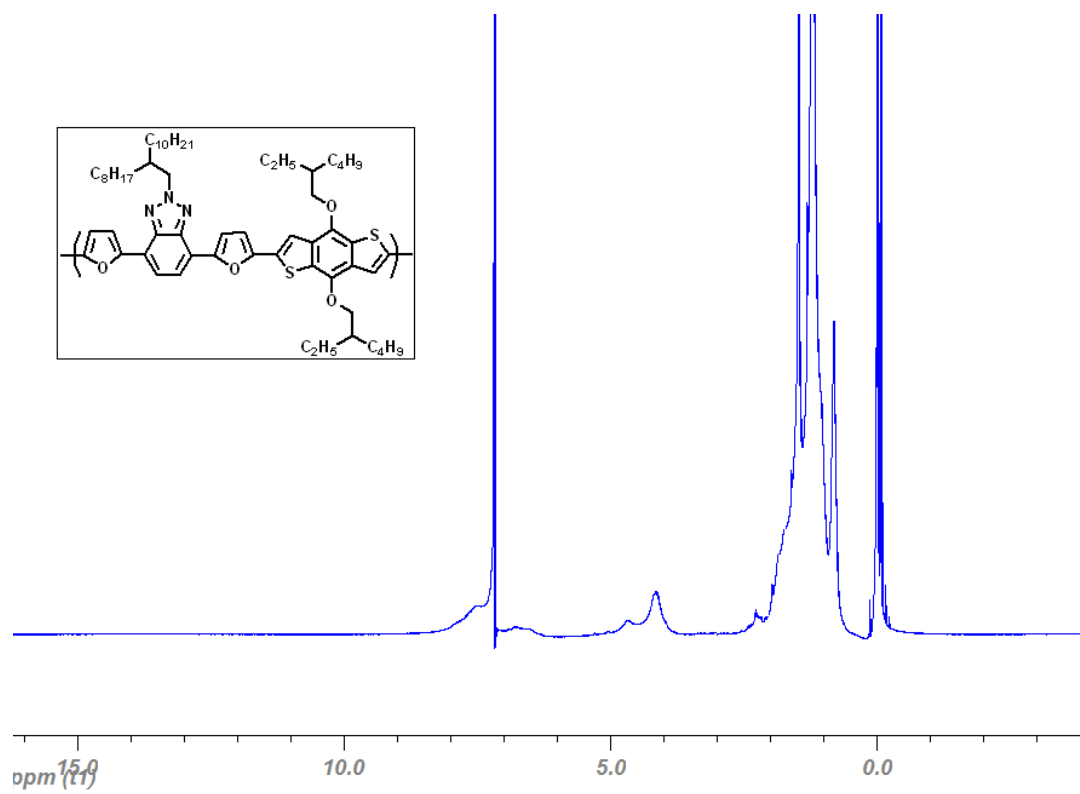


Figure 83 ^1H NMR of PFBTBDT

1. Numune: 13318-1

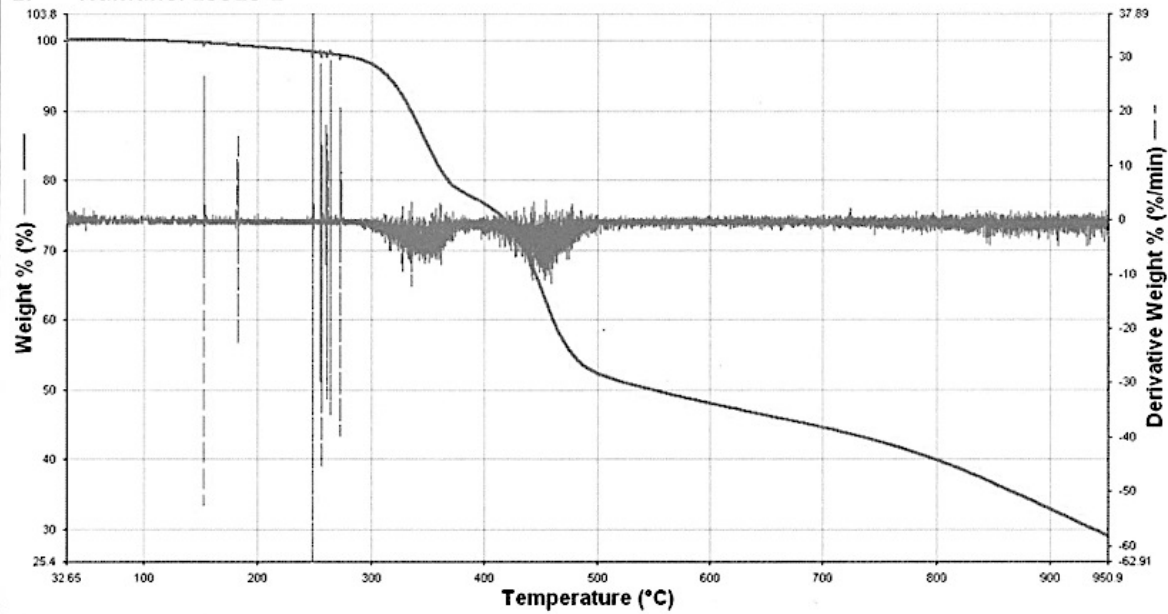


Figure 84 TGA of PTTBTBDT

2. Numune: 13318-2

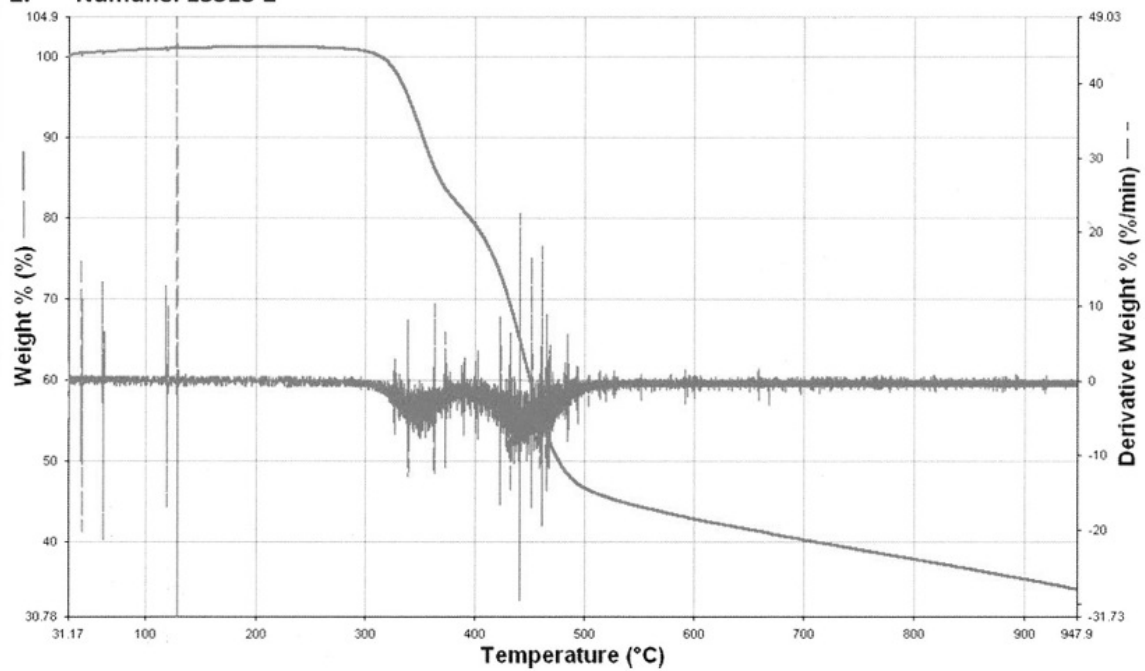


Figure 85 TGA of PFBTBDT

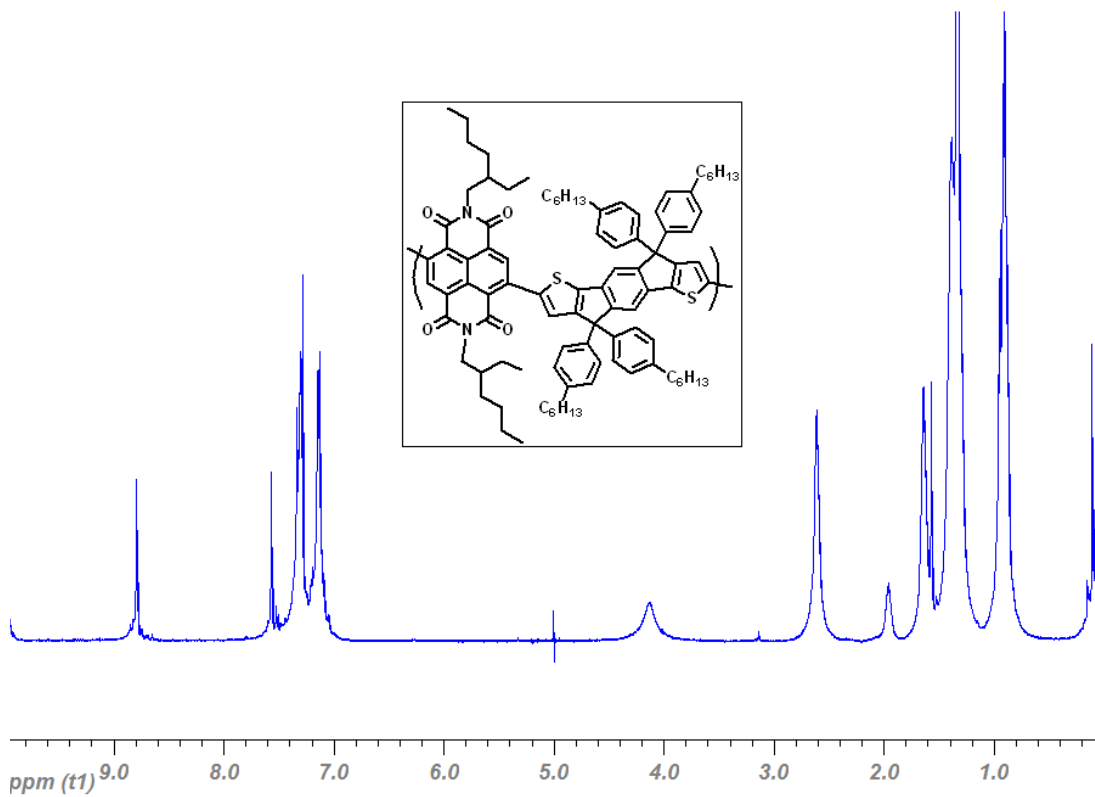


Figure 86 ^1H NMR of PIDTNDI

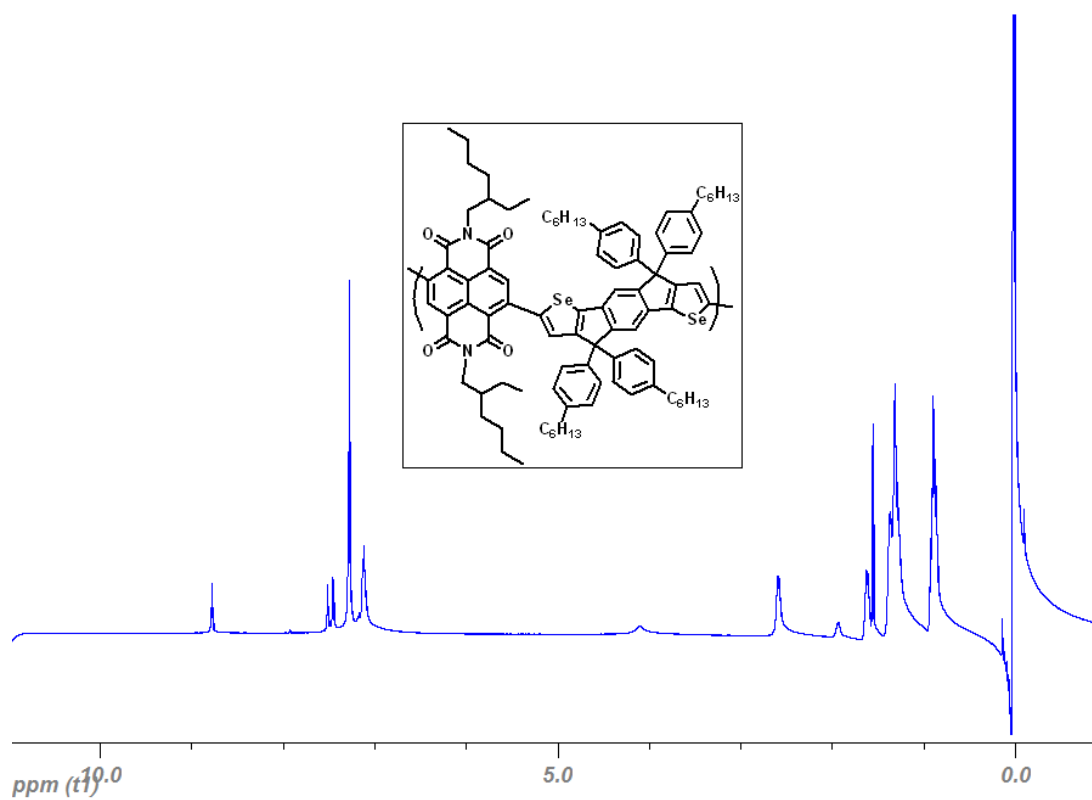


Figure 87 ^1H NMR of PIDSeNDI

CURRICULUM VITAE

PERSONAL INFORMATION

Surname, Name: Akbaşođlu Ünlü, Naime
Nationality: Turkish
Phone: +90 506 246 14 47
Date and Place of Birth: 06 May 1983
email: naimeakbasoglu@gmail.com

EDUCATION AND TRAINING

September 2009-present: Phd. Degree in Chemistry Department of Chemistry,
Polymer Chemistry , METU
Thesis Title: “Organic Bulk Heterojunction Solar
Cells Based on Conjugated Polymers”
Supervisor: Assoc.Prof.Dr. Ali Çırpan
CGPA: 3.56 / 4.00

August 2013- Feb. 2014 TUBITAK SCHOLARSHIP
University of Washington, Material Science and

Engineering Department

Subject Title:

“Indacenodithiophene/selenophene and Naphthalene
Diimide n-Type Copolymers for Efficient All-Polymer
Solar Cells”

“Development of bithiophenedimide based conjugated
large band gap polymers for organic solar cell applications”

Supervisor: Prof. Alex K-Y Jen

Feb. 2008 – Sept. 2009

MSc. Degree in Chemistry Department of Chemistry,
Organic Chemistry, METU

Thesis Title: “Synthesis of linkers and mediators for
electrochemical reactor design and enantiopure synthon
preparation”

Supervisor: Prof. Dr. Ayhan Sıtkı Demir

CGPA: 3.56 / 4.00

Sept. 2002 – Feb. 2008

BS-Major Department of Secondary Science and
Mathematics Education Chemistry Education Program (BS
degree with non-thesis MSc. Degree), METU, CGPA: 3.27 /
4.00

WORK EXPERIENCE

2009-present: Teaching Assistant

Department of Chemistry, Middle East Technical University, 06800
Ankara/TURKEY

Instrumental analysis laboratory for 2 semesters

Physical chemistry laboratory for 6 semesters

General Chemistry laboratory for 3 semesters

PUBLICATIONS

1. Electrochemical and optical studies of furan and thieno[3,2-b]thiophene end capped benzotriazole derivatives, **Naime Akbaşođlu**, Abidin Balan, Derya Baran, Ali Cirpan, Levent Toppare, Polymer Science Part A: Polymer Chemistry, 48,5603–5610 (2010)
2. Synthesis and Electrochemical Properties of a Novel Benzimidazole Derivative as the Acceptor Unit in Donor-Acceptor-Donor Type Polymers, Ali Can Ozelcaglayan, Merve Sendur, **Naime Akbasoglu**; Dogukan H Apaydin, Ali Cirpan, Levent Toppare, Electrochimica Acta, 67, 2012, 224-229.
3. **(Front Cover)** Effect of Dihienopyrrole Unit on electrochromic and optical properties of benzotriazole based conjugated polymers, **Naime Akbasoglu Unlu**, Tugba Kaya Deniz, Merve Sendur, Ali Cirpan, Macromolecular Chemistry and Physics 2012, 213, 1885-1891
4. A.C. Ozelcaglayan, M. Sendur, **N. Akbasoglu**, D.H. Apaydin, A. Cirpan, L. Toppare “Synthesis and Electrochemical Properties of a Novel Benzimidazole Derivative as the Acceptor Unit in Donor-Acceptor-Donor Type Polymers” Electrochimica Acta 2012, 67, 224-229.
5. B. Zaifoglu, M. Sendur, N. A Unlu, L. Toppare, High optical transparency in all redox states: Synthesis and characterization of benzimidazole and thieno [3, 2-b] thiophene containing conjugated polymers, Electrochimica Acta 85 (2012), 78-

6. **(Front Cover)** S. C. Cevher, **N. A. Unlu**, A. C. Ozelcaglayan, D. H. Apaydin, Y. A. Udum, L. Toppare, Ali Cirpan “Fused Structures in the Polymer Backbone to Investigate the Photovoltaic and Electrochromic Properties of Donor-Acceptor Type Conjugated Polymers” *Journal Of Polymer Science, Part A: Polymer Chemistry* 2013, 51, 1933–1941.
7. T.K. Deniz, A.G. Nurioglu, **N.A. Unlu**, M. Sendur, L. Toppare, Ali Cirpan “Syntheses, Electrochemical and Photophysical Properties of Biphenyl Containing Conjugated Copolymers” *Polymer* 54 (2013) 2243-2249
8. M. Kesik, O. Kocer, F. E. Kanik, **N. A. Unlu**, E. Rende, E. A. Gurel, R. M. Rossi, Y. A. Udum, L. Toppare, *Electroanalysis* 25 (2013) 1995-2006.
9. S. D. Uzun, **N.A. Unlu**, M. Sendur, F. E. Kanik, S. Timur, L. Toppare, A novel promising biomolecule immobilization matrix: Synthesis of functional benzimidazole containing conducting polymer and its biosensor applications, *Colloids and Surfaces B: Biointerfaces*, 112 (2013) 74–80.
10. B. Zaifoglu, S.O. Hacioglu, **N.A. Unlu**, Ali Cirpan, L. Toppare “Structure-Property Relations in Donor-Acceptor-Donor Type Benzimidazole Containing Conjugated Polymers” *Journal of Materials Science*, 49 (2014) 225-231
11. S. Toksabay, S. O. Hacioglu, **N. A. Unlu**, Ali Cirpan, L. Toppare “Thieno[3,2-b]thiophene as π -bridge at Different Acceptor Systems for Electrochromic Applications” *Polymer*, 55 (2014) 3093–3099
12. H. Unay, **N.A. Unlu**, G. Hizalan, S. O. Hacioglu, D. E. Yildiz, L. Toppare, Ali Cirpan’ Benzotriazole and Benzodithiophene Containing Medium Band-Gap Polymer for Bulk Heterojunction Polymer Solar Cell Applications, *Journal Of Polymer Science, Part A: Polymer Chemistry*, 53 (2015) 528–535

13. **(Front Cover)** O. Erlik, **N. A. Unlu**, G. Hizalan, S. O. Hacıoğlu, S. Comez, E. D. Yildiz, L. Toppare, A. Cirpan “Silaflorene-based polymers for electrochromic and polymer solar cell applications” 53 (2015) 1533–1628
14. H. Unay, **N.A. Unlu**, S. O. Hacıoğlu, G. Hizalan, L. Toppare, Ali Cirpan: Phosphorus, Sulfur, and Silicon and the Related Elements “Selenophene as a Bridge in Molecular Architecture of Benzotriazole Containing Conjugated Copolymers to Gain Insight on Optical and Electrochemical Properties of Polymers” 190 (2015) 1294-1306

CONGRESS

- XII.Ulusal Kimya Kongresi,Kıbrıs,Magusa, Poster Sunumu
- XXIII.Ulusal Kimya Kongresi,Sivas, Poster Sunumu
- International Enzyme Engineering Symposium. 1-5 October 2008. Kusadasi-İzmir, Poster Presentation
- Nanotr 8- 8. Türkiye Nanobilim ve Nanoteknoloji Konferansı, Ankara, poster sunumu
- 4. Fiziksel Kimya Kongresi, Denizli, Poster Sunumu

SCHOLARSHIP

TUBİTAK 2214/A Yurt Dışı Doktora Sırası Araştırma Burs Programı

PERSONAL SKILLS AND COMPETENCES

Language: Advanced English

COMPUTER SKILLS AND COMPETENCES

MS Office Applications (MS word, MS Excel, MS PowerPoint, FrontPage.)

Knowledge of Chemdraw Ultra 8.0 package

Origin computer programs in Chemistry

HPLC, GC, CV, AAS, AES, FTIR, refractometry, UV-Vis- spectrophotometry